



저작자표시-비영리-변경금지 2.0 대한민국

이용자는 아래의 조건을 따르는 경우에 한하여 자유롭게

- 이 저작물을 복제, 배포, 전송, 전시, 공연 및 방송할 수 있습니다.

다음과 같은 조건을 따라야 합니다:



저작자표시. 귀하는 원저작자를 표시하여야 합니다.



비영리. 귀하는 이 저작물을 영리 목적으로 이용할 수 없습니다.



변경금지. 귀하는 이 저작물을 개작, 변형 또는 가공할 수 없습니다.

- 귀하는, 이 저작물의 재이용이나 배포의 경우, 이 저작물에 적용된 이용허락조건을 명확하게 나타내어야 합니다.
- 저작권자로부터 별도의 허가를 받으면 이러한 조건들은 적용되지 않습니다.

저작권법에 따른 이용자의 권리는 위의 내용에 의하여 영향을 받지 않습니다.

이것은 [이용허락규약\(Legal Code\)](#)을 이해하기 쉽게 요약한 것입니다.

[Disclaimer](#)

Doctoral Thesis

Wearable Hand Exoskeleton Systems
for Virtual Reality and Rehabilitation

Inseong Jo

Department of Mechanical Engineering

Graduate School of UNIST

2019

Wearable Hand Exoskeleton Systems for Virtual Reality and Rehabilitation

Inseong Jo

Department of Mechanical Engineering

Graduate School of UNIST

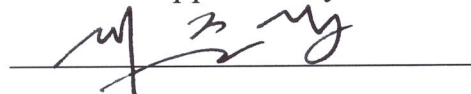
Wearable Hand Exoskeleton Systems for Virtual Reality and Rehabilitation

A thesis/dissertation
submitted to the Graduate School of UNIST
in partial fulfillment of the
requirements for the degree of
Doctor of Philosophy

Inseong Jo

05/30/2019

Approved by



Advisor

Joonbum Bae

Wearable Hand Exoskeleton Systems for Virtual Reality and Rehabilitation

Inseong Jo

This certifies that the thesis/dissertation of Inseong Jo is approved.

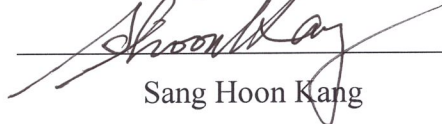
05/30/2019

signature



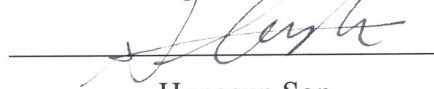
Advisor: Joonbum Bae

signature



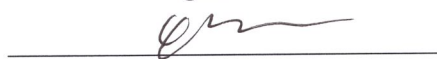
Sang Hoon Kang

signature



Hungsun Son

signature



Hyondong Oh

signature



Gwanseob Shin

Abstract

This thesis reports the development of hand exoskeleton systems, for use in virtual reality (VR) environments and for hand rehabilitation; the aim is to overcome the limitations of conventional systems in terms of both wearability and portability. As the hand receives diverse physical information and manipulates different type of objects, conventional systems contain many sensors and actuators, and are both large and heavy. Thus, hand exoskeleton systems exhibiting high wearability and portability while measuring finger motions and delivering forces would be highly valuable.

For VR hand exoskeleton systems, a wearable hand exoskeleton system with force-controllable actuator modules was developed to ensure free finger motion and force mode control. The linkage structure ensures motion with three degrees of freedom (DOF) and provides a large fingertip workspace; the finger postures assumed when interacting with objects are appropriate. A series elastic actuator (SEA) with an actuator and an elastic element was used to fabricate compact actuator modules. Actuator friction was eliminated using a friction compensation algorithm. A proportional differential (PD) controller, optimized by a linear quadratic (LQ) method featuring a disturbance observer (DOB), was used to ensure accurate force mode control even during motion. The force control performance of the actuator module was verified in force generation experiments including stationary and arbitrary end-effector motions. The forces applied to the fingertips, which are the principal parts of the hand that interact with objects, were kinematically analyzed via both simulations and experiments.

To overcome the weak point of previous system, a wearable hand exoskeleton system featuring finger motion measurement and force feedback was developed and evaluated in terms of user experience (UX). The finger structures for the thumb, index, and middle fingers, which play important roles when grasping objects, satisfy full range of motion (ROM). The system estimates all joint angles of these three digits using a dedicated algorithm; measurement accuracy was experimentally evaluated to verify system performance. The UX performance was evaluated by 15 undergraduate students who completed questionnaires assessing usability and utilitarian value following trials conducted in the laboratory. All subjects were highly satisfied with both usability and the utilitarian nature of the system, not only because control and feedback were intuitive but also because performance was accurate.

For rehabilitation, a highly portable exoskeleton featuring flexion/extension finger exercises was developed. The exoskeleton features two four-bar linkages reflecting the natural metacarpophalangeal (MCP) and proximal phalangeal (PIP) joint angles. During optimization, the design parameters were

adjusted to reflect normal finger trajectories, which vary by finger length and finger joint ROM. To allow for passive physical impedance, a spring was installed to generate the forces that guided the fingers. The moments transmitted to the MCP and PIP joints were estimated via finite element method (FEM) analysis and the cross-sectional areas of the links were manually designed by reference to the expected joint moments. Finger motion and force distribution experiments verified that the system guided the fingers effectively, allowed for the desired finger motions, and distributed the required moments to the joints (as revealed by FEM analysis).

Contents

1	Introduction	8
1.1	Motivation	8
1.1.1	The Hand	8
1.1.2	Applications of the hand exoskeleton systems	10
1.1.2.1	Virtual Reality	10
1.1.2.2	Rehabilitation	10
1.2	State of the Art	11
1.2.1	Hand Force (Kinesthetic) Feedback Systems	11
1.2.2	Hand Rehabilitation Systems	13
1.3	Thesis Overview	15
2	Wearable Hand Exoskeleton Systems for Virtual Reality	17
2.1	A Force-controllable Hand Exoskeleton System	17
2.1.1	Introduction	17
2.1.2	Structure Design	19
2.1.2.1	Design of the Structure	19
2.1.2.2	Kinematic Analysis of the Structure	20
2.1.3	Actuator Module Design	26
2.1.3.1	Series Elastic Actuator (SEA) Mechanism	26
2.1.3.2	Actuator Module Control	30
2.1.4	Implementation of the Hand Exoskeleton	34
2.1.4.1	Analysis of Force Distribution	37
2.1.4.2	Force Transmission Experiment	39
2.1.5	Summary	39

2.2	A Wearable Hand Exoskeleton System with Finger Motion Measurement and Force Feedback	41
2.2.1	Design of the Exoskeleton System for VR	42
2.2.2	Finger Motion Measurement	44
2.2.2.1	Workspace of the Fingertip	44
2.2.2.2	Calculation of Fingertip Position	46
2.2.2.3	Calibration Process	47
2.2.2.4	Joint Angle Measurement of the Index Finger	48
2.2.2.5	Joint Angle Measurement of the Thumb	50
2.2.3	Force Feedback	55
2.2.4	Experimental Verification	56
2.2.4.1	Measurement of the Fingertip Position	56
2.2.4.2	Pinch Motion	56
2.2.4.3	Estimation of Finger Joint Angles	57
2.2.4.4	Performance Evaluation as a Haptic Device	61
2.2.5	Summary	63
2.3	User Experience (UX) Evaluation	63
2.3.1	Introduction	63
2.3.2	Virtual Reality Program	65
2.3.3	Evaluation Framework for Wearable Hand Systems	66
2.3.4	Experimental Setup	70
2.3.5	Result & Discussion	70
2.3.5.1	User Experience (UX) Evaluation	70
2.3.5.2	System Satisfaction	72
2.3.6	Summary	72
2.4	Summary	73
3	A Wearable Spring-guided Hand Exoskeleton for Continuous Passive Motion	77
3.1	Introduction	77
3.2	The Exoskeleton Design	79
3.3	Optimized Design Structure	81
3.3.1	Hand flexion/extension experiment	81

3.3.2	Optimization Algorithm	84
3.3.3	Spring mechanism	89
3.3.4	Force distribution analysis	93
3.4	Performance Evaluation	97
3.4.1	Implementation of the exoskeleton system for the hand	97
3.4.2	Finger Motion Experiment	98
3.4.3	Force Distribution Experiment	100
3.5	Summary	101
4	Conclusion	102
4.1	Wearable Hand Exoskeleton Systems for Virtual Reality	102
4.2	A Wearable Spring-guided Hand Exoskeleton for Continuous Passive Motion	103
4.3	Open Issues	104
4.3.1	Zero Impedance Performance	104
4.3.2	Direction of the Force Feedback	105
	References	106

List of Figures

1-1	Cortical homunculus	9
1-2	Anatomy of the hand	9
1-3	The hand force feedback systems for VR [1–8]	12
1-4	The rehabilitation systems for the hand [9–19]	13
2-1	The system type according to the structure	18
2-2	Anatomy of the finger (edited from [20])	20
2-3	Design candidates of the finger structure	21
2-4	Comparison between design candidates	21
2-5	The proposed design of the linkage structure	21
2-6	The linkage structure	22
2-7	Parameters for kinematic analysis	23
2-8	Linkage 1	24
2-9	Linkage 2	25
2-10	Comparison of the proposed and larger linkage structure	27
2-11	Series elastic actuator (SEA) mechanism	28
2-12	Actuator module design	29
2-13	Maximum contact force	29
2-14	The actuator module	31
2-15	Friction identification	31
2-16	Frequency response of the linearized motor	31
2-17	Overall control structure (P : plant, P_n : the nominal model of P , Q : Q filter in the DOB, C : controller, f_d/f : desired/measured force, x_{Md}/x_M : desired/measured motor position, x_H : finger position, d/\hat{d} : external/estimated disturbance, u : control input, u_d : control input in the DOB, ξ : noise)	32

2-18	Force control performance with stationary motion	34
2-19	Force control performance with arbitrary motion	35
2-20	The proposed hand exoskeleton system	36
2-21	Force distribution analysis	38
2-22	Force transmission experiment	40
2-23	Normal force at the fingertip in experiment	41
2-24	Design of the exoskeleton system for VR	43
2-25	Parameters of finger structures	45
2-26	Fingertip workspace of the index finger	46
2-27	Finger joint angle estimation using inverse kinematics	49
2-28	Estimation algorithm of the finger joint angles	50
2-29	The estimated F/E angle of CMC joint with a constant CMC joint orientation	52
2-30	Thumb structure in calibration posture	53
2-31	Overall control algorithm of the hand exoskeleton system for VR	55
2-32	Fingertip position measurement performance	56
2-33	Pinch motion experiment	58
2-34	Measurement experiment of the index finger joints	59
2-35	Measurement experiment of the thumb joints	60
2-36	Performance evaluation with various physical properties	62
2-37	Evaluation of a haptic interface [21]	64
2-38	VR program	67
2-39	Evaluation framework for wearable devices	68
2-40	Evaluation framework for wearable hand systems for VR (revised from [22])	69
2-41	UX experiment	71
3-1	Proposed kinematic design	80
3-2	Kinematic scheme of the structure	80
3-3	Hand flexion/extension experiment without motion instructions	82
3-4	Hand flexion/extension experiments	83
3-5	Adjusted joint relationship	85
3-6	Design parameters of the exoskeleton structure	86
3-7	Flowchart of the optimization algorithm	88

3-8	Optimized finger motions	89
3-9	Spring mechanism	90
3-10	Deviated postures from the desired trajectory	91
3-11	Force distribution analysis	95
3-12	Applied Moment at MCP and PIP joint	96
3-13	Prototype of the system	98
3-14	Experiment of finger motion	99
3-15	Experimental setup	101
4-1	Magnetic clutch mechanism	104
4-2	The mechanism for various force direction	105

List of Tables

2.1	Parameters of kinematic analysis	23
2.2	Parameters of the spring design	30
2.3	Orientation angle of the trapezium	51
2.4	Familiarity with VR devices	69
2.5	Results of user experience (UX) evaluation	75
2.6	Satisfaction scores of system design	76
3.1	The obtained ROM from the experiment	84
3.2	User information	85
3.3	The optimized design vector	88
3.4	Force distribution experiment	100

Chapter 1

Introduction

1.1 Motivation

1.1.1 The Hand

Of the many body parts, the hand has a particularly large number of sensors that receive diverse physical information (e.g., force, pressure, texture, and temperature) from the environment. This information aids our understanding of the world around us, including nearby objects. Also, the hand performs tasks such as holding or moving objects with the fingers.

The cortical homunculus is a physical representation of the human body based on a neurological map of the brain. The cortical homunculus is a physical representation of the human body based on the neurological map in the brain [23, 24]. Figure 1-1 shows the two-dimensional (2D) homunculus of the motor and somatosensory cortex; the larger the corresponding area in the brain, the greater the neurological complexity of the body part. The hand occupies the second-largest area in the brain, after the mouth. The hand is extremely complex, is capable of very fine motions and is very sensitive to stimuli. Given the exquisite sensitivity and many degrees of freedom (DOF), the hand can interact with objects ranging from a small needle to a large ball, thus facilitating activities of daily living (ADLs).

These bones, and the various associated muscles and ligaments, form joints that are used for diverse motions. Eight carpal bones and four metacarpals (excluding those of the thumb) form the palm, which has a large contact area. Each finger consists of three phalanges (two for the thumb) that can move independently [25]. Thus, the index, middle, ring, and little fingers exhibit flexion/extension (F/E) and abduction/adduction (A/A) motions at the metacarpophalangeal (MCP)

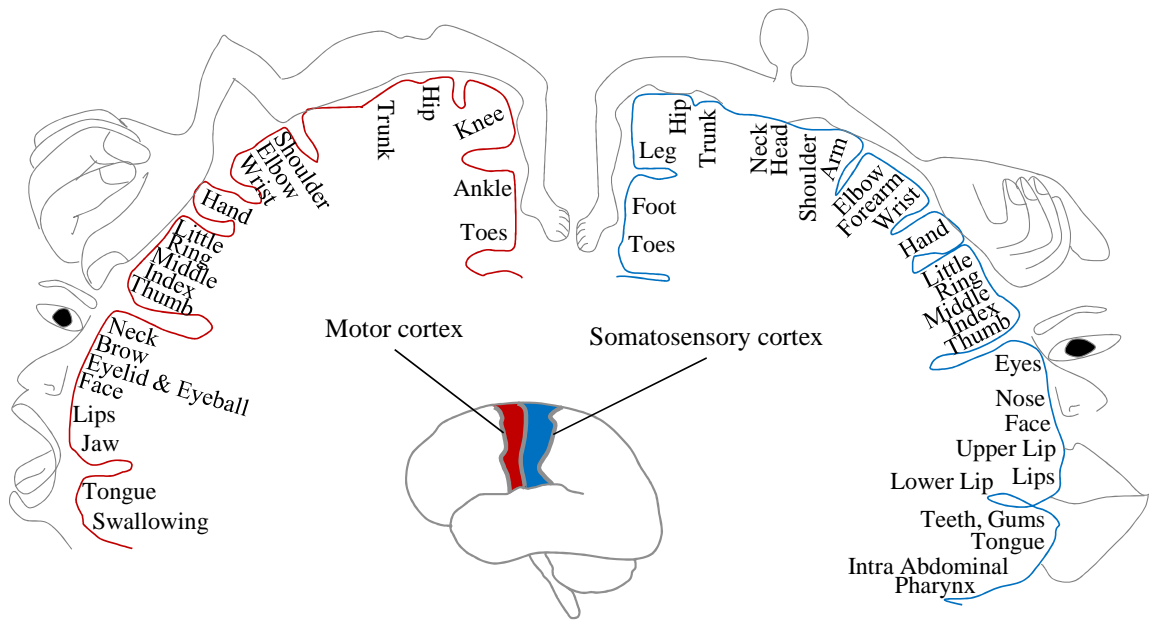


Figure 1-1: Cortical homunculus

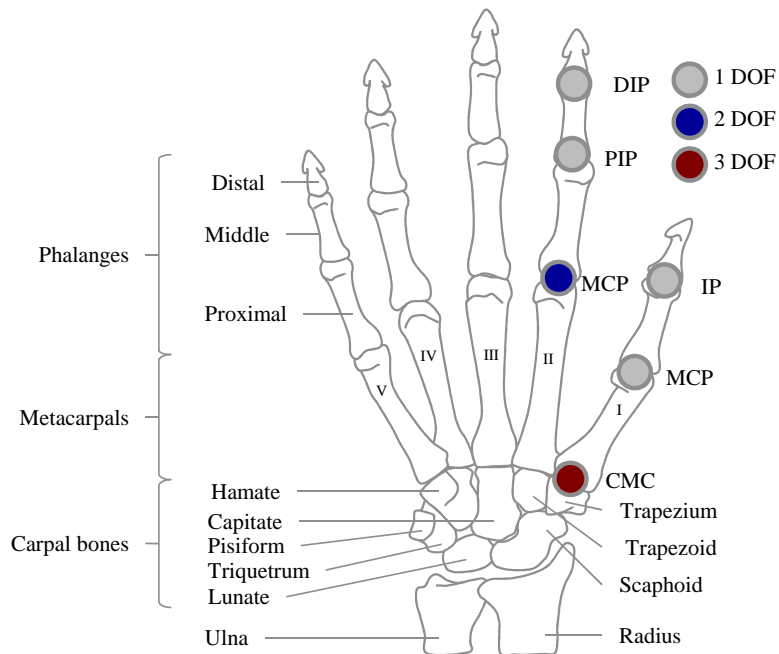


Figure 1-2: Anatomy of the hand

joint, F/E motion at the proximal phalangeal (PIP), and distal interphalangeal (DIP) joints, respectively. The thumb consists of one metacarpal and two phalanges. The first metacarpal engages in complex movements by forming a saddle joint with the trapezium. The carpometacarpal (CMC) joint between the trapezium and the first metacarpal not only exhibits F/E and A/A motions, but also supination/pronation (S/P) [25]. This allows the thumb to curve and engage in pinching with the other fingertips. As complex finger motions are possible given the anatomy of the hand, humans can stably hold objects with various shapes.

1.1.2 Applications of the hand exoskeleton systems

Hand exoskeleton systems have been actively researched due to the importance of hand function in daily life. Such exoskeletons have been applied in a variety of ways, including for virtual reality (VR) applications and hand rehabilitation.

1.1.2.1 Virtual Reality

VR environments can simulate both real and imaginary worlds. As environments beyond the limits of time and space can be implemented in VR, the technique finds applications in various fields; many interfaces (e.g., mouse, keyboard, and joystick) have been developed to connect users to VR environments. However, most systems have the disadvantage that the user must learn how to handle them and the modes of VR interaction differ. Also, most VR systems generate only vibrational feedback from the VR. It would be useful to develop an intuitive interface that measures finger motions and transmits force feedback from the VR to the user. If a virtual hand is to mimic finger motions successfully, such motions must be accurately measured. Finger motion data are used to determine whether the finger is touching an object, or the extent to which an object is being squeezed by the hand. A hand system for VR applications should generate and transmit accurate reaction forces, calculated by reference to the physical properties and extent of deflection of the virtual object. If finger motion measurement and reaction force transmission are inaccurate, the user may misunderstand the virtual environment and objects therein.

1.1.2.2 Rehabilitation

When manipulating an object in daily life, the fingers move and a force is felt during holding of the object. However, finger function can be compromised by disease, surgery, and accidents. Various rehabilitation protocols are used depending on the patient's condition and the aim of therapy.

Conventional therapy requires one-to-one interaction between a patient and a therapist; this is both labor-intensive and expensive [26]. Robotic hand rehabilitation is attractive to ensure recovery of hand function and resumption of normal ADLs.

Two principal groups of patients require rehabilitation. In the first group, the central nervous system (CNS) is affected by disease (usually stroke) [27]. In stroke patients, motor signals are distorted because of abnormalities in the brain that trigger muscle spasticity or fatigue, although the muscles are normal. Through rehabilitation of an affected hand, the unaffected hemisphere comes to control that hand and motor function recovers [28]. In addition, rehabilitation reduces muscle spasticity and restores muscle strength [29].

In the second group of patients, the hand muscles or joints are damaged in an accident or by surgery. Splints are initially used to protect surgical sites; however, blood circulation is compromised and joint edema may develop. Thus, hand rehabilitation via highly intensive and repetitive exercise is essential. Such exercise promotes blood circulation, reduces edema, minimizes joint stiffness, and maintains the range of motion (ROM) [30,31]. To effectively restore hand function, the rehabilitation protocol should consider muscle parameters, the ROM, and hand anatomy. As described above in the context of VR, establishing clear criteria for evaluation of system performance is challenging. Existing methods will be discussed in the next section.

1.2 State of the Art

1.2.1 Hand Force (Kinesthetic) Feedback Systems

Many hand VR interfaces have been developed to transmit force feedback to the user, and hand motions to the VR. The various VR interfaces, categorized according to their mobility and motion measurement systems, are shown in Fig. 1-3. Although many cutaneous feedback systems have been developed, I focus on force feedback systems only.

Force (kinesthetic) feedback systems can be divided into grounded and wearable systems according to mobility, and into finger and hand motion systems according to measurement type. The systems depicted in the top left part of Fig. 1-3 are haptic systems with end-effectors [1, 2]. A user grasps a sphere- or pen-type end-effector and moves the hand in three dimensions. Although only one end-effector is employed, the user feels forces in six directions (i.e., $\pm x$, $\pm y$, and $\pm z$ -axis). Grounded systems transmit forces more accurately than wearable systems because grounding ensures firmness. However, as the position of only the end-effector is measured, these systems mea-




Hand force (kinesthetic) feedback systems		Measurement	
		Hand motion	Finger motion
Mobility	Grounded systems	 <p>Omega.6, Forcedimension Touch, 3D Systems</p>	 <p>SPIDAR-8, TITech MasterFinger, UPM</p>
	Wearable systems	N/A	 <p>Cybergrasp, CyberGlove Systems Dexmo, DextaRobotics</p> <p>ExoHand, Festo RMII-ND, RU</p>

Figure 1-3: The hand force feedback systems for VR [1–8]

sure hand motion rather than finger motion, which is not recognized. Such systems are optimally suited to virtual situations wherein a user performs tasks while holding an object, without any need for finger movement.

The systems depicted in the top right part of Fig. 1-3 are laboratory grounded systems that measure finger motion [3,4]. The user wears several thimbles located at the end-effectors of cables or linkage mechanisms and feels forces while moving the fingers in various directions. As these devices measure fine finger motion, they can be used in complex virtual tasks than the end-effector-type systems. Although the user does not perceive the weight of the system (because it is grounded), he/she cannot move the wrist or arm freely; these are constrained by the system design. Also, the grounded systems are large and heavy, and thus not portable.

To ensure free arm motion, high wearability, and good portability, I focused on wearable systems featuring finger motion measurement and force feedback (lower right part of Fig. 1-3). Cybergrasp and Dexmo are the best-known wearable systems, manufactured by CyberGlove Systems and DextaRobotics, respectively [5, 6]. The ExoHand and RMII-ND are wearable hand systems developed by Festo and RU, respectively [7, 8]. To ensure that the robots could be carried by hand, size and


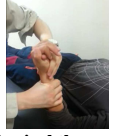







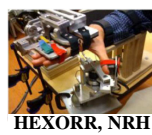



Hand rehabilitation		Purpose		
		Fixation	Continuous passive motion (CPM)	Activities of daily living (ADL)
Actuation	No actuation	 Prometheus Traction Splint, Prometheusmed	 Physical therapy	 Occupational therapy
	Passive actuation (w/ spring)	 SaeboStretch, Saebo	 Hand Exerciser, TheraBand	 SaeboFlex, Saebo  HandSOME, NRH
	Active actuation	N/A	 Kinetic Maestra Portable, TheraTechEquipment  Waveflex Hand CPM, RemingtonMedical  HEXORR, NRH	 HOH, RehabRobotics  Exo-Glove, SNU  Sinfonia, Gloreha

Figure 1-4: The rehabilitation systems for the hand [9–19]

weight reduction was prioritized. The actuator modules and accessory equipment of the Cybergrasps and ExoHand are remote from the hand; however, this degrades system portability to a level similar to that of grounded systems. Also, most such systems (including the Dexmo and RMII-ND) measure only fingertip positions, not finger joint angles. If only fingertip movement is measured, a hand active in a VR cannot accurately mimic real finger motion so the level of VR immersion is low. It is necessary to develop VR systems that measure finger joint angles and transmit force feedback; such systems must exhibit high-level wearability and portability.

1.2.2 Hand Rehabilitation Systems

For effective rehabilitation, the impaired body part must be exercised repetitively and intensively with the help of a therapist. Such conventional therapy is highly protracted and labor-intensive; thus, several robotic rehabilitation systems have been designed and commercialized. Hand rehabilitation systems, including conventional methods, can be classified in terms of purpose and actuation, as shown in Fig. 1-4

Movement of the impaired body part is usually restricted by a splint to prevent tissue tearing or widening after surgery [9]. For stroke patients, splints are also used to reduce the muscle con-

tractions caused by spasticity, but a rigid splint may cause discomfort. A splint with a stiff body, developed by Saebo, allows the flexion posture to be assumed as tone increases, thus gradually repositioning fingers in the extended posture [10].

Physical therapy enhances blood flow and prevents postoperative edema. Also, to reduce muscle spasticity or atrophy, the stroke patient performs intensive and repetitive movements; this is termed continuous passive motion (CPM). The patient usually moves the impaired region with the help of a therapist and a stiff object [11]. However, as the effects of such rehabilitation methods are difficult to maintain over the long term, robotic CPM systems have been developed and commercialized. The Kinetic Maestro Portable Hand CPM and the Waveflex Hand CPM were developed by Thera Tech Equipment and Remington Medical, respectively; they are both wearable, portable, and very simple in design [12, 13]. The fingertips are moved along a defined trajectory; however, circular motion (1 DOF) imparted by an actuator cannot be used to impart 3-DOF fingertip movement. Furthermore, the joint angles are not considered. The HEXORR system generates MCP and PIP joint motions that facilitate functional recovery [14]. As the system guides fingers in which tone is increasing, it was necessary to construct it as a grounded system with large motors and torque sensors transmitting torque of over 1 Nm to each finger.

Conventional rehabilitation, during which the patient performs a task related to the ADL, is termed occupational therapy. The patient grasps objects varying in shape and stiffness, and performs hand and arm motions similar to those required in daily life. To assist and rehabilitate the hand motions of the ADL, various types of system are used. As patients exhibiting muscle spasticity find it difficult to stretch the fingers, simple devices that keep the fingers extended are useful, including springs and rubber bands [10, 15]. Although the systems are compact and light, and stiffness can be varied depending on muscle status, bidirectional assistance cannot be achieved using a passive component. Systems featuring actuators of the ADL have been developed to assist finger motions. The Hand of Hope (HOH) captures patient intention using a surface electromyography (sEMG) sensor on the lower arm, and aids finger motions via a linkage structure [16, 17]. Although the system assists each finger independently, it is relatively heavy (about 700 g) and the ROMs of the MCP and PIP joints are small compared to the full ROMs of the human finger. Sinfonia (developed by Gloreha) assists finger motion using pneumatic actuators [18]. A frictionless support, allowing arm motion and attached to a desk, reduces loading during rehabilitation exercises. Thus, the system is a desktop system. The Exo-Glove Poly, developed by SNU, includes cables that assist thumb, index, and middle finger motions [19]. Use of the cable system allowed for a dramatic reduction

in device size; sensors record finger motions and fingertip forces when various types of objects are grasped. Although the palm component is small, the large actuator box compromises portability.

Both CPM and ADL systems are used to assist intensive finger motions; CPM systems can be employed to facilitate ADL exercises and vice versa. However, the principal feature of a CPM device is that wide-joint ROM is prioritized. CPM devices employ simple and repetitive motions to maintain finger joint ROM, reduce hand spasticity, and enhance blood circulation in a wound. On the other hand, ADL systems typically focus on the holding and moving of objects, and thus control finger postures and fingertip forces when grasping objects of diverse shape and stiffness, while ensuring free arm motion.

Although the system and/or actuator module can be varied depending on patient condition when rehabilitation is underway, rehabilitation systems should exhibit high-level wearability and portability, and must measure finger movements and transmit forces. However, the HEXORR, Sinfonia, and HOH devices shown in Fig. 1-4 are grounded systems with low portability. Also, as the actuator module of the Exo-Glove is remote from the hand, the patient must carry a heavy box. Most commercial CPM devices, such as the Kinetic Maestra Portable Waveflex, control fingertip positions only over a 2D circular trajectory, different from the 3-DOF oval trajectory of a real fingertip. Also, the systems guide only the fingertips; they do not consider joint angles; abnormal angles are thus possible. Therefore, as with VR systems, rehabilitation systems must be wearable and portable, and must measure joint angles to ensure that appropriate forces are imparted.

1.3 Thesis Overview

Various hand exoskeletons featuring measurement of finger motion and delivery of force feedback have been developed for VR and rehabilitation applications. However, most of these systems are large and heavy, limiting wearability and portability. Thus, this thesis aims to develop hand exoskeletons that are highly wearable and portable, and that measure finger motion and deliver force feedback for VR and rehabilitation applications.

Previous studies evaluated finger motion measurement and force feedback via physical experiments. However, subjective features such as wearability and portability are also important, but many systems have not been evaluated in terms of user experience. This thesis thus reports on user experience and is organized as follows.

[Chapter 2: Wearable Hand Exoskeleton Systems for Virtual Reality]

A hand exoskeleton featuring a force-controllable actuator module is developed, which generates force feedback for the VR. The structure ensures 3 DOFs of F/E for each finger, mimicking the real-world situation. A series elastic actuator (SEA) is used to ensure that the system is compact and can operate in force mode. Force is controlled using a linearized motor running a friction compensation algorithm, combined with a disturbance observer (DOB); this represents a robust control algorithm. By combining the exoskeleton, actuator module, and control algorithm, a wearable hand exoskeleton featuring force mode control was developed.

In addition, to revise the weak points of the previous system, a wearable hand system featuring finger motion measurement and force feedback was developed for VR applications. The system measures the joint angles of the thumb, and the index and middle fingers; these play a major role in the manipulation of objects. The finger joint angles are calculated using a closed-loop kinematic model formed by the fingers and the structure under consideration. Accurate force feedback is delivered via motor current control featuring a DOB. The performance of a prototype was evaluated. The estimated finger motions were compared to those measured by a commercial motion capture system. Also, interactions with objects varying in stiffness, size, and shape were evaluated to verify that motion measurement and force feedback functioned well in combination. System performance was verified not only physically, but also from the viewpoint of subjective user experience. Test subjects evaluated the system in the laboratory while moving the fingers and receiving force feedback from virtual objects, and then completed questionnaires. This verified that the system interacted appropriately with the VR.

[Chapter 3: A Wearable Spring-guided Hand Exoskeleton for Continuous Passive Motion]

A portable rehabilitation exoskeleton featuring a spring facilitating finger F/E was developed. The simple wearable exoskeleton afforded 3-DOF finger motion. Using a general finger trajectory measured in a hand F/E experiment, and the joint ROMs of individual patients, the trajectory that the exoskeleton should realize was determined. An optimization algorithm was used to ensure that the desired trajectory was implemented. A spring was employed to generate forces guiding finger F/E. The moments imparted to the MCP and PIP joints by the spring were calculated using the finite element method (FEM). Prototype testing confirmed that the system assisted the fingers to perform the desired motions, and imparted appropriate MCP and PIP joint moments.

[Chapter 4: Conclusion]

This chapter contains concluding remarks and future issues to be addressed.

Chapter 2

Wearable Hand Exoskeleton Systems for Virtual Reality

2.1 A Force-controllable Hand Exoskeleton System

2.1.1 Introduction

Exoskeleton systems have been researched for rehabilitating and assisting the human's motion and force [14, 15, 17, 19, 39–43]. Although interaction with VR is a promising field among the application area of the exoskeleton systems, head-mounted display (HMD) or remote control handsets with vibration feedback were mainly researched [44–48]. However, they are not enough for vivid interaction with VR. Since the hand has a lot of sensory receptors, significant physical data are obtained and a human understands the mechanical properties of objects using the hand. Thus, developing hand force feedback systems with high wearability and portability is crucial to interact with VR vividly.

There are many studies to develop wearable hand systems. Previous systems using electric motors can be categorized into (1) cable-driven glove systems, (2) cable-driven frame systems, and (3) exoskeleton-type systems according to their structure as shown in Fig. 2-1. Exo-Glove is an assistive glove for a stroke patient developed by SNU [49]. The tendons embedded in the glove transmit the force from the small electric motor for helping the finger motions. As the device does not have any rigid part, it is light and easy to wear. However, it is difficult to apply the

The contents of this chapter was published in [32] and will be published in [33] and [34]. Preliminary research results of the paper were published in [35–38]. Reprinted with permission from IEEE and Elsevier.

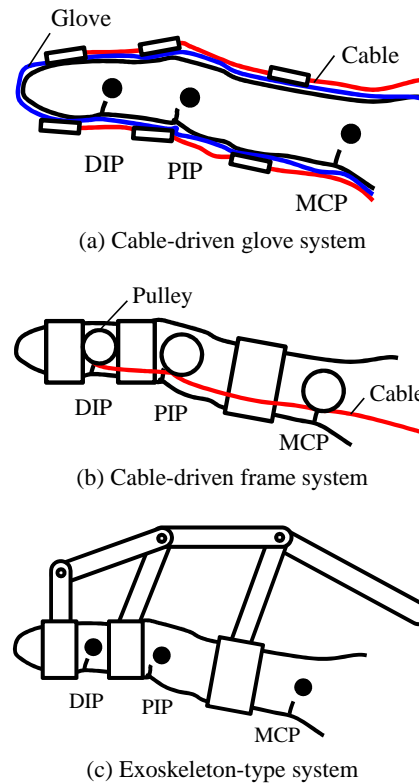


Figure 2-1: The system type according to the structure

accurate force at the specific part and control the cable tension precisely without sensors. The cable-driven frame systems, which have more rigid bodies than the cable-driven glove systems although the force is transmitted by the cable mechanism. The rigid bodies in the cable-driven frame systems are generally used for guiding the cable. To deliver the generated torque, cable pulleys in HANDEXOS were installed at either side of the joint [50]. Thus, it is difficult to put the fingers together, resulting in uncomfortable finger motion. To change the magnitude and direction of the force feedback, the system structure developed by PERCRO laboratory uses three electric motors for one finger [51]. Therefore, the cable-driven mechanism is very large and heavy. CyberGrasp is a commercialized cable-driven frame system developed by CyberGlove Systems [5]. To minimize the interference problem, the cable structure was put on the back side of the fingers, thus the system size is quite large. Additionally, the motors located at the outside of the hand degraded the mobility of the system. As the exoskeleton type system, a variety of systems were developed. HEXOSYS II developed by IIT has a linkage structure and an actuator for each finger [52]. In this system, although the simple structure guarantees the workspace of the fingertip, the various force control was not verified by only focusing on the light system.

The exoskeleton-type system may have the most largest structure among three types of systems. However, since the exoskeleton-type is good for delivering the force due to the rigid bodies, the exoskeleton-type structure was chosen. Additionally, to generate the force feedback from VR, a compact actuator module for force mode control should be studied. Therefore, a hand exoskeleton system consisting of an wearable exoskeleton structure to guarantee natural finger motions and compact actuator modules for force mode control is developed.

In this section, a compact exoskeleton system with force-controllable actuator modules for the hand is proposed by focusing on force generation for force feedback from VR. Inspired by the finger anatomy focusing on the extensor muscles, an exoskeleton structure was designed to guarantee 3 DOF and large ROM. In the actuator module, a series elastic actuator (SEA) mechanism was used to reduce the system size and generate force feedback. In SEA mechanism, the force is precisely generated by controlling the spring deflection. Furthermore, the generated force is calculated using the spring constant and deflected length like a force sensor. A proportional-derivative (PD) controller with disturbance observer (DOB) was applied to satisfy the accurate control of the motor even with the uncertainty due to the finger motions. Therefore, a wearable hand exoskeleton system with force-controllable actuator modules was developed by combining the linkage structure, actuator module, and control algorithm.

2.1.2 Structure Design

2.1.2.1 Design of the Structure

The finger anatomy is very complex because of a lot of bones, tendons, and ligament. Figure 2-2 shows the bones and tendons of the finger [20]. Blue circles are the rotational joints in F/E direction and green colored arrows are the activated muscle during extending the finger. The activation of the muscle when extending the finger, especially extensor digitorum communis (EDC), was mainly focused, since the system transmits the repulsive force from the virtual object. EDC is attached to proximal, middle, and distal phalanges around the joint, thus, it help extending three joints in F/E direction. Dorsal hood which consists of lumbrical and interosseus assists the extension of the PIP and DIP joints while preventing hyperextension of the MCP joint. Additionally, flexor carpi radialis (FCR) is related to the flexion of all three joints in F/E motions. Therefore, the upwards links (red arrows) were designed considering the attached positions (red circles) of the tendon of EDC and then, the linkage structure was design to guarantee the F/E motion of each joint. Although A/A

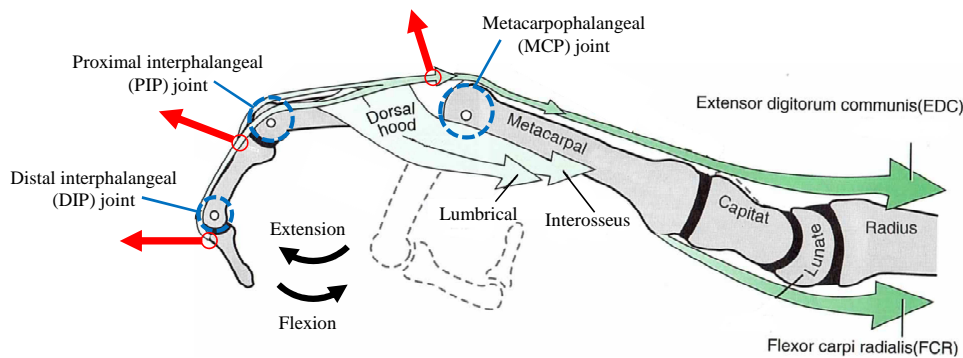


Figure 2-2: Anatomy of the finger (edited from [20])

motion of the finger is also important, F/E motions was only considered to reduce the system size. Since the finger mostly interact with an object using the bottom side, the wearing part was located at the bottom of the fingertip.

To guarantee F/E motion of the finger, various linkage structures were investigated. Figure 2-3 shows design candidates of the linkage structure. The connecting parts (grey parts) were put on each phalanges and dorsum of hand, and the linkage structure was designed at the upper side of the finger to eliminate collision problem between adjacent fingers. The green links are connected grey parts at the similar position to the extensor and the blue links are connecting links between green links and the actuator. The actuators were located at the dorsum of hand for high mobility.

Figure 2-3 (a) shows the first design candidate. The blue links directly connect the motor and green links. Thus, it is the simplest design, however, it has only 2 DOF and cannot be used for the structure for finger motions. The two links were added in design candidate 1 to increase DOF of the structure as shown in Fig. 2-3 (b). Although the structure guarantees the free finger motions, it makes the system size large for large ROM of the finger joints as shown in Fig. 2-4 (a). Therefore, the design candidate 3 was proposed by adding more links and joints as shown in Fig. 2-3 (c). If design candidate 2 and 3 have same ROM of the finger, the system height of the design 2 is 7 mm larger than the that of the design 3 in extension posture as shown in Fig. 2-4. As a result, the design candidate 3 was chosen as the linkage structure, thus Figure. 2-5 describes the exoskeleton structure design for one finger.

2.1.2.2 Kinematic Analysis of the Structure

A person want comfortable movement with the exoskeleton structure, but, several postures are not possible due to the interference between links. Therefore, workspace of the structure was analyzed

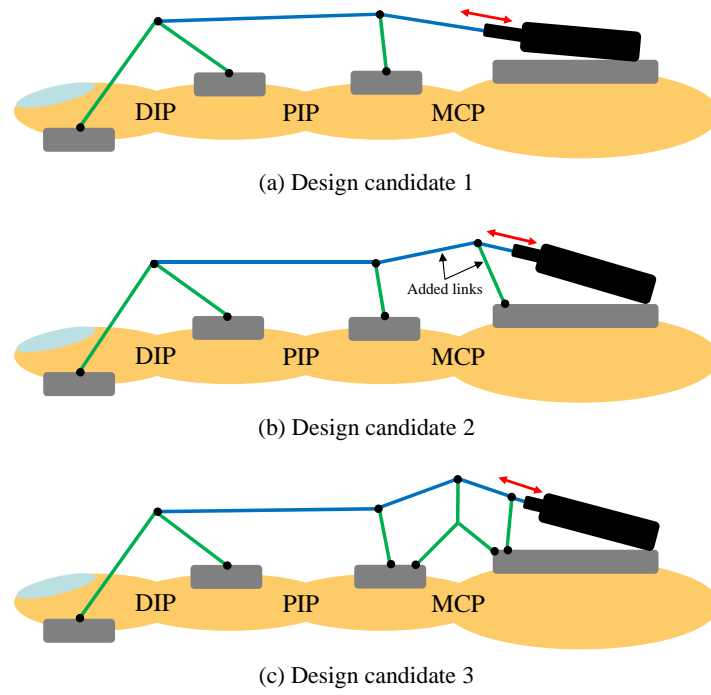


Figure 2-3: Design candidates of the finger structure

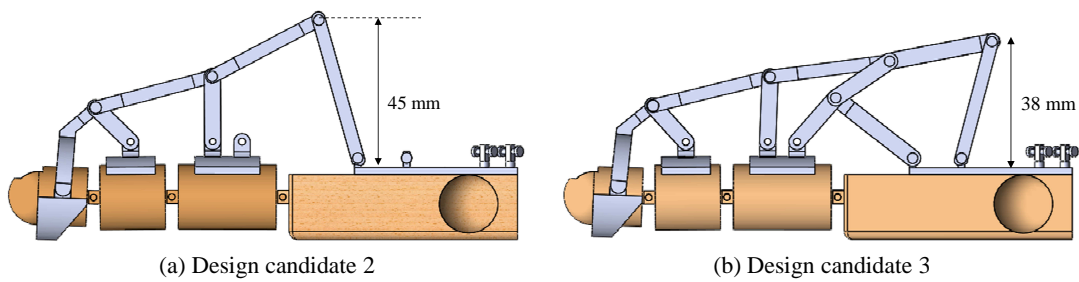


Figure 2-4: Comparison between design candidates

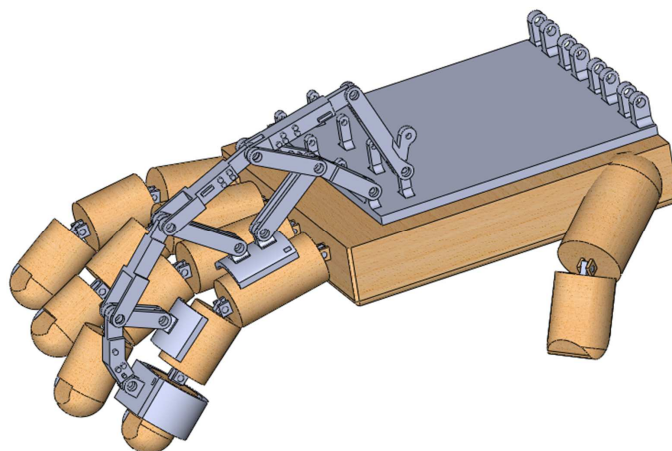


Figure 2-5: The proposed design of the linkage structure

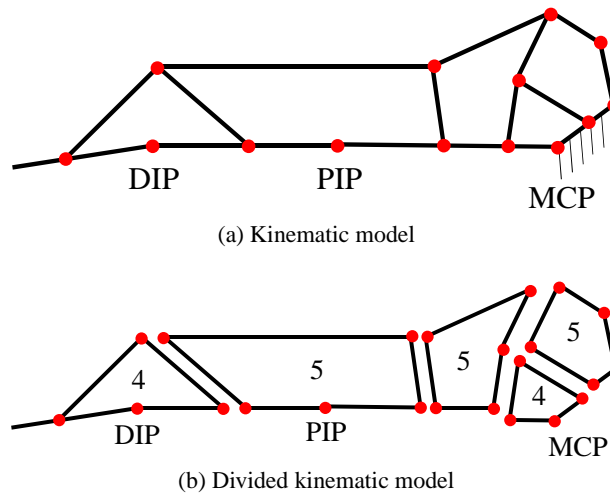


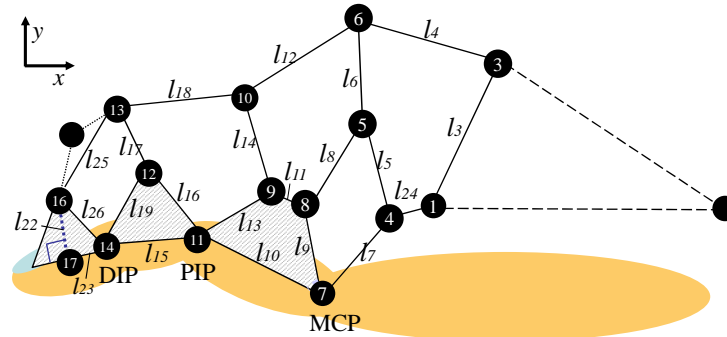
Figure 2-6: The linkage structure

using kinematic model consisting of three five-bar and two four-bar linkages as shown in Fig. 2-6. The linkage type was describe in the numbers inside of the loop in Fig. 2-6 (b).

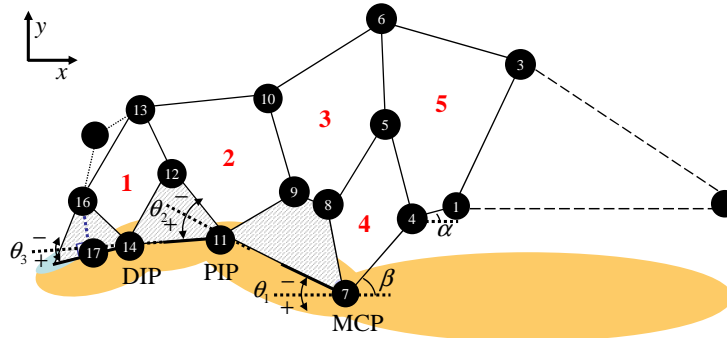
With the structure with 3 DOF, the position of each joint is determined sequentially according to the angles of the MCP, PIP, and DIP joint. To analyze the structure kinematically, the angle and length variable of the structure are shown in Fig. 2-7 (a) and (b), respectively. The x -axis was parallel with the palm and the point 4 located at the dorsum of the hand was set as the origin to investigate the all joint positions. The MCP, PIP, and DIP joint positions were described as point 7, 11, and 14, respectively, and the fingertip position is described as point 17. The exoskeleton device is always worn on the user's hand using same method, thus, the angle α and β were defined as constant values. The θ_1 , θ_2 and θ_3 are the angles of the MCP, PIP and DIP joints controlled by the human, respectively.

Unlike normal ROM, the finger joint angles required to conduct daily tasks like key grip and pinch motion is described as the functional ROM [53]. Since the proposed system was developed for performing the tasks and interacting with objects in VR, the ROM performed by the exoskeleton structure were compared to functional ROM. The parameters for kinematic analysis were summarized in Table 2.1.

Since the several parameters and positions were predetermined and calculated using only joint angles of the finger, the fingertip position is obtained by following equations:



(a) Length parameters



(b) Angle parameters

Figure 2-7: Parameters for kinematic analysis

Table 2.1: Parameters of kinematic analysis

Predefined	angles (°)	α, β
Link	lengths (mm)	l
Position	Origin	pt 4
	MCP joint	pt 7
	PIP joint	pt 11
	DIP joint	pt 14
	fingertip	pt 17
Range of joint angles	MCP (°)	0 ~ 73
	PIP (°)	0 ~ 86
	DIP (°)	0 ~ 57

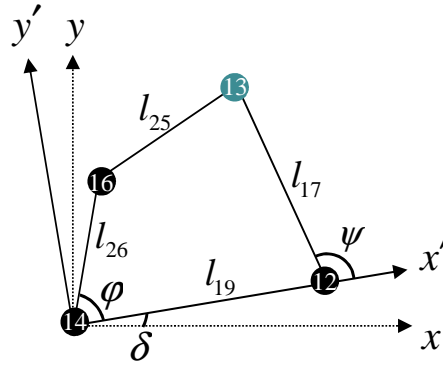


Figure 2-8: Linkage 1

$$\begin{aligned} \vec{P}_{17} &= \vec{l}_7 + \vec{l}_{10} + \vec{l}_{15} + \vec{l}_{23} \\ &= l_7 T(-\beta) + l_{10} T(-\theta_1) + l_{15} T(-\theta_1 - \theta_2) + l_{23} T(-\theta_1 - \theta_2 - \theta_3) \end{aligned} \quad (2.1)$$

where $T(\theta) = [\cos(\theta) \ \sin(\theta); -\sin(\theta) \ \cos(\theta)]$. Thus, the positions of point 8, 9, 12 and 16 are calculated by the equations.

6

The order of the structure was presented as a number in red color to describe the structure clearly as shown in Fig. 2-7 (b). Figure. 2-8 represents the schematic of linkage 1. The joint positions of the linkage 1 except point 13 were determined by previous equations and the position of the point 13 is calculated by the equations for the four-bar linkage analysis. The x' - y' plane is tilted with the angle δ , calculated from the positions of point 12 and 14, from the x - y plane. Additionally, φ is an included angle between links consisting of point 12, 14 and 16 and calculated as following:

$$\varphi = \arccos\left(\frac{l_{26}^2 + l_{19}^2 - \|\vec{P}_{16} - \vec{P}_{12}\|^2}{2l_{26}l_{19}}\right) \quad (2.2)$$

Furthermore, the joint position of point 13 is calculated using the angle φ as follows [54]:

$$(\vec{P}_{16} - \vec{P}_{13}) \cdot (\vec{P}_{16} - \vec{P}_{13}) - l_{25}^2 = 0 \quad (2.3)$$

where $\vec{P}_{16} = l_{26} T(\varphi)$ and $\vec{P}_{13} = l_{19} [1 \ 0]^T + l_{17} T(\psi)$ in the x' - y' plane. It is rewritten as follows:

$$\mathbf{A}(\varphi) \cos \psi - \mathbf{B}(\varphi) \sin \psi + \mathbf{C}(\varphi) = 0 \quad (2.4)$$

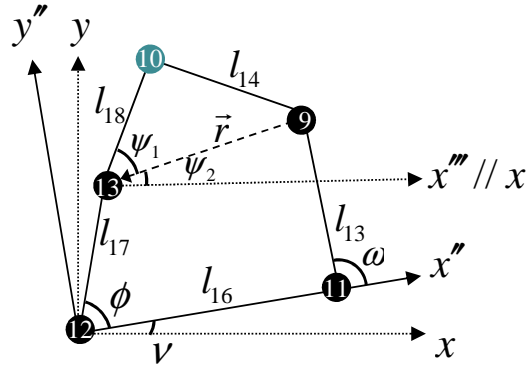


Figure 2-9: Linkage 2

where

$$\mathbf{A}(\varphi) = 2l_{17}l_{19} - 2l_{17}l_{26} \cos \varphi \quad (2.5)$$

$$\mathbf{B}(\varphi) = 2l_{17}l_{26} \sin \varphi \quad (2.6)$$

$$\mathbf{C}(\varphi) = l_{26}^2 + l_{17}^2 + l_{19}^2 - l_{25}^2 - 2l_{26}l_{19} \cos \varphi \quad (2.7)$$

Then, the output angle, ψ , is determined by the input angle, φ by following equation:

$$\psi = \arctan\left(\frac{\mathbf{B}(\varphi)}{\mathbf{A}(\varphi)}\right) \pm \arccos\left(-\frac{\mathbf{C}(\varphi)}{\sqrt{\mathbf{A}(\varphi)^2 + \mathbf{B}(\varphi)^2}}\right) \quad (2.8)$$

Therefore, the position of point 13 can be expressed as follows:

$$\vec{P}_{13} = \vec{P}_{12} + l_{17}T(\delta + \psi) \quad (2.9)$$

Consequently, all joint positions of linkage 1 were calculated by the analysis of the four-bar linkage. Since the linkage 4 is also a four-bar linkage, the positions of the linkage 4 can be determined by above equations. The five-bar linkage with 2 DOF requires two input angles to determine all joint positions. As shown in Fig. 2-9, the position of point 10 is determined by the linkage 2 with two input angles ϕ and ω . The x'' - y'' plane is also rotated with the angle ν , defined by the positions of the point 11 and 12, from the x - y plane. The input angles ϕ and ω are calculated by the cosine law with similar method to the method in linkage 1. Therefore, the position of point 10 can be expressed as follows [55]:

$$\vec{P}_{10} = \vec{P}_{13} + l_{18}T(\psi_1 + \psi_2) \quad (2.10)$$

The vector \mathbf{r} connecting point 9 to point 13 is investigated for obtaining ψ_1 and ψ_2 :

$$\mathbf{r} = \vec{P_9} - \vec{P_{13}} = \vec{l_{16}} + \vec{l_{13}} - \vec{l_{17}} = l_{16}T(\nu) + l_{13}T(\nu + \omega) - l_{17}T(\nu + \phi) \quad (2.11)$$

By using the vector \mathbf{r} , ψ_1 and ψ_2 are calculated as follows:

$$\psi_1 = \arccos\left(\frac{l_{18}^2 + \|\mathbf{r}\|^2 - l_{14}^2}{2l_{18}\|\mathbf{r}\|}\right) \quad (2.12)$$

$$\psi_2 = \arccos\left(\frac{\mathbf{r} \cdot [1 \ 0]^T}{\|\mathbf{r}\|}\right) \quad (2.13)$$

Thus, all joint positions in linkage 2 are obtained consequently and the linkage 3 and 5 that are also investigated using the similar method. Therefore, all joint positions were obtained using the kinematic analysis of the four- and five-bar linkage.

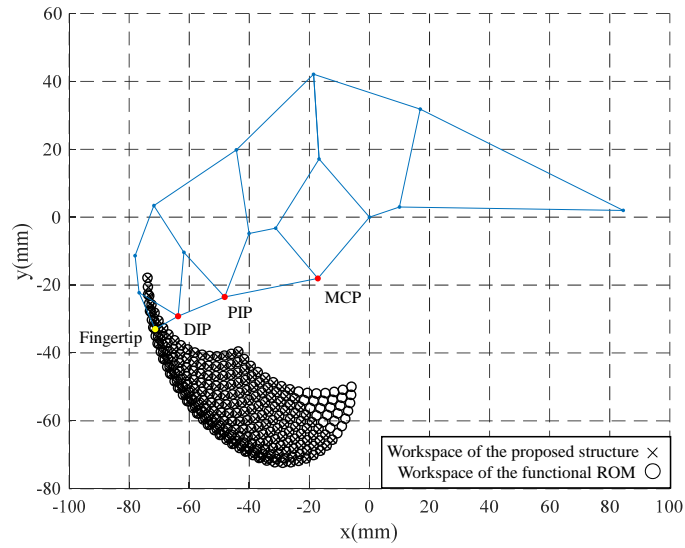
The workspace of the proposed system which means the possible positions of the fingertip with the exoskeleton without any restriction was compared to that of the functional ROM shown in Table. 2.1. The fingertip workspace of the proposed structure and functional ROM were shown in Fig 2-10. As shown in Fig. 2-10 (a), the workspace of the proposed system satisfy 90 % of the that of the functional ROM and the very flexed postures were not realized by the structure interference.

The workspace of the linkage structure can be increased by increasing structure lengths and system size as shown in Fig. 2-10 (b). Even though the larger linkage structure satisfy about 95 % of the functional ROM, the height of the structure should be increased about 20 mm as shown in Fig. 2-10 (c) and (d). Therefore, considering the system size and the fingertip workspace, the system structure design was appositely optimized. With the final structure design, the MCP, PIP, and DIP joint of the finger can move to 93 deg, 89 deg, and 85 deg, which are 93 %, 85 %, and 100 % of the normal ROM, respectively.

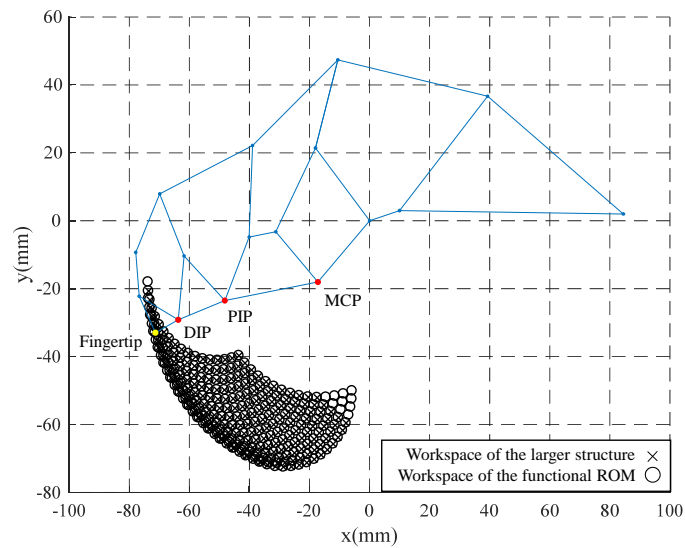
2.1.3 Actuator Module Design

2.1.3.1 Series Elastic Actuator (SEA) Mechanism

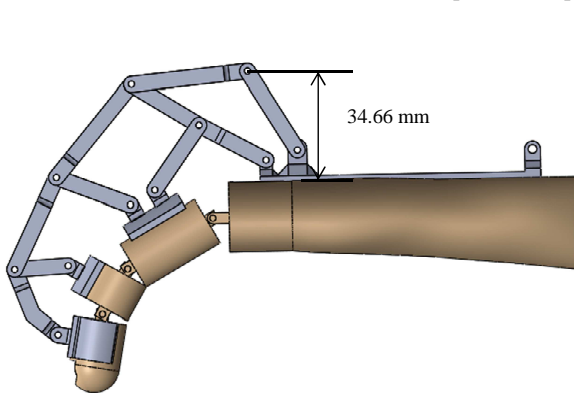
To realize the vivid interaction with VR, the force should be measured for accurate force control. However, since a typical force sensor is quite large and heavy, it is not suitable for the wearable hand systems. Therefore, a series elastic actuator (SEA) mechanism was used to satisfy the force mode control and compact actuator design.



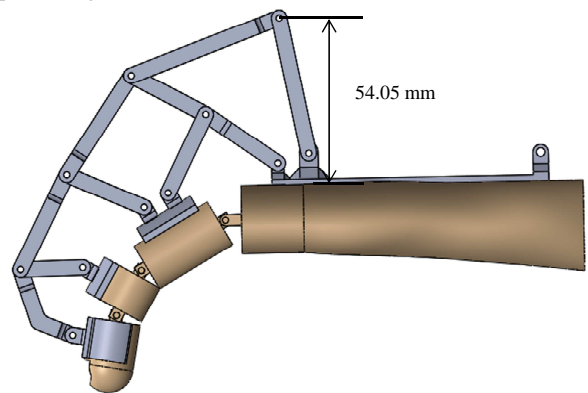
(a) Workspace of the proposed structure



(b) Workspace of the proposed larger structure



(c) Proposed linkage structure



(d) Larger linkage structure

Figure 2-10: Comparison of the proposed and larger linkage structure

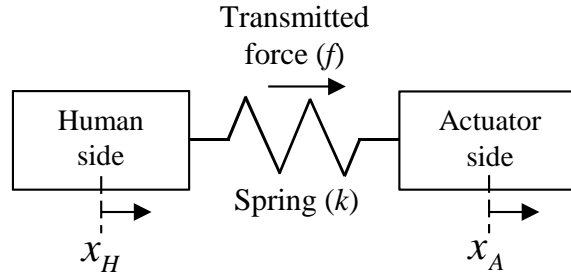


Figure 2-11: Series elastic actuator (SEA) mechanism

In physical human-robot interaction systems, the SEA mechanism has been actively applied for force mode control [56–61]. The force is generated via an elastic element installed between an actuator and human side. The basic schematic of SEA mechanism is shown in Fig. 2-11. By adjusting the spring deflection, the generated force, f , is precisely controlled:

$$f = k(x_A - x_H) \quad (2.14)$$

where k is the spring constant, and x_A and x_H are the positions of the actuator and human side, respectively. The desired actuator position, x_{Ad} , is calculated using the measured human joint position and the given desired force, f_d , as follows:

$$x_{Ad} = \frac{f_d}{k} + x_H \quad (2.15)$$

By controlling the desired motor position, the desired force is generated precisely.

The actuator module with SEA was designed as shown in Fig. 2-12. The positions of the linkage structure and actuators are measured by a potentiometer for the human side and an embedded potentiometer in an actuator, respectively. Since the generated force is calculated by the deflected length of the spring, a force sensor is not required in this hand exoskeleton system. Therefore, the actuator module becomes more compact due to SEA mechanism. Moreover,, the maximum force and the force resolution could be adjusted easily by replacing the elastic element with various stiffness.

To investigate the required force for force feedback, the contact forces in grasping objects were measured experimentally. The subject wore a glove with pressure sensors (Tekscan grip system [62]) attached to the palm side and grasped a cylinder (diameter: 6.4 cm) for 5 s smoothly just before lifting the sphere by only using the fingertips. The researcher measured the contact force at the fingertips during grasp. The subject relaxed the hand some minutes after the trial and repeated

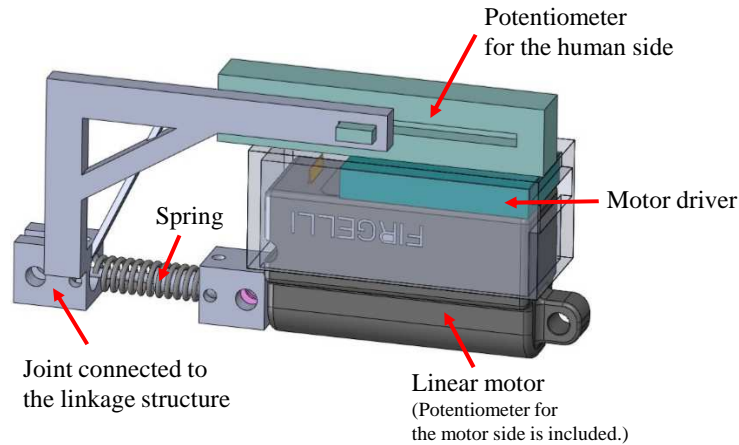


Figure 2-12: Actuator module design

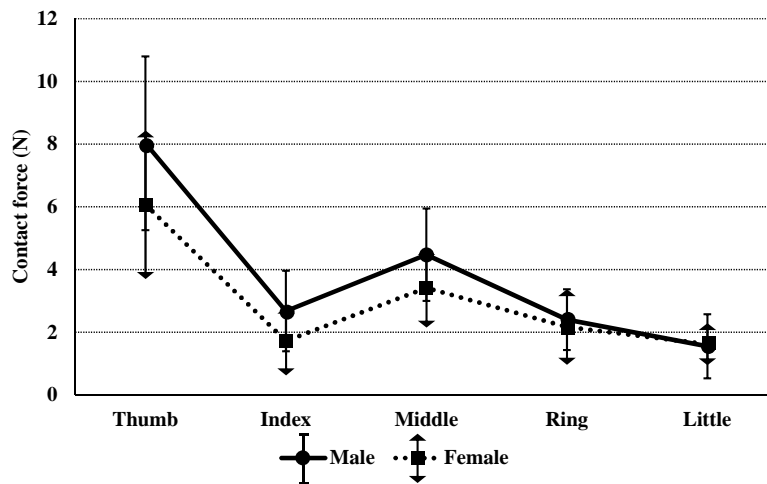


Figure 2-13: Maximum contact force

the grasp 5 times. Seven healthy persons without any known motor diseases (four males, three females, age: 24 ± 4.3) were participated in this experiment. After the experiment, the average of maximum forces was calculated for each person.

Fig. 2-13 shows the experimental results. The solid and dotted lines present the average values for the males and females, respectively. As the experimental results, the contact force at the thumb was the largest for all subjects, about 8 N for males and about 6 N for females. Therefore, the target force for the actuator module was set 8 N. Additionally, about 20 mm linear motions was enough to achieve the fingertip workspace in the simulation in Fig. 2-10 (a). As a result, a linear motor with 9 N maximum force and with a 20 mm stroke (Firgelli PQ12 [63]) was chosen as the electric motors for actuator module.

A spring, as a elastic element, plays an important role in the actuator module for force mode

Table 2.2: Parameters of the spring design

Modulus of rigidity	G (kgf/mm ²)	7500
Diameter of a spring wire	d (mm)	0.6
Mean diameter of a spring	D (mm)	6.5
Number of turns	n	10
Spring constant	k (N/mm)	0.434

control. The average of the force resolution at the MCP and PIP joints is about 0.3 N [64]. If the motor is controlled with less than 1 mm position error, a spring with 0.3~0.5 N/mm is enough considering the force resolution of the finger joint. The design parameters for the spring were determined as in Table 2.2 with regard to the required spring constant and the size of the actuator module. Therefore, the spring constant was calculated as following equation [65]:

$$k = \frac{Gd^4}{8D^3n} \quad (2.16)$$

where G is the modulus of rigidity, d is the diameter of a spring wire, D is the mean diameter of a spring, and n is the number of active coils.

Figure 2-14 (a) and (b) show the manufactured actuator module and manually designed compact motor driver. Since the size of the motor driver is $27 \times 14 \times 4$ mm, it is very compact and suitable for putting on the top side of the motor and hiding the electronic board by a cover. The potentiometer to measure the position for the human side was attached to the top side of the actuator module due to the limited space available. Using the 3D technology, the actuator module except the motor and sensors was manufactured. Its size was about $18 \times 77 \times 36$ mm, and its weight was 30 g.

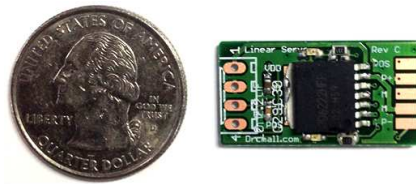
2.1.3.2 Actuator Module Control

The electric motor used for the actuator module includes a gear box for adjusting the range of velocity and force. Although the gear reducer is installed to amplify the output torque, it generates the motor friction which makes the system nonlinear. Therefore, the motor friction is reduced though friction compensation algorithm to improve the control performance.

To apply the friction compensation algorithm for elimination of the actuator friction, the friction model was experimentally investigated. Figure 2-15 presents the required control input of the motor at a variety of velocities. Although a signum function is typically used for the friction model, the sudden increase of the control input at zero velocity makes undesired vibration of the motor. Therefore, the control input calculated by the friction compensation algorithm was determined to



(a) Manufactured actuator module



(b) Manually designed motor driver

Figure 2-14: The actuator module

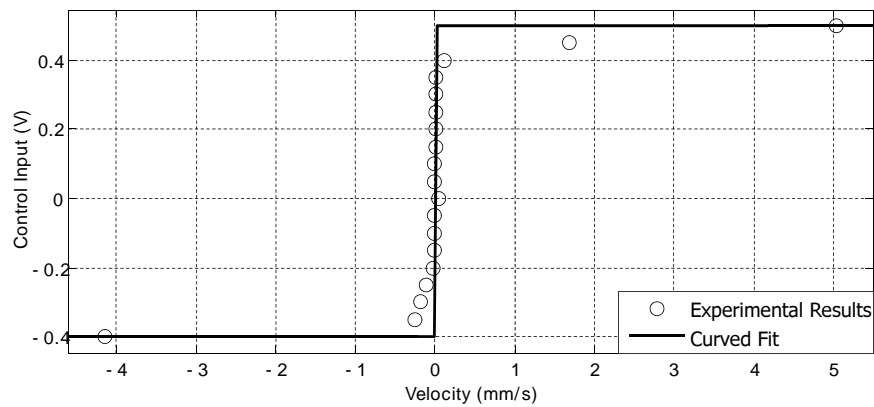


Figure 2-15: Friction identification

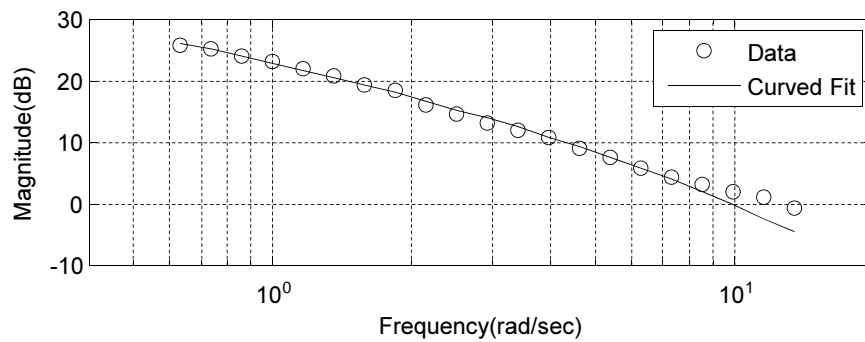


Figure 2-16: Frequency response of the linearized motor

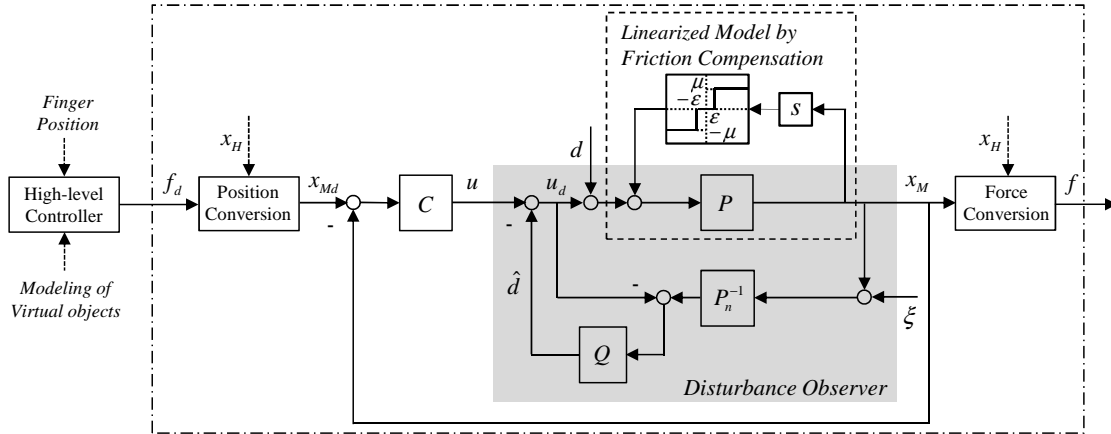


Figure 2-17: Overall control structure (P : plant, P_n : the nominal model of P , Q : Q filter in the DOB, C : controller, f_d/f : desired/measured force, x_{Md}/x_M : desired/measured motor position, x_H : finger position, d/\hat{d} : external/estimated disturbance, u : control input, u_d : control input in the DOB, ξ : noise)

be zero if the motor is in the stationary state. Thus, the friction compensation input, V_{fric} , was generated as follows:

$$V_{fric} = a + b \cdot \text{sgn}^*(v_A) \quad (2.17)$$

where v_A is the actuator velocity. Also, the function $\text{sgn}^*(v_A)$ was defined as following.

$$\text{sgn}^*(v_A) = \begin{cases} -1, & v_A < -\epsilon \\ -a/b, & -\epsilon \leq v_A < \epsilon \\ 1, & v_A \geq \epsilon \end{cases} \quad (2.18)$$

The velocity range of the actuator (ϵ in 2.18) for eliminating the vibration was set considering the measurement noise of the velocity. Coefficients a and b in (2.17) mean bias and Coulomb friction, respectively. The parameters were determined through curve fitting the experimental data as $a = 0.05$, $b = 0.45$. Also the range ϵ was set to 0.3 considering the measurement noise. The frequency response of the motor with the friction compensation algorithm is shown in Fig. 2-16. Since the actuator position should be controlled in SEA mechanism, the linearized actuator model was obtained as following:

$$P(s) = \frac{124.7}{s^2 + 8.527s + 3.708} \quad (2.19)$$

In SEA mechanism, the position of the actuator should be precisely controlled. A PD controller

was used for the position control and its gain was optimized by a linear quadratic (LQ) method. The cost function of the LQ method was expressed as following.

$$J = \int_0^{\infty} \{e^T(t)Qe(t) + u^T(t)Ru(t)\}dt \quad (2.20)$$

where e and u are the tracking error and control input, respectively, Q and R are weighting factors for system state and control input. Since the weighting factor for system state Q is a 2×2 matrix, (1,1) and (2,2) elements are values for position and velocity error, respectively. Additionally, as the motor position should be controlled precisely, the weighting factor for the position has larger value than that for the velocity. The weighting factor for the control input R was obtained experimentally to control the motor position successfully while preventing saturation of the control input. The matrix Q and value R were experimentally determined, and Q and R were selected as $[1 \ 0; 0 \ 0.0001]^T$ and 0.2, respectively.

The system with the optimized PD controller and the plant linearized by the friction compensation may precisely control the motor position. However, uncertainties, especially introduced by the interaction between the linkage and the human, degraded the control performance of motor. Therefore, disturbance observer (DOB), which is mostly used among the robust control algorithms, was used to enhance the system robustness. In DOB algorithm, the disturbance from the system is estimated and compensated. The Q filter in DOB is used to filter the disturbance from the calculated control input. Thus, by considering the actuator and human finger speed, it was designed as a low-pass filter with cut-off frequency of 3 Hz.

Fig. 2-17 shows the overall control algorithm for actuator modules. The high-level controller was not considered in this research to focus on development of the hand exoskeleton system. When the position of the human side and the desired force, f_d , are determined, the desired motor position, x_{Md} is calculated by (2.15) ('Position Conversion' box in Fig. 2-17). The PD controller ('C' in Fig. 2-17) is applied to control the motor position. The geared motor, 'P' in Fig. 2-17), is linearized through the friction compensation algorithm, and DOB, as the robust control algorithm, minimize the uncertainties from interaction with the human. The precisely controlled motor position, x_M , is converted to the force feedback, f , by the spring deflection(2.14) ('Force Conversion' box in Fig. 2-17).

To investigate the performance of the force mode control, an experiment for generation of the desired force was tested with sinusoidal and arbitrary motions of the human side. The desired force

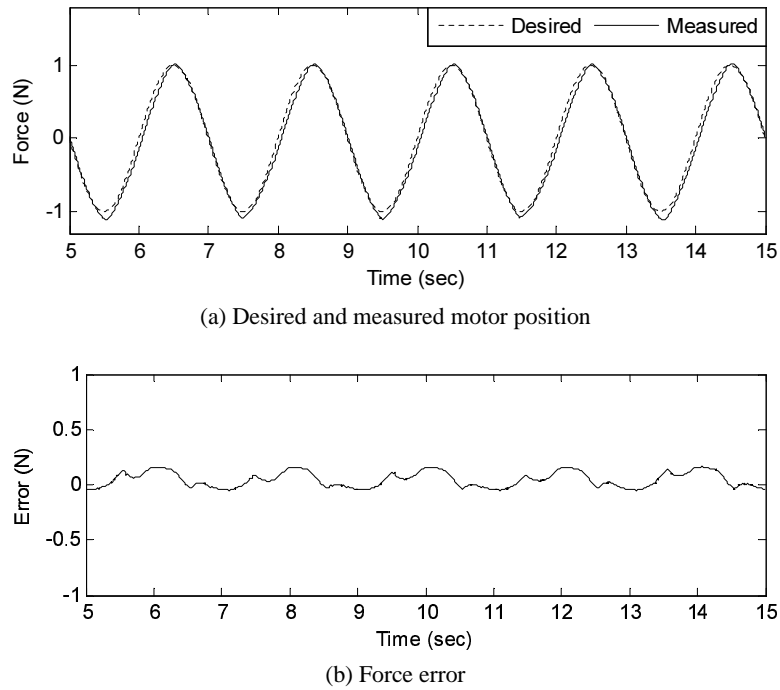
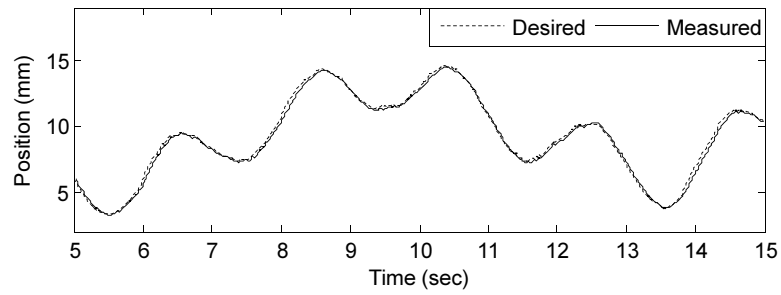


Figure 2-18: Force control performance with stationary motion

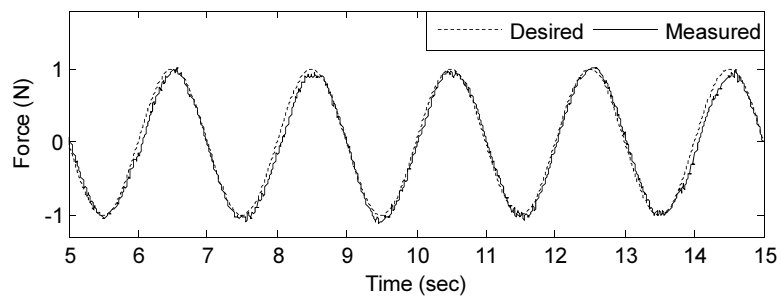
was defined as a sinusoidal signal, and also, the motion at the human side, x_H in (2.14) and (2.15), maintain stationary. As shown in Fig. 2-19 (a), the sinusoidal force is generated successfully and the maximum force error is below 0.3 N. In addition, the end-effector position is changed to the arbitrary finger motion in the Fig. 2-19. Fig. 2-19 (a) shows the performance of the position control of the motor. In SEA mechanism, the motor is position-controlled in real-time by (2.15) although the actuator module generates the force. As shown in the figure, the motor tracked the desired position well. Therefore, the desired force was accurately produced despite of arbitrary motion at the end-effector, as shown in Fig. 2-19 (b) and (c). The maximum force error was about 0.27 N and the root-mean-squared error (RMSE) of force was 0.09 N, which was smaller than the force resolution of the finger joints [64].

2.1.4 Implementation of the Hand Exoskeleton

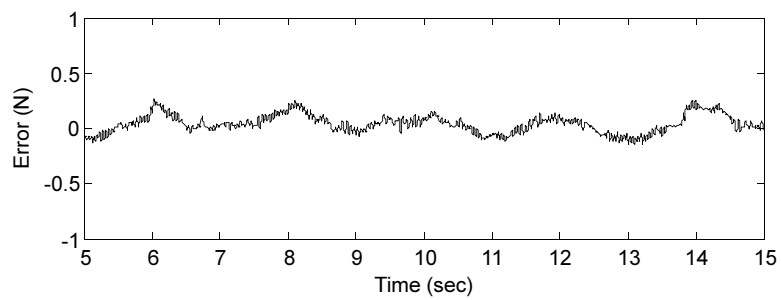
Fig. 2-20 (a) and (b) shows the 3D design and prototype of the integrated hand exoskeleton system with the proposed structure and actuator modules, respectively. Also, its size is $88 \times 230 \times 83$ mm and weight is 298 g. The overall rigid structures were attached to a glove for high wearability. The force feedback was generated by actuator modules which were put on the dorsum of hand for free hand and arm motions. Even though the system has five actuator modules are on the hand, its size



(a) Desired and measured motor position

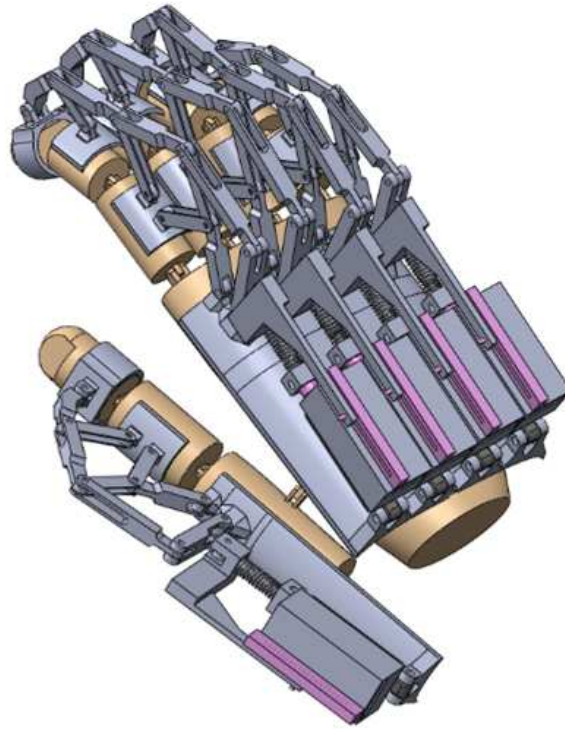


(b) Desired and measured force

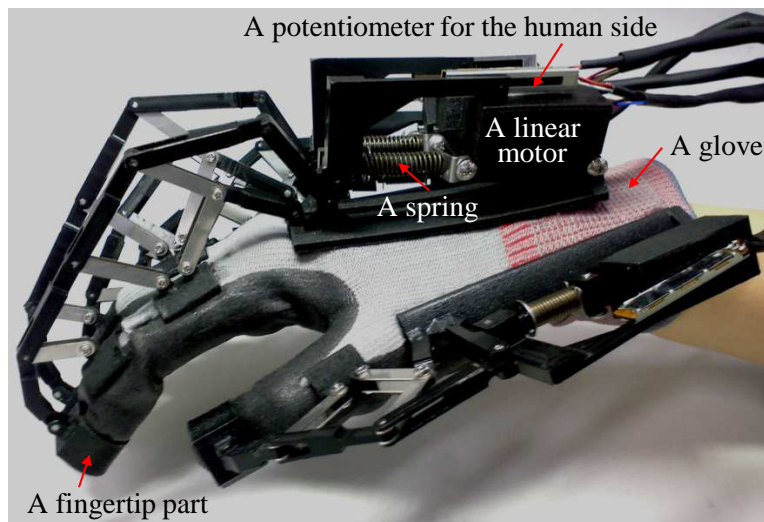


(c) Force error

Figure 2-19: Force control performance with arbitrary motion



(a) Design of the hand exoskeleton



(b) Prototype of the hand exoskeleton

Figure 2-20: The proposed hand exoskeleton system

and weight are small and the user can move the arm comfortably. Since all structure and actuators were placed on dorsum of the hand, the proposed system has high wearability and portability.

2.1.4.1 Analysis of Force Distribution

Since the force generated by the motor is distributed through the linkage structure, force distribution through the structure is analyzed to evaluate the exoskeleton system.

As the speed of the finger motion is slow when the force feedback is applied, the structure was assumed in a quasi-static situation. The schematic of linkage structure for force distribution was shown in Fig. 2-21. The circles with numbers in Fig. 2-21 (a) present the joints in the structure and the red arrows are the transmitted forces to each joint. When the posture of the structure was determined by the joint angles of the finger, the force vectors at each joint were calculated by the equations of force equilibrium.

F and F_{tip} in the figure show the force feedback by the actuator module and applied force in normal direction to the fingertip, respectively. Since people generally feel reactive forces in normal direction when grasping an object, the normal force at the fingertip was mainly focused. The finger phalanges and palm contact to the exoskeleton through the grey-colored parts (4, 9, 12, 16 in Fig. 2-21 (a)). Therefore, force equilibrium equations were investigated and the equations for one loop shown in Fig. 2-21 (b) can be expressed as follows:

$$F_{9x} + F_{9y} - F_{10a} - F_{5a} = 0 \quad (2.21)$$

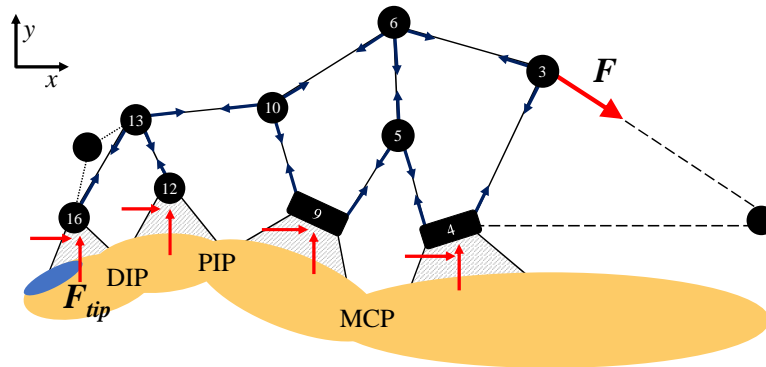
$$F_{10a} + F_{10b} - F_{6b} = 0 \quad (2.22)$$

$$F_{6a} + F_{6b} - F_{3a} = 0 \quad (2.23)$$

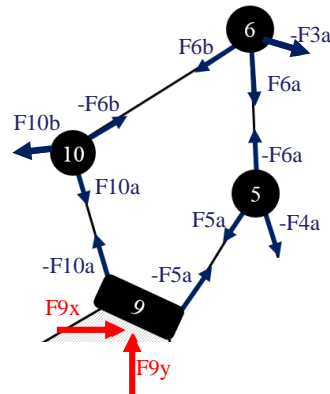
$$F_{5a} - F_{4a} - F_{6a} = 0 \quad (2.24)$$

The equations can be calculated by linear algebra after investigating all equations of the rotational joints and expressing the equations as the matrix and vector. Therefore, the normal force at the fingertip F_{tip} was calculated by the force distribution analysis. The joint ROM used in kinematic analysis was same with the ROM from Table. 2.1. Since the DIP joint angle depends on the PIP joint, it was set as 2/3 of the PIP joint angle [66]. Also, the generated force by the motor (F in Fig. 2-21 (a)) was assumed as 3 N in the force distribution analysis.

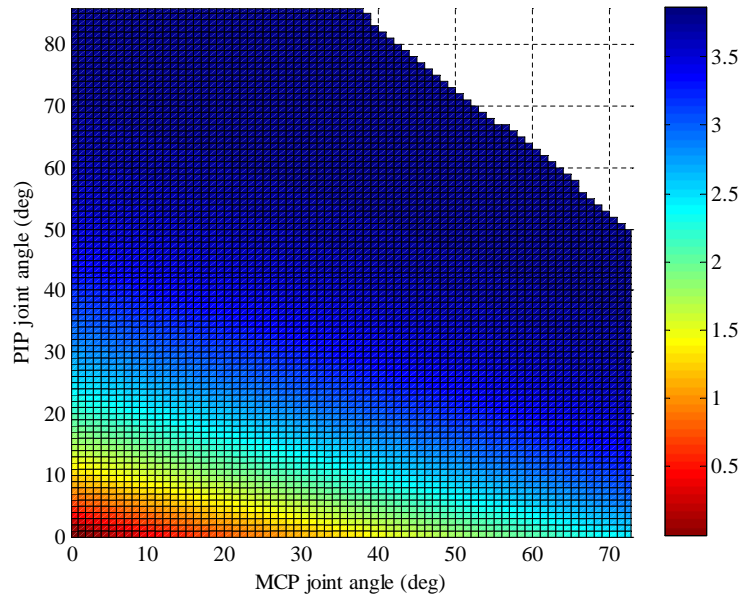
Figure 2-21 (c) shows the applied force in normal direction at the fingertip calculated by the



(a) The whole structure



(b) One loop



(c) Force feedback to the fingertip

Figure 2-21: Force distribution analysis

force analysis. Since the DIP joint angle is varied with the change of the PIP joint angle, the DIP joint angle was not expressed. The only colored area shows the delivered force to the fingertip in the workspace of the proposed structure. The applied force to the fingertip, F_{tip} , is highly dependent on the joint angles of the finger; as the joint angles increase, the fingertip force is also decreased. As the finger flexed, the angle between the actuator module and the normal direction of the fingertip is increased, and the normal force of the fingertip is decreased. Without the PIP joint motion, the force at the fingertip is decreased from maximum 3.5 N to 1.5 N according the MCP joint angle. Also, without the MCP joint motion, the force is also decreased according to the change of the PIP joint angle. Since the normal direction of the fingertip is more dramatically changed due to both PIP and DIP joint motion, the decrease of the force by the change of the PIP joint angle is larger than that by the change of the MCP joint angle.

2.1.4.2 Force Transmission Experiment

The performance to transmit the force feedback to the fingertip was also tested using the prototype of the exoskeleton system. A wearing part of the fingertip was revised to attach a load cell (CLS-20NA, TML [67]) at the bottom part as shown in Fig. 2-22 (a). The normal force applied to the fingertip was measured when the force feedback is generated by the actuator module. Figure 2-22 (b) shows the setup of the force transmission experiment: a subject wearing the system made three finger postures ((DIP, PIP, MCP): (0, 0, 30), (0, 0, 45), (10, 15, 30) deg) 10 times, and 3 N force was generated by the actuator module.

Figure 2-23 shows the experimental results; the solid dots and dashed lines represent average and standard deviation, respectively. Similar to the results of the kinematic analysis in previous section, the delivered force is reduced as the finger flexed. The amount of the transmitted forces were smaller than those of simulation, which may be caused by the imperfect hardware manufacturing such as joint friction. As expressed in results of the kinematic analysis and the experiment, the fingertip force is decreased as the joint angles of the finger increased.

2.1.5 Summary

In this section, a wearable hand exoskeleton system with force-controllable actuator modules was developed. The linkage structure with 3 DOF and large ROM was designed by inspiring the finger anatomy. The fingertip workspace of the linkage structure was kinematically investigated and compared to the that of the functional ROM. Since the workspace of the proposed structure satisfy 90 %

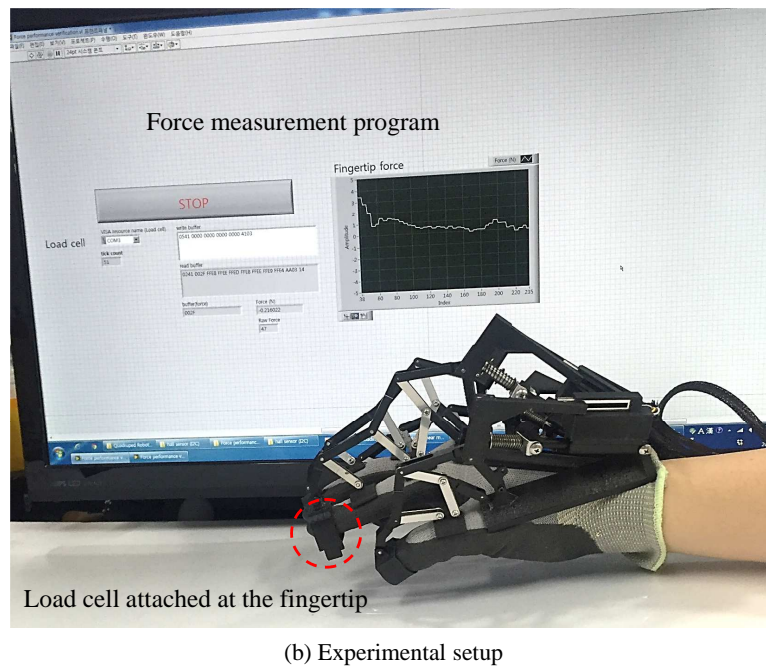
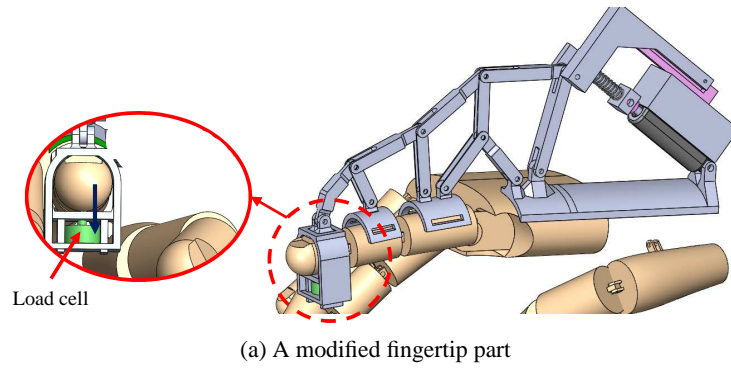


Figure 2-22: Force transmission experiment

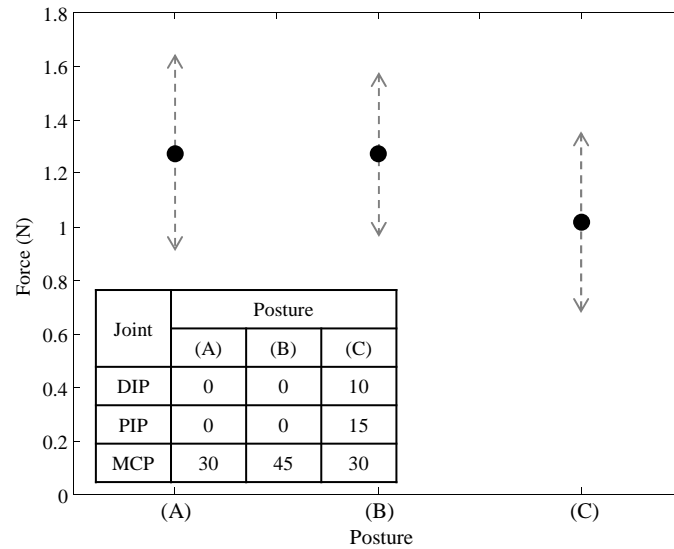


Figure 2-23: Normal force at the fingertip in experiment

of that of the functional ROM, it is verified that the user can make the most of the required postures to interact with objects. For the actuator modules, SEA mechanism which consists of the actuator and elastic element was applied. Considering the required stiffness and actuator module, the spring was designed manually. The measurement experiment of the contact force when the subjects grasp the object was conducted to determine the maximum force of the actuator. The motor friction was eliminated through the friction compensation algorithm to linearize the motor model, and DOB was applied to achieve accurate force mode control even with the human motion. Since the compact actuator modules were attached to the dorsum of the hand, the user can move the hand and arm freely. The actuator module generated the desired force accurately even with the stationary and arbitrary finger motions. However, the normal fingertip force was smaller than the generated one due to the drastic change in the normal direction of the fingertip as the finger is flexed.

2.2 A Wearable Hand Exoskeleton System with Finger Motion Measurement and Force Feedback

In previous study, since the finger structure is very complex to be worn on all phalanges, full joint ROM was not guaranteed and the transmitted force to the fingertip is distributed to other phalanges through the structure. With the proposed structure, the users with various hand sizes could not wear the system. In addition, the previous research focused only on the force feedback to the hand. However, in order to manipulate a virtual object, the finger motions should be measured. Although

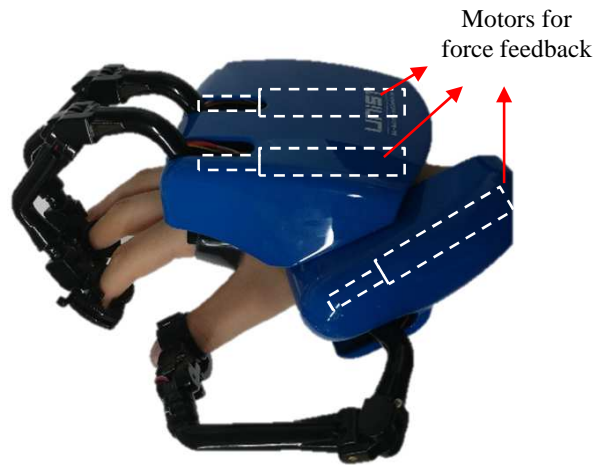
the system was designed with high wearability and portability, it was not verified by the experiment. Therefore, a wearable hand exoskeleton was developed considering these problems.

Since the finger structure was designed as a structure in which two bent links are connected by one rotational joint and it is worn only by the fingertips unlike the previous system, full joint ROM can be guaranteed while minimizing the collision between links and the users with various hand sizes can use the system without replacing the parts. Additionally, the force is transmitted to only the fingertip through the fingertip structure and the each joint angles was measured by using the fingertip position and the finger length. Since the finger motion measurement and the force feedback were simultaneously implemented, interaction performance with VR was also evaluated. Furthermore, although the system wearability and portability was described by only qualitative description in previous study, the system performance was also evaluated by UX evaluation in this study.

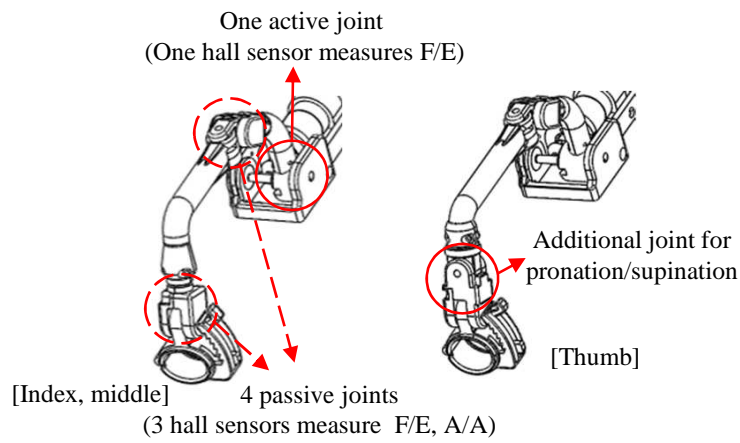
Thus, in this section, a wearable hand system with finger motion measurement and force feedback for VR is researched. The system has simple structures worn on the fingertips and palm and guarantee full ROM for natural finger motions. In addition, the finger structure can be worn on a variety of finger lengths without replacing the links. The system measure 5 DOF motion of the thumb, 4 DOF motion of the index and middle finger after only one calibration posture unlike previously developed systems. The forces are controlled by an the robust control algorithm to compensate the uncertainties arising from the interaction with the user. The system performance for finger motion measurement and interaction with VR was verified by the experiment.

2.2.1 Design of the Exoskeleton System for VR

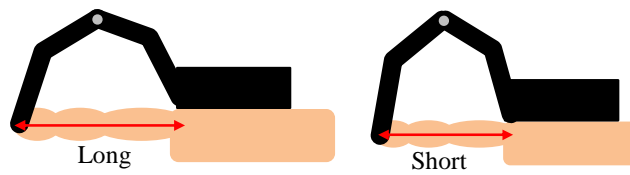
Figure 2-24 describe the system characteristics. The system for the hand was designed as shown in Fig. 2-24 (a), and its weight and size are 488 g and $120 \times 230 \times 80 \text{ mm}^3$, respectively. The system is worn on only fingertips of the thumb, index and middle fingers, which are important to interact with the environment and objects [68–70]. The finger linkages and motors for the ring and little fingers were not added for reducing the system weight. The finger structure for the index and middle finger has one active joint controlled by the motor for force feedback and 4 passive joints for free motions as shown in Fig. 2-24 (b). The finger structure for the thumb has one more passive joint than that for index finger to guarantee S/P motion. Hall sensor and magnet module is attached to each joint for measuring the fingertip position with respect to the motor shaft. Since the finger structure consists of two bent links with one rotational joint, the users with various hand sizes can use this system without



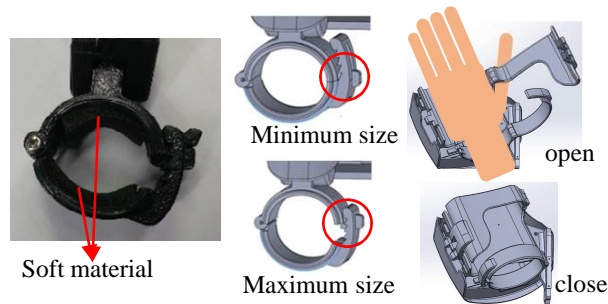
(a) Prototype of the system



(b) Finger structure



(c) Adaptable to different hand sizes



(d) Wearing part

Figure 2-24: Design of the exoskeleton system for VR

replacing the links as shown in Fig. 2-24 (c). The electric motors (DCX 16S, Maxon motors [71], finger structures and even a system controller are located on dorsum of the hand, thus, the user can move the arm and wrist freely without any restriction. For better wearability, the structures for the fingertips and palm were made as the clicking structure for wearing the fingertip and adjusting the size easily as shown in Figs. 2-24 (d). Moreover, the silicon material is coated on the wearing part for comfortable fit to the user.

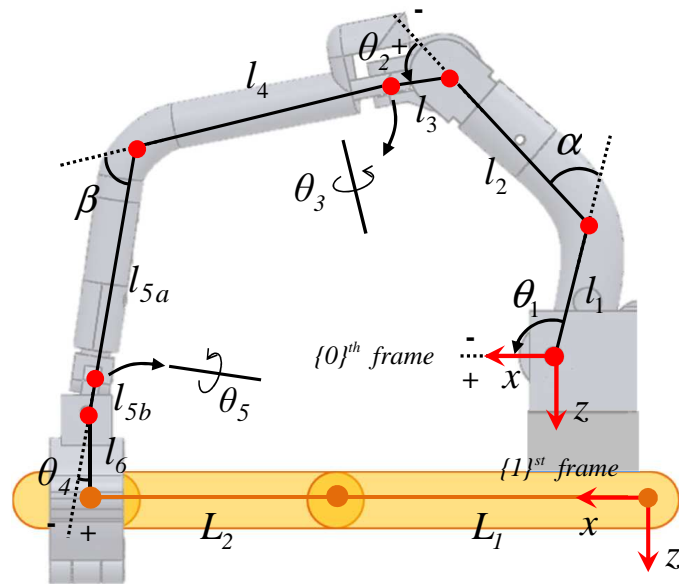
2.2.2 Finger Motion Measurement

The systems for finger motion measurement, especially joint angle measurement of the fingers, has been actively researched. Most of the wearable glove-type systems are using cables and strain or bending sensors [72–76]. However, since their performance depends highly on the alignment of the sensor and joint, the sensor position should be adjusted well whenever wearing the systems. In addition, more than two calibration postures are required before finger motion measurement, resulting in longer preparation time. To achieve high wearability and functionality, a finger motion measurement algorithm using only one calibration posture was developed although the system is worn on only the fingertip and the palm.

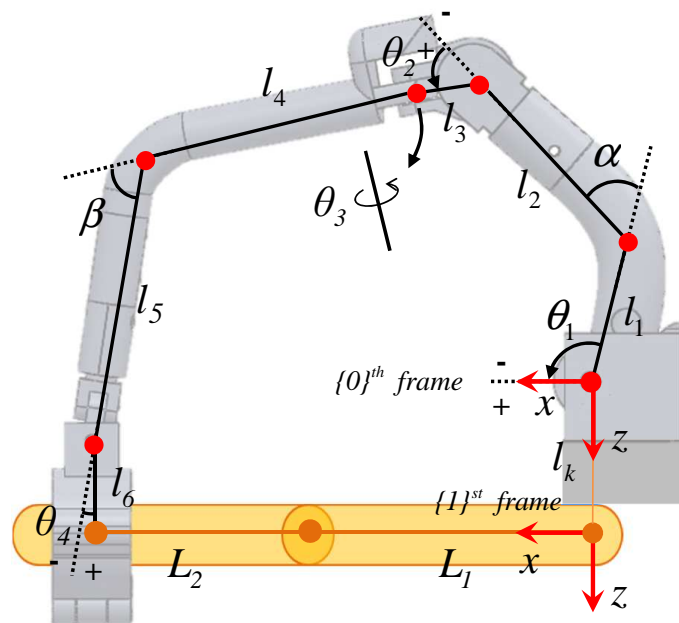
2.2.2.1 Workspace of the Fingertip

Since hall sensors embedded in the structure measure the rotation angle of the joints, the fingertip position with respect to the motor can be calculated by the forward kinematics. The required parameters for calculating the forward kinematics of the finger structure for the thumb and index finger are shown in Fig. 2-25 (a) and (b), respectively. The lengths ($l_1 \sim l_6$) and angles (α, β) of the links were optimized manually to satisfy various hand size and free finger motions. To guarantee 3 DOF motions of index and middle fingers, active rotational joint θ_1 and passive joints $\theta_2 \sim \theta_4$ were introduced and their angles were measured by embedded hall sensors. In addition, θ_5 is added to support S/P motion of the thumb.

Based on the finger structure, the fingertip workspace of the index finger and the finger structure was simulated as shown in Fig. 2-25. The ROM of each joint is from -90° to 90° in the simulation. Furthermore, the finger joint ROM in F/E motion is $\pm 90^\circ$ and in A/A motion is $\pm 30^\circ$. The workspace of the designed structure shows much larger than that of the human finger motions. Therefore, the system guarantee full workspace of the finger.



(a) Finger structure for the thumb



(b) Finger structure for the index and middle fingers

Figure 2-25: Parameters of finger structures

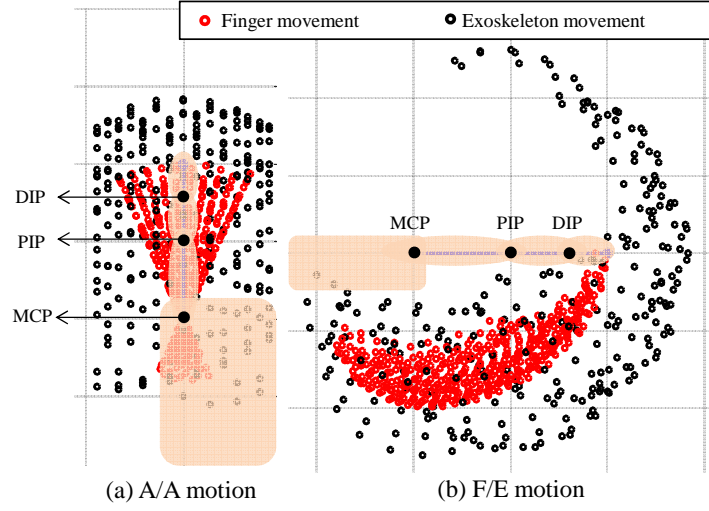


Figure 2-26: Fingertip workspace of the index finger

2.2.2.2 Calculation of Fingertip Position

The fingertip position of the index finger with respect to $\{0\}^{th}$ frame is calculated using forward kinematics as follows:

$$\begin{aligned}
 P_{x0} = & l_1 \cos \theta_1 + l_2 \cos(\alpha + \theta_1) + l_3 \cos(\alpha + \theta_1 + \theta_2) + l_4 \cos(\alpha + \theta_1 + \theta_2) \cos \theta_3 \\
 & + l_5(-\sin \beta \sin(\alpha + \theta_1 + \theta_2) + \cos \beta \cos(\alpha + \theta_1 + \theta_2) \cos \theta_3) \\
 & + l_6(-\sin(\beta + \theta_4) \sin(\alpha + \theta_1 + \theta_2) + \cos(\beta + \theta_4) \cos \theta_4 \cos(\alpha + \theta_1 + \theta_2)) \quad (2.25)
 \end{aligned}$$

$$P_{y0} = -(l_4 + l_5 \cos \beta) \sin \theta_3 + l_6 \cos(\beta + \theta_4) \quad (2.26)$$

$$\begin{aligned}
 P_{z0} = & l_1 \sin \theta_1 + l_2 \sin(\alpha + \theta_1) + l_3 \sin(\alpha + \theta_1 + \theta_2) + l_4 \sin(\alpha + \theta_1 + \theta_2) \cos \theta_3 \\
 & + l_5(\sin \beta \cos(\alpha + \theta_1 + \theta_2) + \cos \beta \sin(\alpha + \theta_1 + \theta_2) \cos \theta_3) \\
 & + l_6(\sin(\beta + \theta_4) \cos(\alpha + \theta_1 + \theta_2) + \cos(\beta + \theta_4) \cos \theta_3 \sin(\alpha + \theta_1 + \theta_2)) \quad (2.27)
 \end{aligned}$$

where P_{x0}, P_{y0}, P_{z0} are the index fingertip positions with respect to $\{0\}^{th}$ frame in the direction of x, y and z axes, respectively. The fingertip position of the middle finger could be calculated in the same equations. In addition, the thumb tip position with respect to $\{0\}^{th}$ frame is calculated as

follows:

$$\begin{aligned}
P_{x0}^{th} = & l_1 \cos \theta_1 + l_2 \cos(\alpha + \theta_1) + l_3 \cos(\alpha + \theta_1 + \theta_2) + l_4 \cos(\alpha + \theta_1 + \theta_2) \cos \theta_3 \\
& + l_{5a}(-\sin \beta \sin(\alpha + \theta_1 + \theta_2) + \cos \beta \cos(\alpha + \theta_1 + \theta_2) \cos \theta_3)) \\
& - l_{5b}(\sin \theta_3 \sin \theta_4 \cos(\alpha + \theta_1 + \theta_2) + \cos \theta_4(\sin \beta \sin(\alpha + \theta_1 + \theta_2) \\
& - \cos \beta \cos \theta_3 \cos(\alpha + \theta_1 + \theta_2))) \\
& - l_6 \cos \theta_5(\sin \theta_3 \sin \theta_4 \cos(\alpha + \theta_1 + \theta_2) - \cos \theta_4(\cos \beta \cos \theta_3 \cos(\alpha + \theta_1 + \theta_2) \\
& - \sin \beta \sin(\alpha + \theta_1 + \theta_2))) \\
& - l_6 \sin \theta_5(\sin \beta \cos \theta_3 \cos(\alpha + \theta_1 + \theta_2) + \cos \beta \sin(\alpha + \theta_1 + \theta_2)) \quad (2.28)
\end{aligned}$$

$$\begin{aligned}
P_{y0}^{th} = & -(l_4 + l_{5a} \cos \beta + l_6 \sin \beta \sin \theta_5) \sin \theta_3 \\
& - (l_{5b} + l_6 \cos \theta_5)(\cos \beta \sin \theta_3 \cos \theta_4 + \cos \theta_3 \sin \theta_4) \quad (2.29)
\end{aligned}$$

$$\begin{aligned}
P_{z0}^{th} = & l_1 \sin \theta_1 + l_2 \sin(\alpha + \theta_1) + l_3 \sin(\alpha + \theta_1 + \theta_2) + l_4 \sin(\alpha + \theta_1 + \theta_2) \cos \theta_3 \\
& + l_{5a}(\sin \beta \cos(\alpha + \theta_1 + \theta_2) + \cos \beta \cos \theta_3 \sin(\alpha + \theta_1 + \theta_2) \cos \theta_3)) \quad (2.30)
\end{aligned}$$

where P_{x0}^{th} , P_{y0}^{th} , P_{z0}^{th} are the thumb tip positions with respect to $\{0\}^{th}$ frame.

In case of the index finger, since the finger joint angles should be calculated from the MCP joint, the reference frame is changed from the motor shaft to the MCP joint, i.e., from the $\{0\}^{th}$ frame to the $\{1\}^{st}$ frame. l_k , which is the distance from the rotational joint at the motor to MCP joint, is assumed to be constant because all users wear the system in the same way. Thus, the finger joint estimation algorithm can be calculated based on the fingertip position with respect to the MCP joint. In case of the thumb, the method to convert the fingertip position with respect to $\{0\}^{th}$ frame to that with respect to the CMC joint was researched in next section.

2.2.2.3 Calibration Process

Before measuring the finger motions, a calibration process is required to obtain the finger lengths of the user. The user opens between the thumb and index finger, and closes between the index and middle finger while extending all fingers during the calibration process. When a user poses this calibration posture, the system captures the lengths of three fingers using forward kinematics. Since the fingertip structure is worn on the distal phalanx, the length of the distal phalanx was not considered. As the ratio of the lengths of the proximal and middle phalanges is 5 : 3 [77], the length of each phalanx can be estimated. Using the obtained phalanx lengths, the fingertip positions with

respect to MCP joint are converted to the finger joint angles through the proposed algorithm.

2.2.2.4 Joint Angle Measurement of the Index Finger

The fingertip position with respect to the MCP joint can be converted to the 3 DOF of F/E motion and 1 DOF of A/A motion through the joint angle estimation algorithm.

The A/A angle of the MCP joint can be measured easily using position of the fingertip shown in $\{1\}^{st}$ frame using P_{y1} and P_{x1} as follows:

$$\theta_{A/A} = \tan^{-1} \left(\frac{P_{y1}}{P_{x1}} \right) \quad (2.31)$$

To calculate F/E angles, the frame of the fingertip position should be converted into $\{2\}^{nd}$ frame to eliminate the effect of A/A motion. Additionally, since the DIP joint angle is coupled with the PIP joint due to the musculoskeletal structure [78], the DIP joint angle is estimated to be 2/3 of the PIP joint angle [66]. Thus, MCP and PIP joint angles in F/E direction can be calculated by inverse kinematics using fingertip position and finger phalanx lengths as follows:

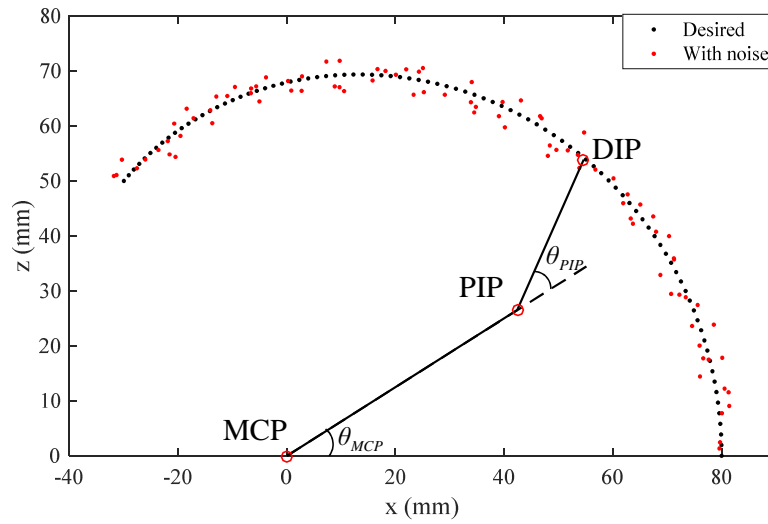
$$\theta_{MCP} = \tan^{-1} \left(\frac{P_{z2}}{P_{x2}} \right) - \cos^{-1} \left(\frac{P_{x2}^2 + P_{z2}^2 + L_1^2 - L_2^2}{2L_1 \sqrt{P_{x2}^2 + P_{z2}^2}} \right) \quad (2.32)$$

$$\theta_{PIP} = \cos^{-1} \left(\frac{P_{x2}^2 + P_{z2}^2 - L_1^2 - L_2^2}{2L_1 L_2} \right) \quad (2.33)$$

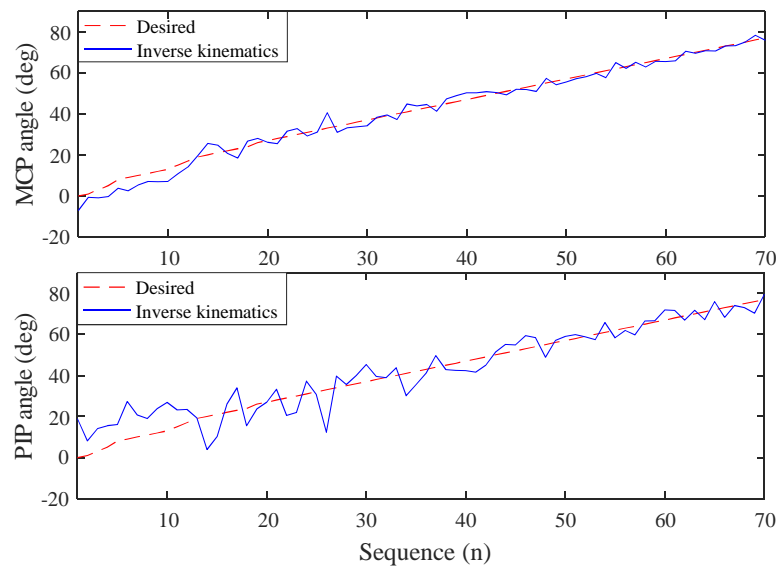
where P_{x2} , P_{y2} and P_{z2} are the positions with respect to $\{2\}^{nd}$ frame in the direction of x , y and z axes, respectively, and L_1 and L_2 are obtained lengths of proximal and middle phalanges in the calibration process.

However, inverse kinematics cannot be applied to estimate joint angles because of the high sensitivity to the position errors as shown in Fig. 2-27. Figure 2-27 (a) shows the fingertip positions with measurement errors. By using the equations (2.32) and (2.33), the estimated MCP and PIP joint angles were compared with the desired angles as shown in Fig. 2-27 (b). However, the estimated joint angles show very high errors according to the noise. It is because the result value of inverse cosine has $0 \sim 90^\circ$ angle range according to the $0 \sim 1$ input data change.

Therefore, another finger motion measurement method is proposed as follows. As shown in Fig. 2-28, $P_{(n)}$ is the measured fingertip position by the forward kinematics and $P'_{(n)}$ is the calculated fingertip position by the proposed method. If the fingertip position changes (Fig. 2-28 (a) and (b)), possible joint angles are calculated by adding -1° , 0° , $+1^\circ$ to the MCP and PIP joint angles of



(a) Fingertip position with measurement errors



(b) MCP joint angle in F/E motion

Figure 2-27: Finger joint angle estimation using inverse kinematics

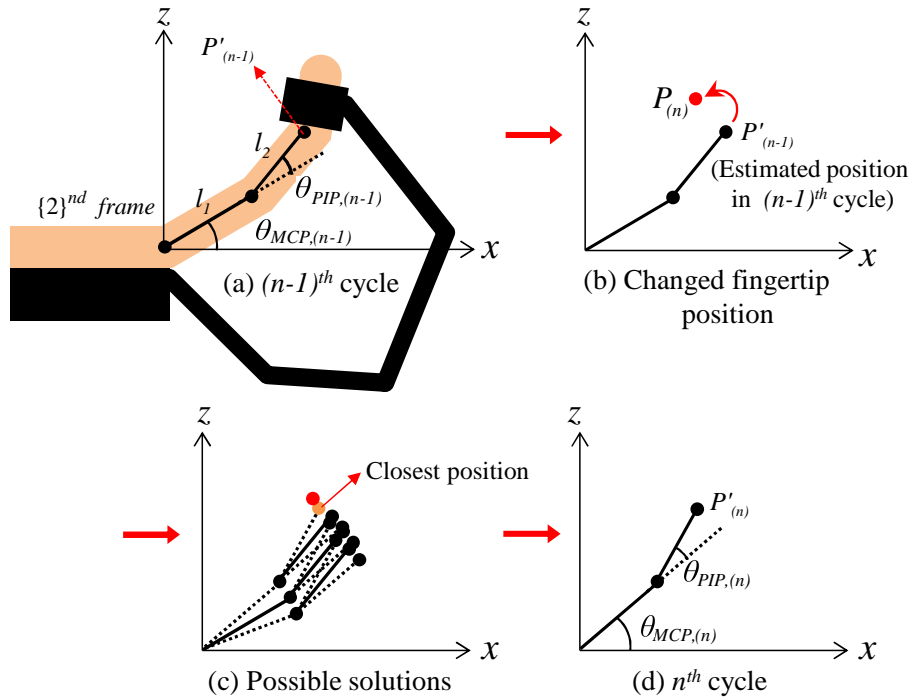


Figure 2-28: Estimation algorithm of the finger joint angles

the $(n-1)^{th}$ cycle (Fig. 2-28 (c)). By combining possible MCP and PIP joint angles, total nine candidates of fingertip positions are calculated. Finally, the calculated fingertip position ($P'_{(n)}$) which has the minimum distance with the measured fingertip position ($P_{(n)}$) is selected as the solution of the n^{th} cycle as shown in Fig. 2-28 (d). Thus, the MCP and PIP joint angles of the $P'_{(n)}$ are the estimated finger joint angles in $(n)^{th}$ cycle. The joint angles of the middle finger are also estimated by the same algorithm.

The angle change of 1° and the sampling time of the system (1 ms) can cover natural speed of finger motions, considering the bandwidth of fast finger motion ($4 \sim 8\text{ Hz}$ of writing, typing and tapping) [79].

2.2.2.5 Joint Angle Measurement of the Thumb

Although the thumb has very complex motions, previous studies indicate that A/A and S/P motions of the MCP joints are very limited and not significant([80–82]). Thus, Therefore, the kinematic model of the thumb consists of 5 DOF motions which have F/E, A/A, S/P motions at CMC joint, F/E motion at MCP and IP joints and the structure for the thumb has one more passive joint than that for other finger. In addition, the motor for the thumb was placed in consideration of the workspace of the thumb rather than the position of the CMC joint, thus, it was not possible to separate A/A and

Table 2.3: Orientation angle of the trapezium

	Flexion (°)	Abduction (°)	Pronation (°)
Mean	46	35	82
Range	40-53	25-43	75-89
Median	48	38	80

F/E motion through frame conversion similar to the algorithm for the index finger. Therefore, a new algorithm was developed to measure joint angles of the thumb accurately.

Similar to the angle estimation for the index finger, previous studies on the thumb motions was investigated to check the relationship between joint angles. Several researchers indicated that a muscle, called as flexor pollicis brevis, covers the CMC and MCP joint together and the F/E angle of the MCP joint depends on that of the CMC joint([80,81]). Additionally, S/P motion of the thumb is coupled with the F/E motion of the CMC joint, thus, it is estimated as 0.9 of the F/E angle of the CMC joint([80, 82]). By using the joint angle relationships, the fingertip position candidates and corresponding computational load could be minimized.

To convert the thumb tip with respect to the motor to that with respect to the CMC joint, not only the position but orientation of the CMC joint are required. The CMC joint position with respect to the hand exoskeleton was set as a constant vector due to same wearing method despite of various hand sizes. In case of CMC joint orientation, the researchers have been studied the orientation angle determined in ten cadaver hands [83]. They attached *T*-shaped markers to the first metacarpal of the thumb, and proximal phalanges of the index and middle fingers and measured the tilted angles of the thumb with respect to the third metacarpal.

Table 2.3 shows the orientation angle of the trapezium which consists of the CMC joint. Although the cadaver hand has relatively high flexion angle and partially flexed hand posture, the finger joint angles generally measured based on the full extended posture. Thus, the median values of orientation angles obtained from cadaver hands were converted to 0° of flexion, 38° of abduction, and 36° of pronation using the joint angle relations.

Therefore, the thumb tip position with respect to the motor could be converted to that with respect to the CMC joint using the CMC joint orientation (R_C) and tilted motor angle (R_M) with respect to the dorsal of the hand and position difference vector between the motor and CMC joint position (Tr_C) as following.

$$P_{tip,C} = R_C(R_M^{-1}P_{tip,C} + Tr_C) \quad (2.34)$$

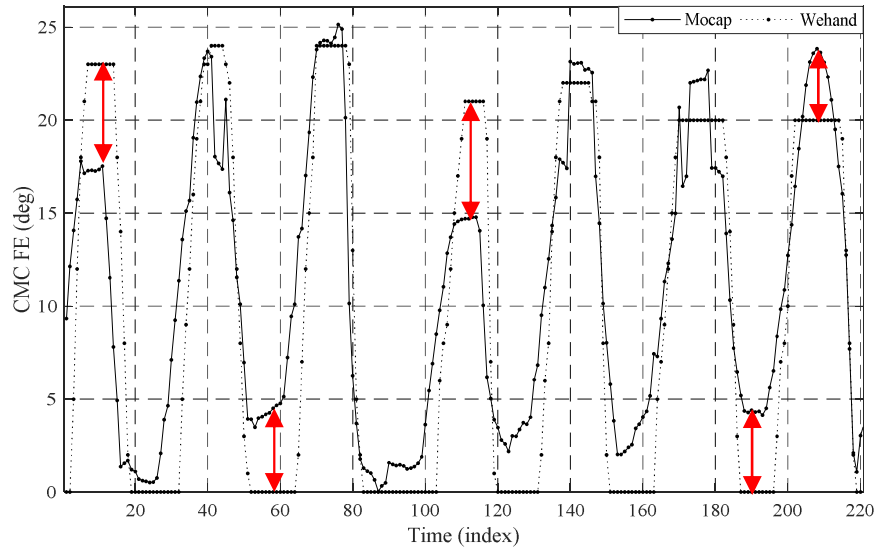
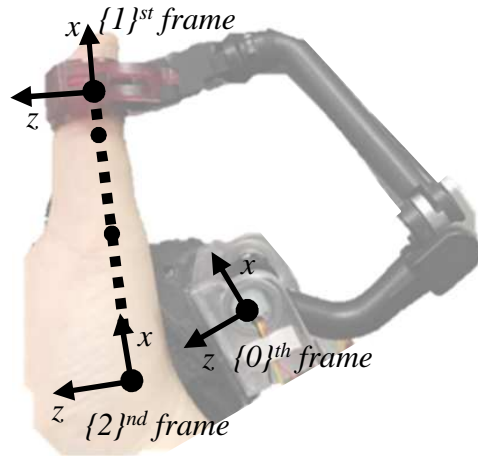


Figure 2-29: The estimated F/E angle of CMC joint with a constant CMC joint orientation

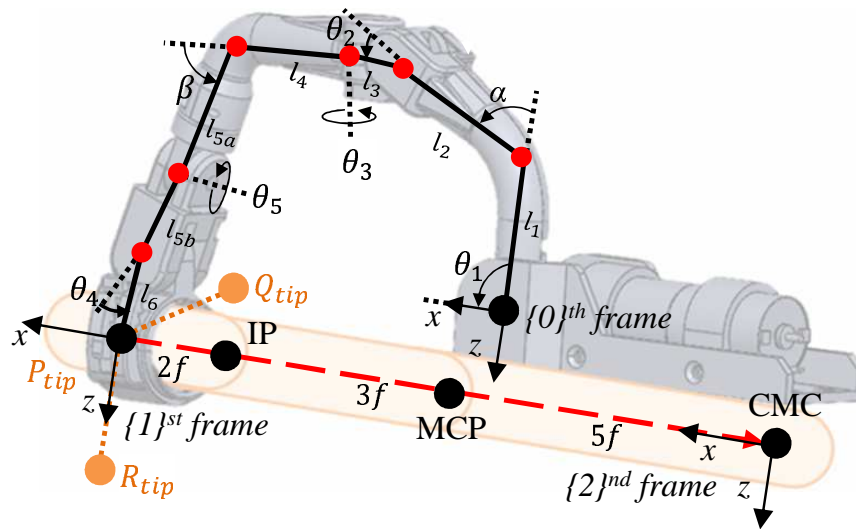
Since this method used a constant CMC joint orientation, the estimation algorithm is very simple. However, as shown in Table. 2.3, the CMC joint has wide orientation ranges with 13° range of flexion, 18° range of abduction, and 14° range of pronation. The estimated joint angles were not accurate accordingly when they compared to the measured angle by the camera-based motion capture system as shown in Fig. 2-29. Consequently, the CMC joint orientation of each user should be measured and applied to the algorithm.

Figure 2-30 (a) shows the CMC joint orientation at the calibration posture. The orientation of the thumb tip at the calibration posture where all the thumb joints are extended coincides with that of the CMC joint axis. Thus, the measured orientation of the thumb tip is used to convert the fingertip position of the thumb with respect to the motor to that with respect to the CMC joint.

As shown in Fig. 2-30 (b), the fingertip calculated by forward kinematics of the structure is the thumb tip position P_0 with respect to the $\{0\}^{th}$ frame and it is the same with the origin of the $\{1\}^{st}$ frame. Then, assume that there are two more positions called as Q_{tip} and R_{tip} . Q_{tip} and R_{tip} are the positions located at a distance of 1 mm from the fingertip on the y_1 -axis and z_1 -axis, respectively.



(a) The calibration posture



(b) Parameters for the thumb structure

Figure 2-30: Thumb structure in calibration posture

They are also can be expressed with respect to the $\{0\}^{th}$ frame as follows:

$$\begin{aligned} P_{tip} &= 0\hat{i}_1 + 0\hat{j}_1 + 0\hat{k}_1 \\ &= P_{x0}\hat{i}_0 + P_{y0}\hat{j}_0 + P_{z0}\hat{k}_0 \end{aligned} \quad (2.35)$$

$$\begin{aligned} Q_{tip} &= 0\hat{i}_1 + 1\hat{j}_1 + 0\hat{k}_1 \\ &= Q_{x0}\hat{i}_0 + Q_{y0}\hat{j}_0 + Q_{z0}\hat{k}_0 \end{aligned} \quad (2.36)$$

$$\begin{aligned} R_{tip} &= 0\hat{i}_1 + 0\hat{j}_1 + 1\hat{k}_1 \\ &= R_{x0}\hat{i}_0 + R_{y0}\hat{j}_0 + R_{z0}\hat{k}_0 \end{aligned} \quad (2.37)$$

By using these three positions, P_{tip} , Q_{tip} , and R_{tip} , the rotation matrix $[R]$ between $\{0\}^{th}$ frame and $\{1\}^{st}$ frame was calculated in the calibration process as follows:

$$[\hat{i}_1 \ \hat{j}_1 \ \hat{k}_1]^T = [\hat{i}_0 \ \hat{j}_0 \ \hat{k}_0]^T [R] \quad (2.38)$$

Then, the length of the thumb (10*f*) was calculated using the estimated CMC joint position according to the system design and the CMC joint position of the user was determined to be located at a distance of the thumb length in the direction of $-x_1$ -axis from the fingertip. The $\{2\}^{nd}$ frame with the CMC joint as the origin was determined, and the thumb tip can be expressed as the position with respect to the $\{2\}^{nd}$ frame as follows:

$$[P_{x2} \ P_{y2} \ P_{z2}] \begin{bmatrix} \hat{i}_2 \\ \hat{j}_2 \\ \hat{k}_2 \end{bmatrix} = [P_{x0} \ P_{y0} \ P_{z0}] \begin{bmatrix} \hat{i}_0 \\ \hat{j}_0 \\ \hat{k}_0 \end{bmatrix} [R] + [T] \begin{bmatrix} \hat{i}_2 \\ \hat{j}_2 \\ \hat{k}_2 \end{bmatrix} \quad (2.39)$$

where $[T]$ is the translation vector from $\{0\}^{th}$ frame to $\{1\}^{st}$ frame. Through the calibration process, the matrix $[R]$ and vector $[T]$ are measured and the fingertip position with respect to $\{0\}^{th}$ frame by forward kinematics is simultaneously converted to the position with respect to $\{2\}^{nd}$ frame. Thus, as with the algorithm for the index finger, the joint angles of the thumb are also calculated based on thumb phalanx lengths and the fingertip position with respect to the CMC joint.

Since F/E motion of the MCP joint and S/P motion of the CMC joint depend on the F/E joint of the CMC joint, the independent motions among 5 DOF are A/A motion of CMC joint and F/E motions of CMC and IP joints. Thus, three independent angles were obtained through the estimation

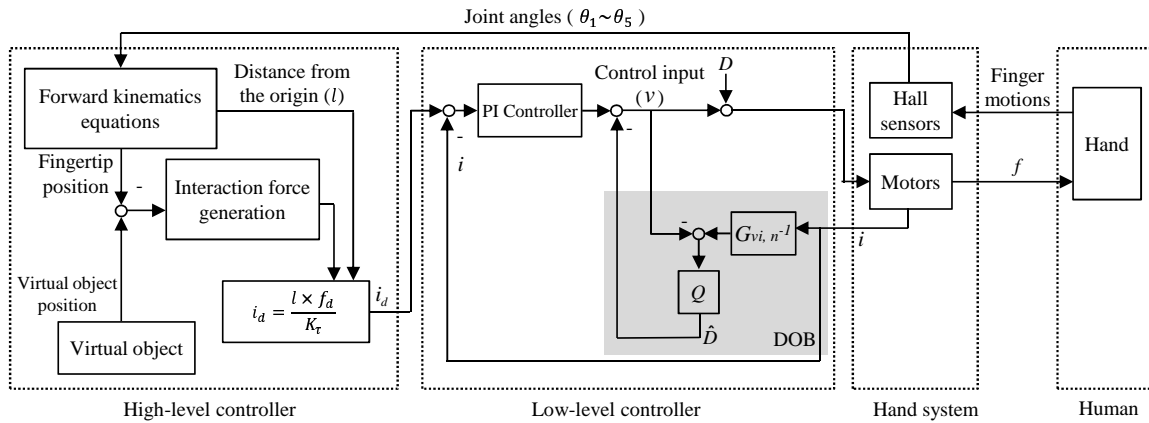


Figure 2-31: Overall control algorithm of the hand exoskeleton system for VR

algorithm used for motion measurement of the index finger. Although there are 2 unknown angles in case of the index finger, there are 3 unknown angles in case of the thumb and total 27 position candidates are considered. The fingertip position with respect to the motor is converted to that with respect to the CMC joint by applying the matrix $[R]$ and vector $[T]$, and the fingertip position is converted to the 5 DOF of finger joint angles through the estimation algorithm using 27 position candidates.

2.2.3 Force Feedback

The overall control algorithm for generating the force feedback is shown in Fig. 2-31. The proposed control algorithm is divided into a high-level and low-level controllers. In the high-level controller, the fingertip position is calculated using the hall sensor data. When an virtual object is realized, and its position and physical properties are already known by the virtual environment. Thus, the desired interaction force is calculated through the interaction force generation algorithm using the fingertip position and virtual object information. In the low-level controller, a PI controller with DOB, which is the mostly used as a robust control algorithm, was applied for compensating the uncertainties from the user. The motors for force feedback are generate the force feedback accurately by the high and lower controller and the force feedback is transmitted to the user's hand.

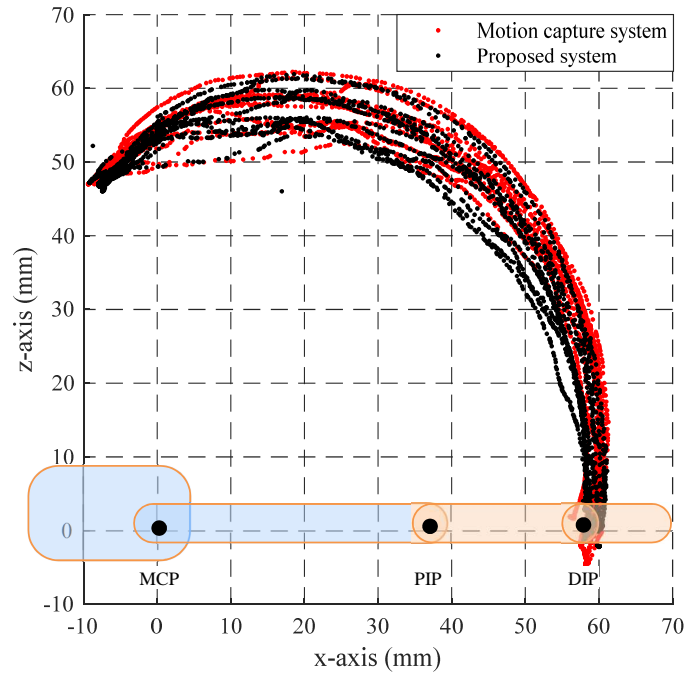


Figure 2-32: Fingertip position measurement performance

2.2.4 Experimental Verification

2.2.4.1 Measurement of the Fingertip Position

The performance experiment of the fingertip position measurement was conducted to verify the measurement accuracy using the commercialized motion capture system. As a reference system to compare with the proposed system, a motion capture system (Optitrack, Prime 13 [84]) which has position accuracy in three dimension of 0.8 mm . The markers for the motion capture system were attached to the MCP joint and fingertip structure for tracking the fingertip position with respect to the MCP joint. Therefore, the fingertip trajectory with respect to MCP joint captured by the reference system is compared to that measured by the hand exoskeleton system using forward kinematics of the proposed structure. Figure 2-32 shows the fingertip trajectories measured by the motion capture system and the proposed system. The fingertip trajectory measured by the proposed system is closely matched to that of the motion capture system with a maximum distance of 6 mm .

2.2.4.2 Pinch Motion

The proposed system measures the fingertip positions firstly and converts the fingertip position to the finger joint angles through the joint estimation algorithm. The accuracy of the fingertip position

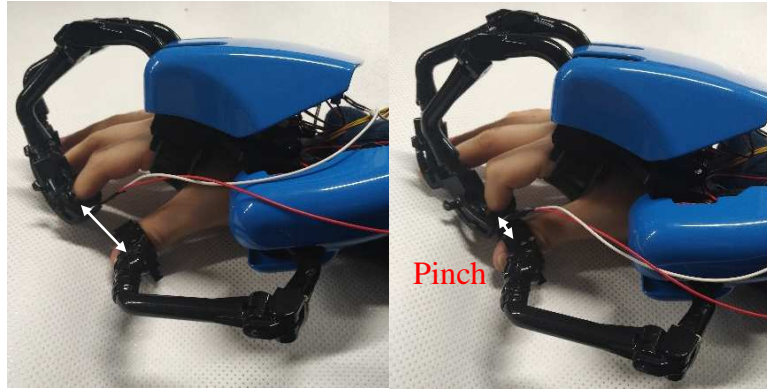
was verified in previous experiment and the maximum error of the position measurement at the fingertip was about 6 *mm*. Since the measurement of the fingertip position eventually affects the pinch motion and the pinch motion is a dominant posture among the precision grasps [85], the fingertip position measurement performance was also verified by the pinch motion experiment using the thumb and index finger before the experimental verification of the joint angles. Fig. 2-33 shows the experimental setup and results of the pinch motion using the thumb and index finger. As shown in Fig. 2-33 (a), the pressure sensor was attached to the fingertip structure of the thumb and its signal is increased when the pressure is applied. The sensor signal and the distance between the fingertip structures of the thumb and index finger were measured during pinch motion to confirm that pinch motion was captured by this system well.

Fig. 2-33 (b) shows the sensor signal and the distance between two fingertips. When the distance between the thumb and index fingertips is closer than 45 *mm*, the signal of the pressure sensor is dramatically increased. Since the fingertip distance was measured based on the center of the fingertip structure, the distance of 45 *mm* was made by the thickness of the structure. It was found that the distance between the fingertips, that is, the positions of the thumb and the index finger, were measured constantly, as the distance between the fingertip structures maintained about 45 *mm* when the sensor signal was increased even in several trials. Therefore, the pinch motion using the thumb and index finger was captured successfully using the proposed system.

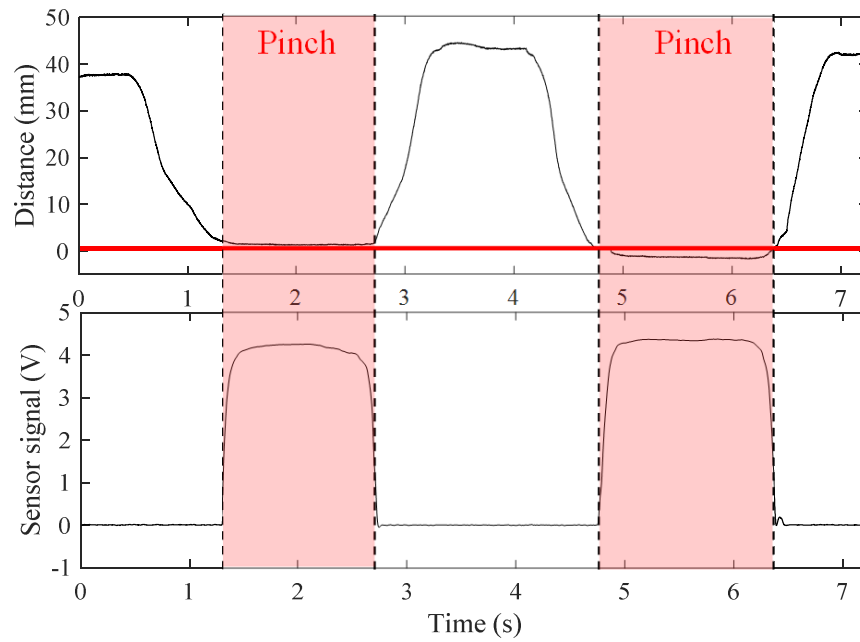
2.2.4.3 Estimation of Finger Joint Angles

The performance of the finger joint angle estimation was verified by comparing with a motion capture system. The markers were attached to the palm and MCP, PIP joints to capture the joint angles of the index finger. Simultaneously, the finger joint angles were measured by the proposed system. Fig. 2-34 shows the experimental results of joint angles for the index finger. Finger joint angles obtained by the proposed system are similar to those by the motion capture system. Since the DIP joint angle was estimated by the PIP joint angle in this system, the MCP and PIP joint angles were only experimented. The root mean square errors (RMSE) of the MCP joint angles in F/E and A/A motion, and PIP joint angle in F/E motion are approximately 2.03°, 2.45° and 3.20°, respectively. As the just noticeable difference (JND) of position sensing resolution of MCP and PIP joints are about 2.5° [86], the joint angle accuracy of the proposed system is acceptable for VR applications.

Furthermore, the measurement performance of the proposed system for the thumb was also

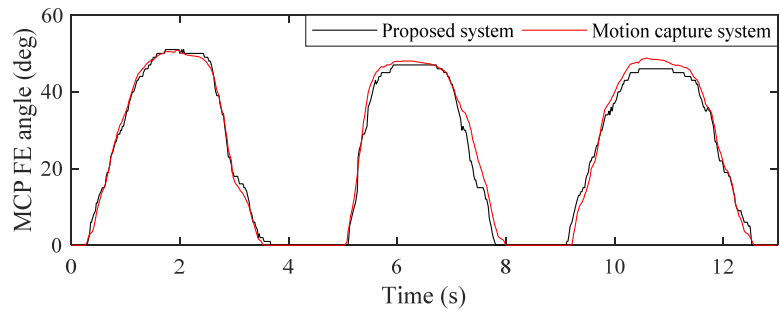


(a) Experimental setup

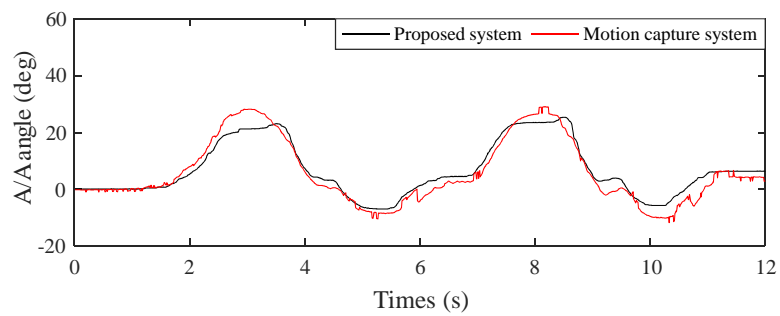


(b) Experimental results

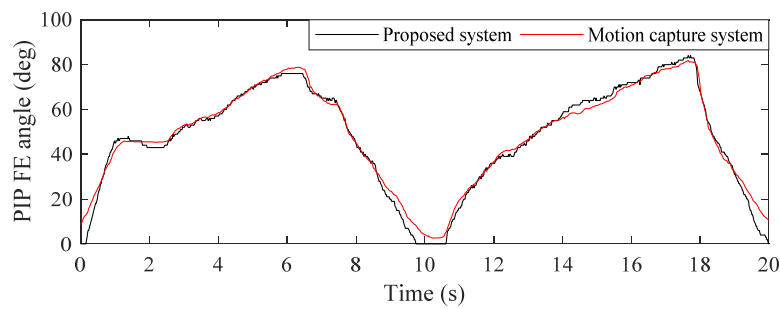
Figure 2-33: Pinch motion experiment



(a) MCP joint angle in F/E motion

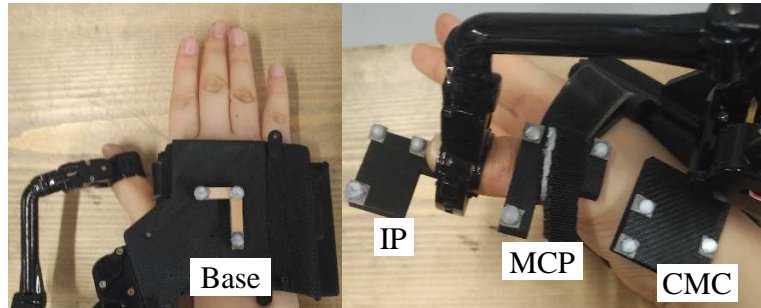


(b) MCP joint angle in A/A motion

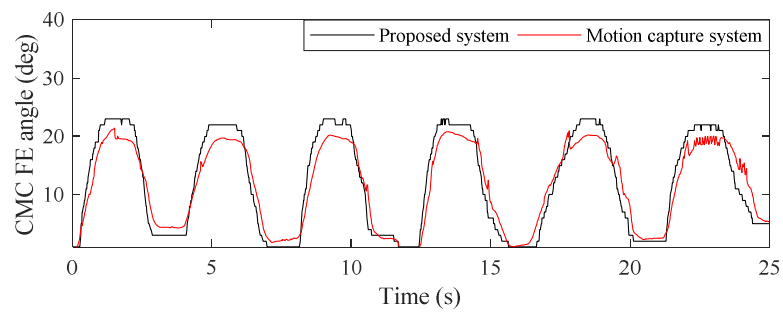


(c) PIP joint angle in F/E motion

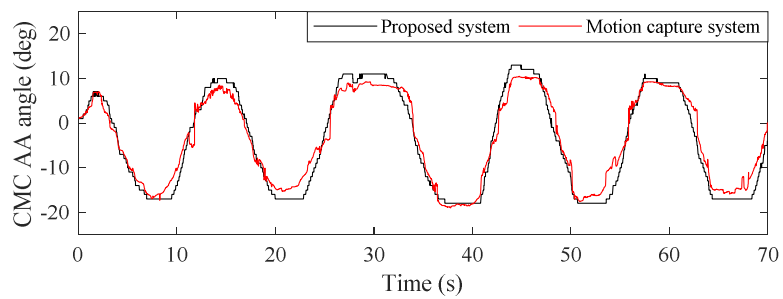
Figure 2-34: Measurement experiment of the index finger joints



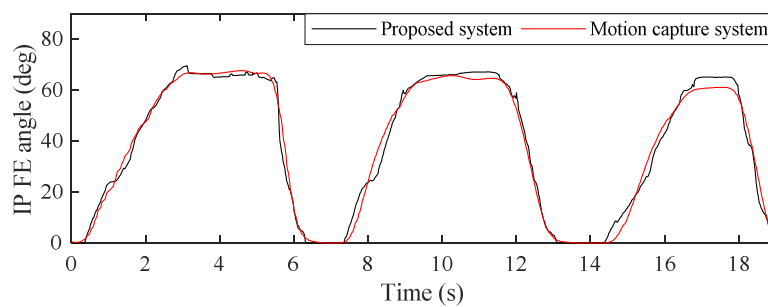
(a) Attached markers



(b) CMC joint angle in F/E motion



(c) CMC joint angle in A/A motion



(d) IP joint angle in F/E motion

Figure 2-35: Measurement experiment of the thumb joints

verified using the motion capture system. Fig. 2-35 shows the experimental results of joint angles for the thumb. Since other motions were coupled with the CMC F/E motion, the 3 independent motions (i.e., CMC F/E, CMC A/A, IP F/E motions) among the 5 DOF motions were verified in this experiment. The markers were attached to the palm and each metacarpal and phalange. The finger joint angles measured by the proposed system are very similar to those by the motion capture system. The RMSE of the CMC joint angles in F/E and A/A motions and that of the IP joint angle in F/E motion are 2.57° , 2.42° , and 3.06° , respectively. Thus, it was verified that the proposed system captures accurately the joint angles of the thumb and index finger.

2.2.5 Summary

In this section, a wearable hand exoskeleton system with finger motion measurement and force feedback for VR was developed. The finger structure is worn only on the fingertips and palm for high wearability and guarantee full ROM for natural finger motion. The system measure 5 DOF motion of the thumb, 4 DOF motion of the index and middle finger after only one calibration posture unlike previously developed systems. In addition, the forces are controlled by an algorithm, which is robust to the uncertainties arising from interaction with the human. The system was implemented and evaluated the performance of the finger motion measurement and interaction with VR for verification of the functional requirement. Thus, the experimental results showed that the developed system measure the finger motions accurately.

2.3 User Experience (UX) Evaluation

2.3.1 Introduction

The proposed system was evaluated in physical perspective in previous section. However, the subjective factors such as wearability and portability could not be evaluated by physical evaluation method although they are important factor as a haptic system. Thus, the performance of the subjective factors of the proposed system were evaluated in this section.

Various wearable hand systems have been developed as haptic systems for VR. Since they were developed for human use, both the performance of the system itself and its interaction with the user should be considered. Therefore, it is important to consider the evaluation methods and perform experiments accordingly, verifying the interaction performance of the system with the user to allow for a comprehensive performance evaluation.

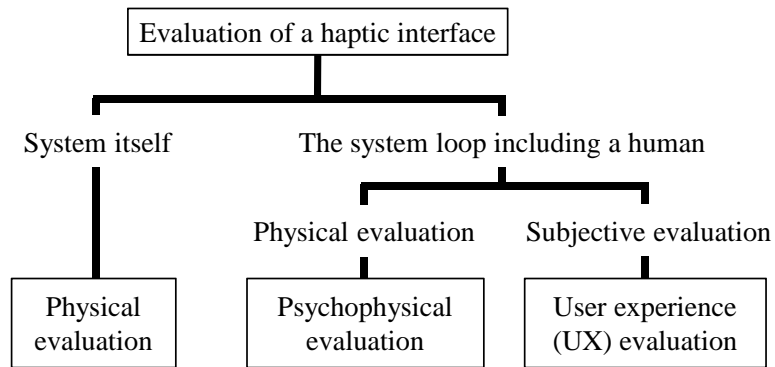


Figure 2-36: Evaluation of a haptic interface [21]

It is necessary to investigate the performance criteria used to evaluate wearable hand systems for VR. The environment for evaluating the haptic interface is divided into two parts: the system itself and the system loop including a human as shown in Fig. 2-37. The performance of the system itself is verified in physical evaluation experiments. The method for evaluating the performance of the interaction between the system and the user can be divided into psychophysical evaluation, which is a physical evaluation, and user experience (UX) evaluation, which is a subjective evaluation. For the psychophysical evaluation, the quantitative relationship between the force feedback and the corresponding sensation and perception of the user [87] was determined. For the UX evaluation, the subjective evaluation of the subject using the system was obtained.

Most wearable hand force feedback systems have been evaluated in terms of their physical performance with respect to force feedback and finger motion measurement; these parameters represent the performance of the system itself. Rutgers Master II is a haptic interface developed for interaction with VR [8]. Researchers have measured the performance of the finger motion measurement and force generation, such as maximum force, sensor resolution, and finger workspace, by conducting physical experiments. The performances were compared with those of the CyberGlove with CyberGrasp [5], which are the most well-known wearable force feedback systems that have been commercialized for VR. However, this physical evaluation is insufficient for assessing the system because the interaction performance is not considered.

In previous studies, the verification of the interaction performance (such as psychophysics and UX) of wearable cutaneous systems was conducted. Murray *et al.* applied the psychophysical evaluation to a wearable vibrotactile glove which has five miniature voice coils [88]. They obtained the psychophysical relation between vibrotactile stimulation and perceived magnitude, and performed telemanipulation experiments to evaluate the system effectiveness. Maisto *et al.* evaluated wearable

haptic systems for the fingers by writing, pick and place, and ball balancing tasks [89]. Fourteen subjects were performed tasks with five different feedback conditions and the completion time, force magnitude, and perceived effectiveness were measured. They validated that the user wearing the haptic device for the fingertip shows better performance than the user without the system. Prattichizzo *et al.* evaluated a 3 DOF wearable haptic interface through curvature discrimination experiment [90]. The subjects with the cutaneous feedback device distinguished smoother curvature than those without the feedback. In addition, they verified that the system is highly wearable and easy to use through the UX survey.

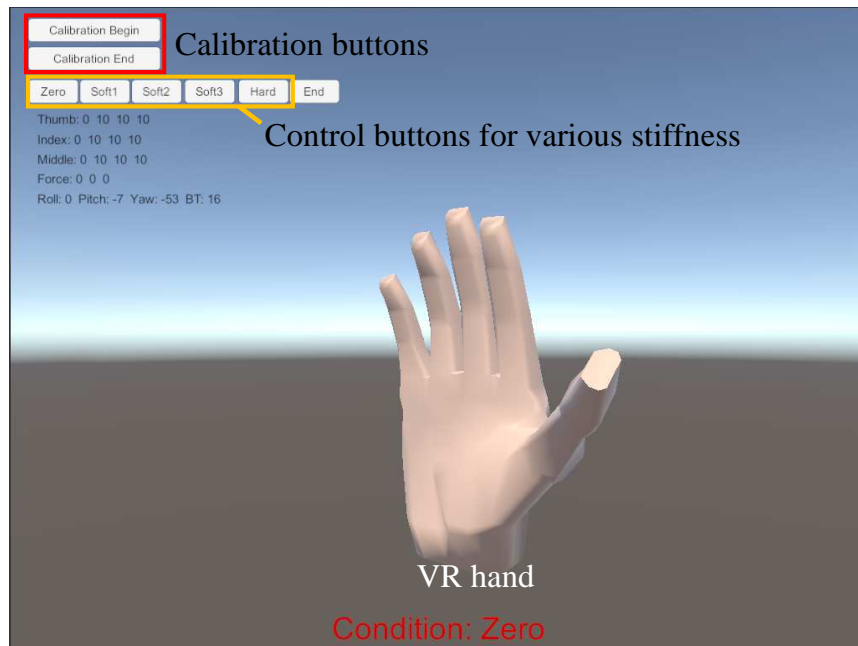
Although the evaluation of the interaction performance has been actively conducted for the wearable cutaneous systems, there are few studies to assess wearable hand kinesthesia systems. The interaction performance of the wearable hand force system was evaluated in terms of the psychophysical and UX perspectives. The evaluation of haptic interfaces is divided into physical, psychophysical, and UX evaluations. The evaluation criteria and experimental environments were determined considering the characteristics of the system. The quantitative results of the psychophysical evaluation was verified by comparing them with those of other haptic devices and human perception threshold. The results of the UX evaluation were analyzed with the opinions from the subjects. In this research, the subjective evaluation using UX evaluation was only considered for evaluation of the haptic interface.

2.3.2 Virtual Reality Program

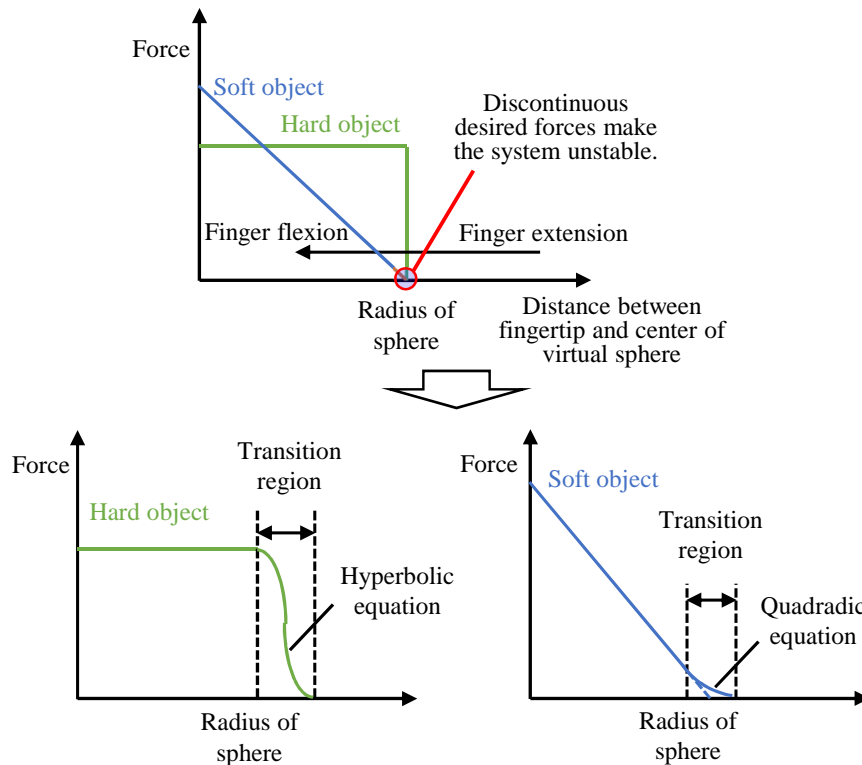
To use and evaluate the proposed system, VR environment suitable for the proposed system performance was needed. Therefore, a VR which meets the characteristics of this system was developed using UNITY and C# programming.

Figure 2-41 (a) shows the developed VR visual interface. When the calibration button in the upper left corner of the interface is clicked, lengths for the thumb, index and middle fingers are measured. Then, as soon as the calibration process is completed, the finger motions are measured. The finger joint angles are applied to the virtual hand model to show the finger motions measured by the hand exoskeleton system simultaneously. Since the system does not measure motions of the ring and little fingers, the rest fingers of the virtual hand moves along with the middle finger.

A virtual sphere was introduced to generate the force feedback from VR, which was designed to have three levels of stiffness (i.e., zero impedance, soft object, and hard object). When the control buttons for various stiffness in visual interface were clicked, the corresponding stiffness was



(a) VR visual interface



(b) Force profile

Figure 2-37: VR program

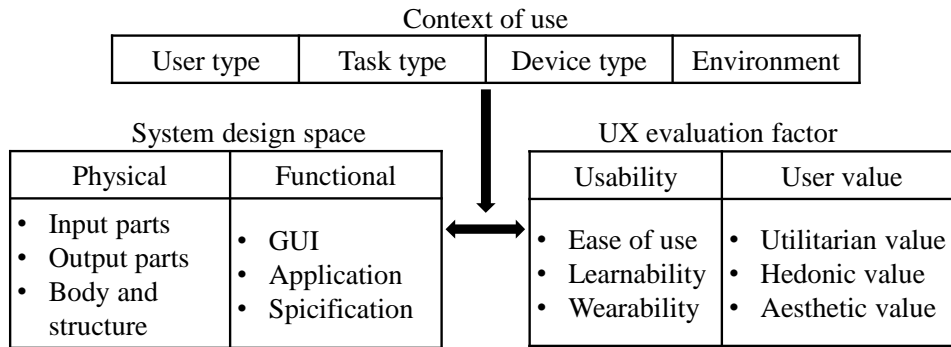


Figure 2-38: Evaluation framework for wearable devices

implemented. In case of a soft object, the magnitude of the force increased from the surface to the center of the object. In case of a hard object, the sudden and constant force was applied from the object surface. However, since sudden changes in force magnitude might make the system unstable, an algorithm smoothing the force profile was researched.

As the distance between fingertip and center of the sphere decreases, no force was applied to the fingertip until the fingertip reaches the surface. When the fingertip touches the sphere’s surface, discontinuous forces should be applied to realize the soft and hard object as shown in Fig. 2-41 (b). To make the system stable, a transition region was set to change discontinuous force profile to continuous profile. Thus, a hyperbolic and quadratic equation were introduced to the hard object and soft object condition, respectively.

2.3.3 Evaluation Framework for Wearable Hand Systems

The UX is defined as a person’s perceptions and responses to the use and/or anticipated use of a product, system or service [91]. Various methods (e.g., lab studies, field studies, surveys, and expert evaluations) have been used, and especially, the survey method is particularly frequently used because it is easy to implement and data can be obtained quickly for many subjects [92]. Many UX survey methods have focused on evaluating software interfaces or graphical user interfaces [93]. UX evaluation methods for physical user interfaces, especially for wearable hand systems, have not been well-researched. A previous paper which proposed a UX evaluation framework for wearable devices was deeply investigated for UX evaluation of this haptic system [22] and Figure 2-39 shows the proposed framework.

The UX evaluation framework suggested the essential components of the UX evaluation experiment. The evaluation framework consists of three components: context of use, system design

space and evaluation factor. Context of use refers to external factors which can affect to the evaluation results, system design space refers to the components of the system, and UX evaluation factor refers to the items of the system to be evaluated. The context of use is a combination of the user, task, device, and environmental factors. Since the UX evaluation is subjective assessment, these factors influence the perception of, and experience of using, the system. Thus, they should be considered deeply when designing the experiment. The context of use for the evaluation experiment will be described in next section. The system design space is divided into physical and functional design spaces. The physical design space is the external area that physically interacts with the user and consists of input parts, output parts, and body and structure. Since input and output parts are actually connected parts with the user, they are more important than the body and structure. The functional design space is the embedded functions that is required to realize the system's purpose and consists of user interface (UI), application and specification. Since most of wearable devices interact with the user using screen, graphical user interface is considered as a factor of functional space. Application refers the embedded softwares in the devices and specification refers the physical functions such as battery operation time, storage capacity, and so on. Regarding to the evaluation factor, usability is composed of ease of use, learnability, and wearability, which together represent the subjective characteristics of the system, and user value is composed of utilitarian, hedonic and aesthetic values which the user can receive while experiencing the system. Utilitarian value is the user's experience when utilizing the system and hedonic value is to the subjective feeling of using the system. In addition, aesthetic values refers a user's feeling when the user just watch the device.

The proposed UX evaluation framework was designed for the wearable devices. However, the evaluation framework should be revised according to the characteristics of the system although this system is also a wearable device. Figure 2-40 shows the revised framework for wearable hand system for VR.

In case of this system, since a fingertip structure is responsible for the measurement (input) and feedback (output), the physical space consists of two parts as fingertip structure and the structure on the palm. Additionally, the finger motion measurement and force feedback, which constitute two major functions of the system, belong to the functional space component.

Regarding to user value in evaluation factor, hedonic and aesthetic values were excluded to assess the user value of the system. Hedonic value is highly related to the VR contents, which are not considered in the development stage and aesthetic values was also not considered, such as the appearance of the system, when designing the prototype. Thus, total eight statements for four

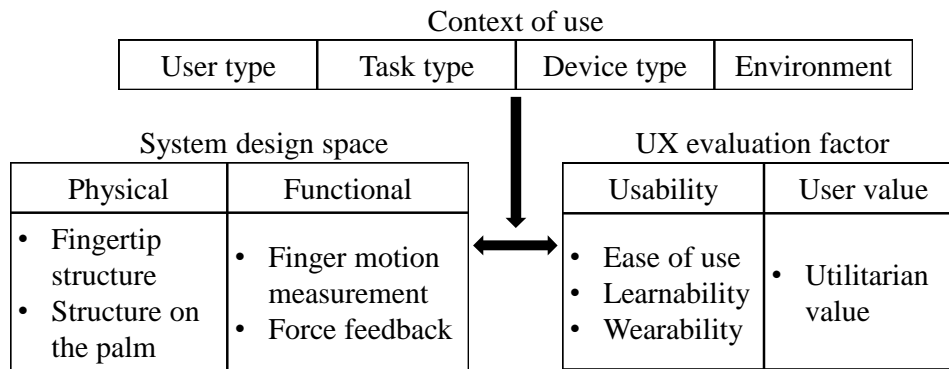


Figure 2-39: Evaluation framework for wearable hand systems for VR (revised from [22])

Table 2.4: Familiarity with VR devices

	How many hours have you used VR devices?		
Q1	Below 1 h	1 h ~5 h	More than 5 h
	8	6	1
	Interest in VR technology and wearable devices		
Q2	High	Medium	Low
	6	6	3

evaluation factors (ease of use, learnability, wearability, utilitarian value) were designed for the UX evaluation by reference to previous studies([94–96]). All statements and satisfaction scores were evaluated using a 7-point Likert scale, with high scores indicating a positive attitude toward the system. Additionally, the statements were randomly ordered to eliminate the influence between questions.

Similar to UX evaluation factor, the satisfaction score for system design space was assessed to capture the influence of the system design on the evaluation factor. After responding to all statements, each subject was asked to write down the reasons underlying their highest- and lowest-scoring statements. The subjective comments about the system were used in analysis of the UX results.

2.3.4 Experimental Setup

The context of use mainly considered such as the user, task, device and environment. The UX experiment was conducted under laboratory conditions for short-time experiment. A total of fifteen right-handed subjects (eleven males, four females) participated in the UX experiment. They were all undergraduate students aged 20 ~ 26 (23.6 ± 2.0) with hand sizes 17 ~ 20 cm; this range covers about 80 % of South Korean adults aged between 20 and 60 years old [97]. Moreover, since

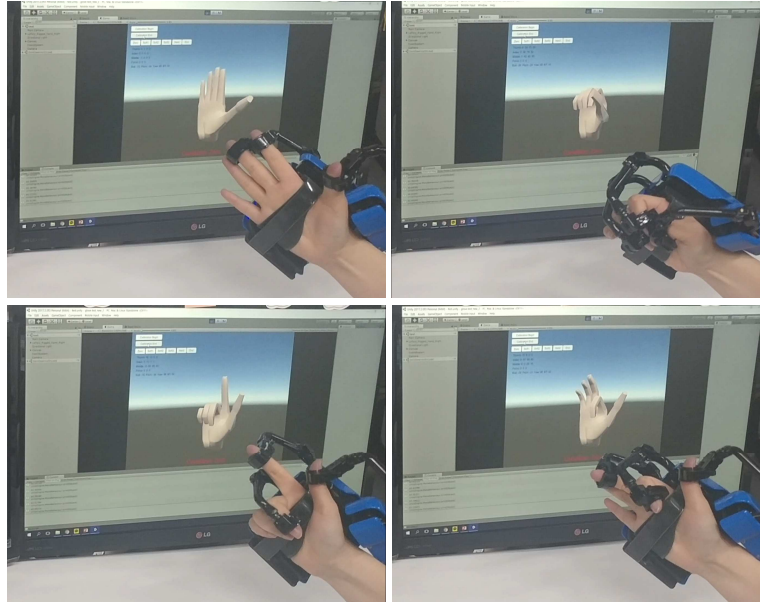
the degree of experience in using VR devices could affect the UX results, the subjects answered two questions pertaining to their familiarity with VR devices to, as shown in Tab. 3.2. Many subjects had used VR devices for less than 1 hour and most of the subjects reported a high or medium level of interest in VR technology and wearable devices.

Before the subjects experiences the proposed system for VR, a description of its purpose, characteristics and performance was provided for understanding the system and VR. After explaining the system, the subjects pose the calibration posture and they moved their fingers more than five times to obtain sufficient experience of the various levels of stiffness (i.e., zero impedance, hard object, and soft object). Under the zero impedance condition as shown in Fig. 2-41 (a), the users could move their fingers easily without resistive forces and their finger motions were represented simultaneously by the VR hand. Since the ring and little fingers do not captured by the system, they show same motions with the middle finger. The conditions of the resistive forces were divided into hard and soft objects as shown in Fig. 2-41 (b). The stiffness of the objects were changed by the control buttons and their stiffness were already determined experimentally. When the subjects touch the virtual object (i.e., blue sphere), a constant resistive force was applied to the fingertip at the object surface under the hard object condition, whereas a linearly increasing force was applied under the soft object condition, from the object surface to its center. The virtual objects with various levels of stiffness were realized by varying the slope of the increasing force. The user completed the questionnaire after feeling the zero impedance, hard and soft objects for a sufficient duration.

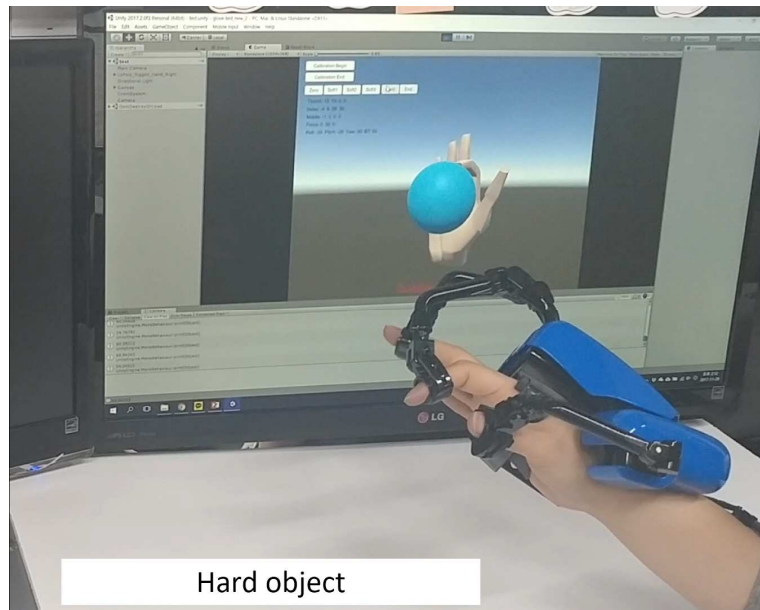
2.3.5 Result & Discussion

2.3.5.1 User Experience (UX) Evaluation

Table 2.5 lists the questionnaire statements of evaluation factor. All statements, except those pertaining to wearability, received scores exceeding 5.5 points on average, and it showed that the subjects generally had a positive attitude toward the developed hand system for VR. The scores of statement Q4 and Q6 pertaining to the wearability of the device were 4.07 and 4.93, respectively. Although their scores are also larger than the middle point (3.5) of the Likert scale, these statements typically produced lower scores than other statements. The predominant opinion about the wearability was that the system was heavy, and also that it was difficult to maintain the fingertips in close proximity to each other due to the large fingertip structures of the device. The learnability statements produced the highest scores, in accordance with the intuitiveness and simplicity of wearing and using the de-



(a) Finger motion measurement



(b) Force feedback

Figure 2-40: UX experiment

vice. Similar reasons were cited for the high scores on the ease of use factor. In addition, since even the subjects who have experienced the VR system have used only the remote control type systems, they responded positively to the system's intuitiveness and force feedback and gave good grade to the utilitarian value.

2.3.5.2 System Satisfaction

The satisfaction score for each design space parameter is shown in Tab. 2.6. The satisfaction score for the system was 5.87 out of 7 which shows relatively high score. The scores for the physical space parameters were relatively low because, as noted previously, the system was perceived as being heavy and the fingertip structures were large. The satisfaction score for the finger motion measurement was high, because the accuracy was high and the device control method is intuitive, in contrast to haptic devices with remote controls (e.g., Vive controller [48], Odyssey controller [47]). Furthermore, the force feedback score was relatively high because most subjects find this to be an intuitive feedback method, such that it enhances the sense of immersion.

2.3.6 Summary

The proposed system was evaluated by the UX perspective. The evaluation criteria of haptic interface were determined considering the characteristics of the proposed system. The experiments for the psychophysical evaluation were conducted in the context of three perception modes: detection, discrimination, and identification. The quantitative results of the detection and discrimination experiments verified that the interaction performance of the system was better than that of other commercialized grounded systems, and force discrimination thresholds were similar to those of humans. In addition, the results show that most users could distinguish between three sizes and three shapes, where the correct response rate and identification level exceeded 90 % and 2.5 level, respectively. For the UX evaluation, the evaluation framework was revised and a questionnaire was designed using 7-point Likert scales, attitude toward its usability and utilitarian value. Many users considered the learnability of the system as its greatest advantage. In addition, since the proposed system enables users to interact with a VR environment via an intuitive control and feedback method, they were highly satisfied with the functional design. In addition to these advantages, the users also reported some disadvantages, namely that the system was heavy and uncomfortable, and that the force feedback sensation was different to the feel of real objects.

2.4 Summary

In this chapter, wearable hand exoskeleton systems for VR were proposed. In first research, a wearable hand exoskeleton system with force-controllable actuator modules was developed. For compact and light-weight system, a SEA mechanism consisting of the actuator and elastic element was used. In control algorithm of the actuator module, the motor friction was eliminated through the friction compensation algorithm to linearize the motor model, and DOB was applied to achieve accurate force mode control even with the human motion. Since the compact actuator modules were attached to the dorsum of the hand, the user can move the hand and arm freely. The actuator module generated the desired force accurately even with the stationary and arbitrary finger motions.

However, the previous research cannot measure finger motions and the normal fingertip force was smaller than the generated one due to the drastic change in the normal direction of the fingertip as the finger is flexed. In this section, a wearable hand exoskeleton system with finger motion measurement and force feedback for VR was developed. The finger structure is worn only on the fingertips and palm for high wearability and guarantee full ROM for natural finger motion. The system measure 5 DOF motion of the thumb, 4 DOF motion of the index and middle finger after only one calibration posture unlike previously developed systems. In addition, the forces are controlled by an algorithm, which is robust to the uncertainties arising from interaction with the human. The system was implemented and evaluated the performance of the finger motion measurement. Thus, the experimental results showed that the developed system measure the finger motions accurately.

The proposed system was evaluated by the UX perspective. The evaluation criteria of haptic interface were determined considering the characteristics of the proposed system. The experiments for the psychophysical evaluation were conducted in the context of three perception modes: detection, discrimination, and identification. The quantitative results of the detection and discrimination experiments verified that the interaction performance of the system was better than that of other commercialized grounded systems, and force discrimination thresholds were similar to those of humans. In addition, the results show that most users could distinguish between three sizes and three shapes, where the correct response rate and identification level exceeded 90 % and 2.5 level, respectively. For the UX evaluation, the evaluation framework was revised and a questionnaire was designed using 7-point Likert scales, attitude toward its usability and utilitarian value. Many users considered the learnability of the system as its greatest advantage. In addition, since the proposed system enables users to interact with a VR environment via an intuitive control and feedback

method, they were highly satisfied with the functional design. In addition to these advantages, the users also reported some disadvantages, namely that the system was heavy and uncomfortable, and that the force feedback sensation was different to the feel of real objects.

Table 2.5: Results of user experience (UX) evaluation

UX evaluation factor	Statement No.	Statement	Avg.	Std.
Ease of Use	Q1	The system was easy to use.	5.87	0.83
	Q7	The system was simple to use.	6.40	0.51
Learnability	Q2	I think that most people could easily remember how to wear and use the system.	6.60	0.51
	Q8	I think that a novice can learn to wear and use the system quickly.	6.67	0.49
Wearability	Q4	I felt comfort while wearing the system.	4.07	1.03
	Q6	The system guaranteed free movement of my hand and fingers.	4.93	1.53
Utilitarian value	Q3	I think the system is useful to manipulate objects in VR.	5.93	0.80
	Q5	I think the system is effective to manipulate objects in VR.	6.00	0.76

Table 2.6: Satisfaction scores of system design

Design space		Avg.	Std.
Overall system		5.87	0.92
Physical	Fingertip structure	5.33	1.11
	Structure on the palm	5.13	1.06
Functional	Finger motion measurement	6.00	0.93
	Force feedback	5.60	1.06

Chapter 3

A Spring-guided Hand Exoskeleton for Continuous Passive Motion

3.1 Introduction

As discussed in Chapter 1, finger motion measurement, force feedback, high wearability, and portability are important factors for rehabilitation systems, as well as VR systems. However, previous rehabilitation systems have not satisfied these conditions sufficiently. Most rehabilitation systems for the hand have been developed using a variety of actuators and sensors [14, 100]. Many sensors and actuators allow the system helping the impaired body in various ways, but typically results in complex and heavy systems. Thus, the patient feels uncomfortable due to the fixed parts to these systems which are made as the desk- or splint-mounted systems to distribute the system weight. On the other hand, to decrease the system load on the hand while maintaining functions using a lot of sensors and actuators, cable mechanisms were usually applied to the hand rehabilitation systems and the required parts were located on the outside of the system. [101, 102]. Although this method can decrease the system weight on the hand, the external box for the actuator and sensor modules degrades the portability of the system.

In this research, a portable and wearable hand exoskeleton system for rehabilitation with finger motion measurement and force feedback system was developed. Due to finger motion measurement and force feedback functions, different to the exercise with the physical therapist, the patient's movement condition is measured as quantitative data in real time. In addition, the force feedback

The contents of this chapter was published in [98]. Preliminary research results of the paper were published in [99]. Reprinted with permission from IEEE and Elsevier.

can be adjusted according to the joint stiffness of the impaired part, different to the position control system. Thus, since a spring mechanism for force feedback is added to the system, it is possible to adjust the deviated motion range and force magnitude based on the given trajectory by adjusting the spring stiffness.

Moreover, subjective properties except safe were not generally focused for rehabilitation systems with high performance. However, since the hand is the most distal part among the upper limbs, body parts which affect to the hand position (i.e., trunk, shoulder, elbow) may have some restrictions when the grounded rehabilitation system is worn on the hand. This restriction may cause inconvenience to the patient, thus, the portable system should be developed for comfort rehabilitation. In addition, the system with high wearability reduces short preparation time and reduce the fatigue during rehabilitation exercise. The hand system with high portability and wearability enables high repetitive and intensive exercise by the patient.

Continuous passive motion (CPM) is a frequently used rehabilitation method for patients by stroke, surgery, and etc. In case of stroke patients, since they suffer from the muscle spasticity due to neurologic deficits, about 4 Nm torque is required for fully extended posture of the high tone patients [15] and this large torque cannot be realized by the small size motor which could be put on the dorsum of the hand. However, to develop a hand rehabilitation system of high wearability and portability, the huge motor cannot be applied. Thus, in this research, a rehabilitation system was developed for patients who want to maintain or recover the full joint ROM without undesired muscle contraction.

Therefore, in Chapter 3, a portable hand exoskeleton for exercising F/E motion of the fingers using the spring mechanism was proposed. A 1 DOF structure satisfying motions of MCP and PIP joint was proposed for exercising four fingers except the thumb. A hand F/E motion experiment was conducted to investigate general finger motions by normal people and determine the finger trajectory of the structure. The linkage structure design was optimized through the proposed optimization algorithm using the user's finger size and full ROM of the joint for effective exercise. Furthermore, a spring is introduced and installed at the structure to generate guiding forces when the patient's fingers have some deviated motion. Therefore, the spring plays a role of physical passive impedance and realize force control without a complex algorithm for force mode control. The transmitted torque by the spring at the MCP and PIP joint were investigated by finite element method (FEM). Consequently, the experiments using the proposed rehabilitation system for finger motions and force distribution was conducted for performance verification.

3.2 The Exoskeleton Design

The proposed hand exoskeleton should assist the F/E motion of the patient's fingers. Although four fingers except the thumb typically have 4 DOFs including 1 DOF of A/A motion, the A/A motion did not focused on this research to reduce the system size. Furthermore, since the DIP joint motion highly depends on the PIP joint motion, only the motions of the MCP and PIP joint were considered. Thus, the exoskeleton of simple linkage structure with a single motor was designed to help the patient's finger motions successfully.

Figure 3-1 shows how the linkage structure was designed for exercising F/E motions of the finger. The linkage structure should guide the both MCP and PIP joints simultaneously as shown in Fig. 3-1 (a). As the connecting links with the finger and the linkage structure and the linear motor located at dorsum of the hand were introduced, each phalange and the palm formed triangular plane as shown in Fig. 3-1 (b). The linear motor was used to control the motion of the linkage structure of the exoskeleton. Therefore, as the inclined angle of each plane is controlled by the linear motor, the angles of MCP and PIP joint were consequently controlled. Since the four-bar linkage has 1 DOF, the two four-bar linkages were designed to guide the MCP and PIP joint angles independently as shown in Fig. 3-1 (c). With this design, two actuators were required to uniquely define the finger posture. Thus, one joint angle at the proximal phalanx was fixed to decrease the structure DOF. Finally, the system has only 1 DOF, and the PIP joint angles were determined by the MCP joint as shown in Fig. 3-1 (d). The proposed design guarantee natural F/E motion of the MCP and PIP joint with the single actuator of 1 DOF.

The detailed structure design which consists of two four-bar linkages (green and blue linkages) is shown in Fig. 3-2. The angles of MCP and PIP joints were determined by the green and blue links, respectively. In addition, the bent link with the fixed angle is included in both green and blue links. The green link moves as the length of the motor stroke increases, which in turn affects the movement of the blue links. Therefore, since the bent link connects two four-bar linkage and determine the DOF of the linkage structure as 1, the MCP and PIP joint angles were simultaneously controlled by the motor stroke length.

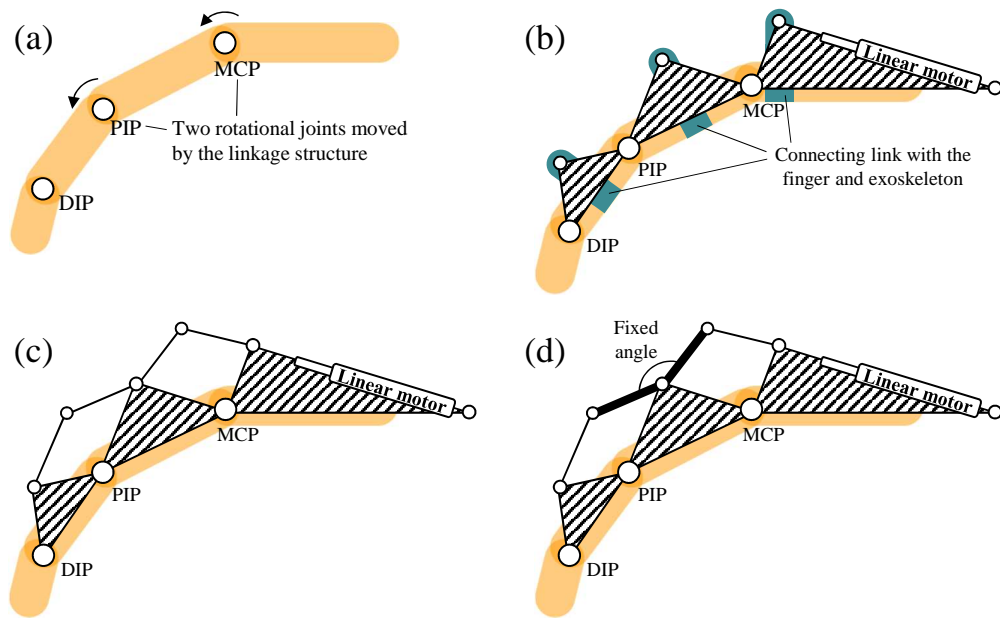


Figure 3-1: Proposed kinematic design

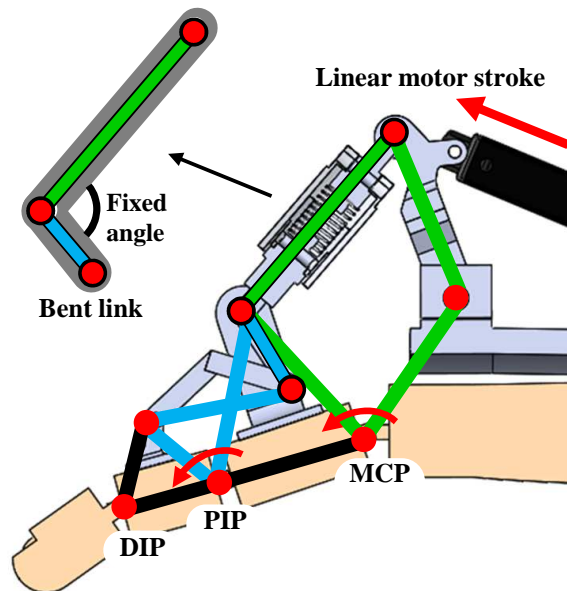


Figure 3-2: Kinematic scheme of the structure

3.3 Optimized Design Structure

3.3.1 Hand flexion/extension experiment

The hand rehabilitation system in this research is exercising the patient's impaired fingers with natural motions repetitively and intensively. Therefore, the research for the finger trajectory generated by the rehabilitation system is important issue during the design process of the exoskeleton structure.

Previous studies for finger motions were reviewed to investigate a suitable trajectory of the finger F/E motion. Kamper *et al.* studied the fingertip trajectory when the subjects grasped a variety of objects. [103] They found that the DIP joint angle shows linear relation to the PIP joint angle, however, there was no specific dependency between the MCP and PIP joints because the human can control two joints independently. Conti *et al.* captured the joint trajectory of a normal person and designed an exoskeleton for the hand following the normal person's trajectory [104]. In addition, Yang *et al.* researched a finger exoskeleton using the tendon mechanism based on the relationship between finger joints [105]. When a normal person moved the index finger, the researchers measured the angles of the three joints in F/E motion and investigated their relationships during motions. Since the finger joints were adapted to the size and shape of the objects for stable grasp, investigating the specific relationship between the angles of MCP and PIP joint during grasping various objects is difficult. Furthermore, since the most of people have their own habits according to the specific hand anatomy, it is hard to obtain the similar motions by many people. Therefore, many researchers were used one normal person's motion to design the finger trajectory of the rehabilitation structure, but it is difficult to verify whether the motion by only one person with the individual habit is good for the rehabilitation of the patient's finger. Thus, the hand F/E motion experiment by a variety of people was conducted to investigate the general relationship between the MCP and PIP joint angles.

First of all, five subjects with normal hands were participated in the hand flexion/extension experiment. They wore a finger motion measurement glove with inertial measurement unit (IMU) on right hand and flexed/extended the hand without specific motion instructions. After all subjects' movements were measured, the MCP and PIP joint angles were calculated separately.

Figure 3-3 shows the MCP and PIP joint angles during the hand flexion/extension without motion instructions. Although the curved fit was obtained using a first-order equation, the angle data

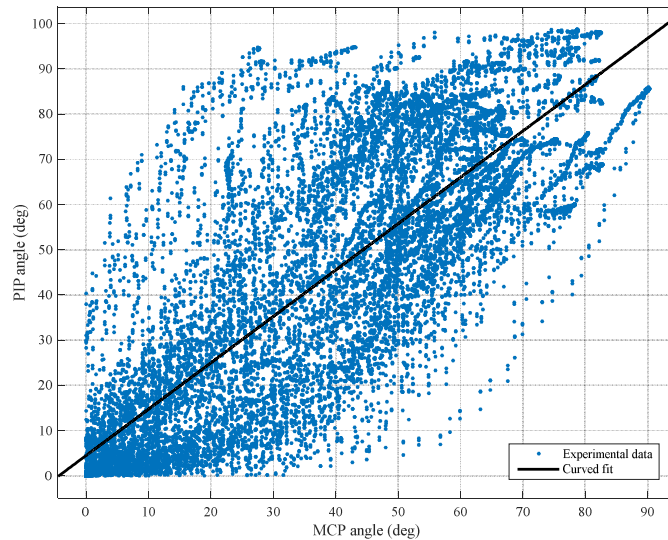
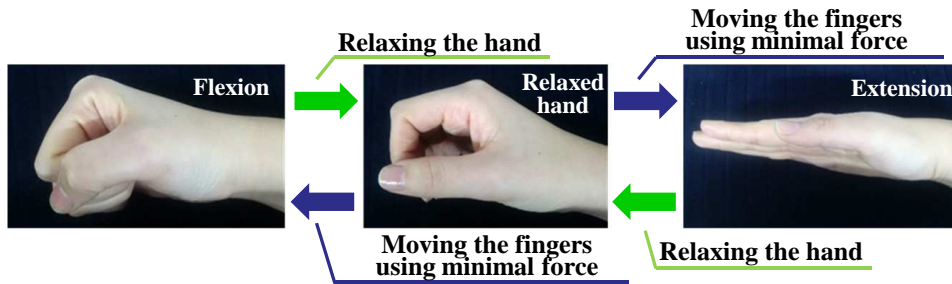


Figure 3-3: Hand flexion/extension experiment without motion instructions

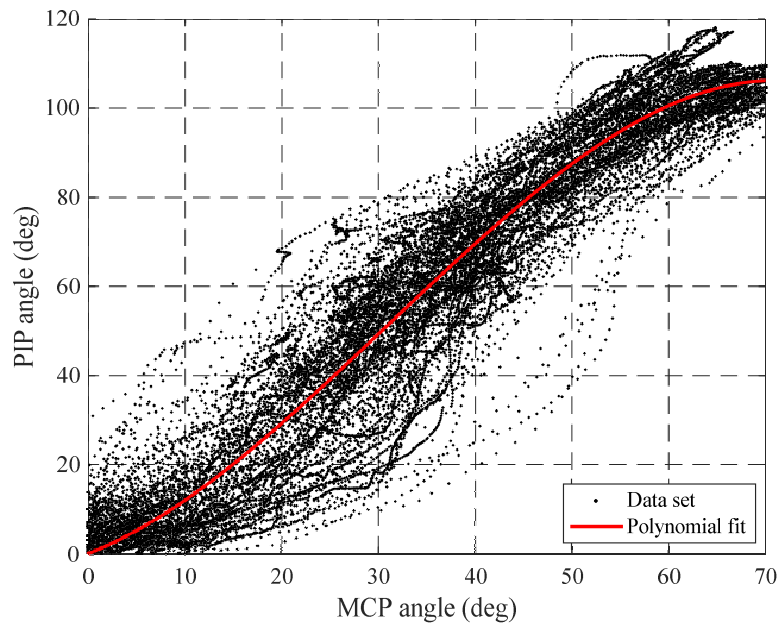
were distributed throughout the ROM of the MCP and PIP joints and did not follow the curved fit well. Since the MCP and PIP joints can move independently, the instructions to minimize the individual habits should be required. Therefore, a new experiment for measuring hand motions was conducted.

The subjects participated in this experiment should have followed the instruction described in Fig. 3-4 (a) to eliminate the effect of the individual habits when they grasped the fingers. The figure shows three postures of the hand: flexion, relaxed hand, and extension. The relaxed hand shows a partially flexed posture, induced by the passive recoil force generated by flexor digitorum profundus (FDP) [20]. To perform the grasping motion according to the instruction, the subject relaxed his/her hand from the flexion posture and made minimal force to move their fingers to the extension posture. By contrast, the subject with an extended hand relaxed his/her hand, then moved the hand to a flexion posture. By using the minimum force and natural contraction of the fingers, the potential for idiosyncratic motions was minimized. Therefore, by these instructions for hand F/E motion, the general finger motions with similar tendency were obtained although many subjects participated in the experiment.

In the hand F/E experiment, four subjects (aged: 25.3 ± 1.71 years) participated while following the given instructions. The subjects proceeded to flex/relax/extend their hands for 1 min per trial while attaching the markers for capturing the finger motions at the joints of the index finger. There were three trials with 1 minute rest between trials. The positions of the markers were captured by the motion capture system (Prime 13, Optitrack, USA) during the experiment and the finger joint



(a) Instructions for hand flexion/extension



(b) Relationship between MCP and PIP joint angles

Figure 3-4: Hand flexion/extension experiments

angles of the subjects were analyzed. All experiments were conducted with the approval of the institutional internal review board (IRB) (IRB approval number: UNISTIRB-17-23-A).

Figure 3-4 (b) presents the experimental results for MCP and joint angles performed by the subjects. The black dots and the red line represent the obtained joint angles by the subjects and its polynomial curve fitted to the experimental data, respectively. The polynomial fit followed the curvilinear trend and the finger motions by the subjects were distributed around the polynomial curve. Therefore, the equation for the obtained polynomial in the experiment was as follows:

$$y = -0.0004239x^3 + 0.0392x^2 + 0.8507x \quad (3.1)$$

where x and y are the MCP and PIP joint angles, respectively. The ROM by the subjects is presented in Table 3.1.

Table 3.1: The obtained ROM from the experiment

Joint	Range of motion (ROM)
MCP (°)	0 - 70
PIP (°)	0 - 106

3.3.2 Optimization Algorithm

The exoskeleton structure was designed considering the natural finger motion and the general hand F/E motion was obtained through the experiment by normal subjects. Thus, the parameters of the exoskeleton structure should be designed to satisfy the obtained hand motions.

Before the optimization of the design parameters, the obtained general hand motion should be adjusted to fit the user's hand. Since the rehabilitation exercise was conducted with a physical therapist and the exercise movement could not be measured, the representative hand motion trajectory has not been proposed. However, based on the hand anatomy, the MCP joint is firstly extended in the early stage of extension from fully flexed posture, and then, PIP and DIP joints are extended by EDC [20]. Furthermore, lumbrical and interosseous muscles are activated to help the extension of the PIP and DIP joints and prevent hyperextension of the MCP joint. This tendency is also captured in the hand F/E experiment. In addition, CPM system should guarantee the wide ROM because the rehabilitation system have to satisfy the user's full ROM [106]. Therefore, the polynomial fit was revised to guarantee the patient's individual ROM of the finger while maintaining the tendency between the angles of the finger joints.

To maintain the tendency between the joint relation while changing the joint ROM of the system, the measured joint trajectory from the experiment was expanded/contracted according the user's joint ROM. Thus, the polynomial fit equation from the experiment was changed by multiplying the joint angles by the ratio between the maximum ROM according to the experimental results and the user's maximum ROM. The revised MCP and PIP joint angles were expressed as x' and y' , respectively. Therefore, new equations were introduced as follows:

$$x = \frac{X}{X'}x', \quad y = \frac{Y}{Y'}y' \quad (3.2)$$

where X and Y represent the maximum MCP and PIP joint angles, respectively, according to the fitted polynomial equation, and X' and Y' represent the user's maximum MCP and PIP joint angles, respectively. The polynomial equation optimized to the patient's finger size and ROM was obtained by substituting (3.2) to (3.1).

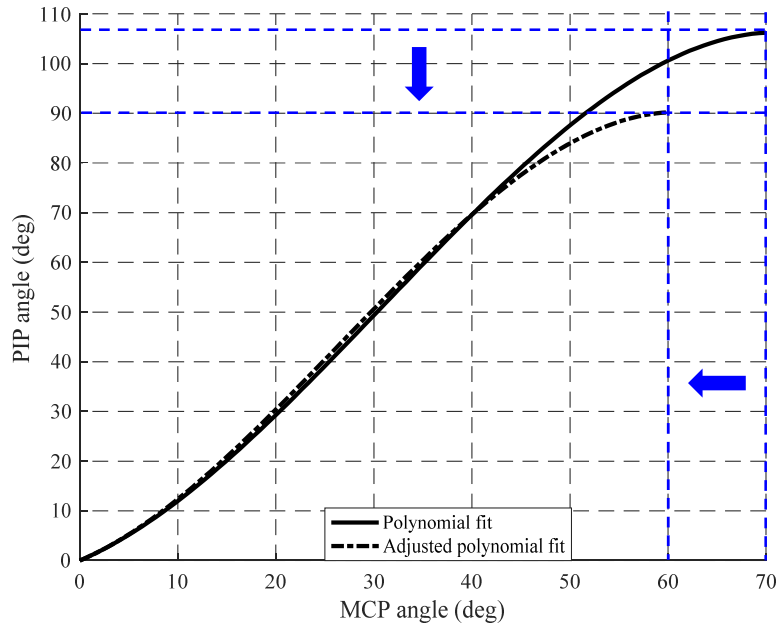


Figure 3-5: Adjusted joint relationship

Table 3.2: User information

Index finger	Length(mm)	Proximal phalanx	40
		Middle phalanx	24
	Range of motion (°)	MCP joint	0~60
		PIP joint	0~90

The user formation about the finger size and ROM is presented in Table 3.2. Since the maximum angles of the MCP and PIP joint were 60 ° and 90 °, the polynomial equation was changed using 3.2 as shown in Fig. 3-5. The adjusted polynomial equation was applied to optimize the design parameters of the linkage structure for each patient.

When a patient wore the exoskeleton system on the impaired hand, the finger motions by the exoskeleton have to satisfy the desired finger motions obtained through the adjusted polynomial. Therefore, the optimization algorithm of the design parameters should be studied.

The design parameters of the exoskeleton structure was shown in Fig 3-6. l_p and l_m are the phalange lengths of the patient’s finger, expressed in Table 3.2, and l_{act} is the length of the linear motor stroke. There are 19 parameters for 14 links ($l_1 \sim l_{11}$, l_b) and 5 angles ($\alpha \sim \epsilon$) in total; however, 9 independent parameters except the dependent and predefined parameters were used in the optimization algorithm. The design parameter vector used in the optimization algorithm was defined as follows:

$$l_i = [l_2 \ l_4 \ l_5 \ l_6 \ l_7 \ l_b \ l_{11} \ \alpha \ \epsilon] \quad (3.3)$$

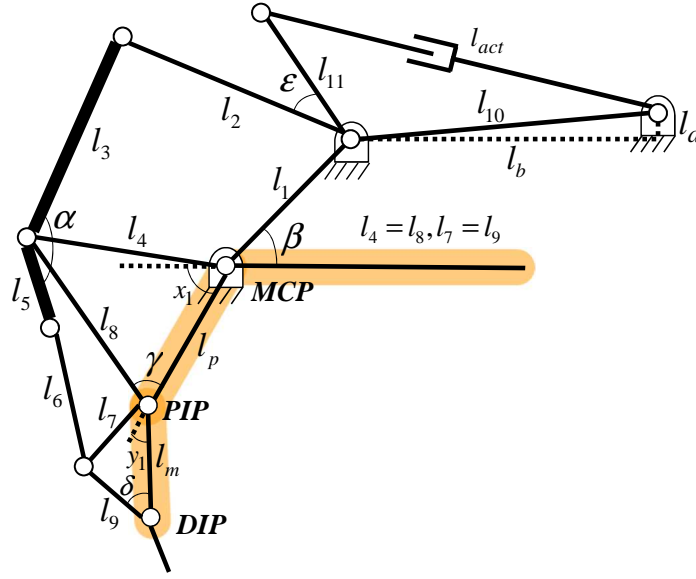


Figure 3-6: Design parameters of the exoskeleton structure

The vector l_i which produce the trajectory most similar to the desired trajectory is chosen as the optimized design parameter through the optimization algorithm. The difference between the exoskeleton trajectory by the vector l_i and the desired finger trajectory is described as a cost function of the optimization algorithm. Therefore, x_1 is the MCP joint angle of the linkage structure driven by the length of motor stroke l_{act} , and y_1 and r_1 are the PIP joint angle driven by the proposed structure and the desired angle of PIP joint, respectively. These parameters were described as functions of the design parameter vector l_i and the length of motor stroke l_{act} as follows:

$$\begin{aligned}
 x_1 &= f_{MCP}(l_i, l_{act}) \\
 &= \beta + \arccos\left(\frac{l_p}{2l_4}\right) + \arctan\left(\frac{l_2 \sin \psi}{l_1 + l_2 \cos \psi}\right) \\
 &\quad - \arccos\left(\frac{l_1^2 + l_2^2 + l_4^2 - l_3^2 + 2l_1 l_2 \cos \psi}{2l_4 \sqrt{l_1^2 + l_2^2 + 2l_1 l_2 \cos \psi}}\right) - \pi
 \end{aligned} \tag{3.4}$$

$$\begin{aligned}
 y_1 &= f_{PIP}(l_i, l_{act}) \\
 &= \arccos\left(\frac{l_m}{2l_7}\right) + \arccos\left(\frac{l_p}{2l_4}\right) + \arctan\left(\frac{l_5 \sin \omega}{l_8 + l_5 \cos \omega}\right) \\
 &\quad + \arccos\left(\frac{l_8^2 + l_5^2 + l_7^2 - l_6^2 + 2l_8 l_5 \cos \omega}{2l_7 \sqrt{l_8^2 + l_5^2 + 2l_8 l_5 \cos \omega}}\right) - \pi
 \end{aligned} \tag{3.5}$$

$$r_1 = g(x_1) = -0.0004239x_1^3 + 0.0392x_1^2 + 0.8507x_1 \tag{3.6}$$

where f_{MCP} and f_{PIP} are the functions for generating motion by the exoskeleton, and g is the

function to generate the desired trajectory. The angles ψ and ω were calculated as follows:

$$\psi = \epsilon - \beta + \arccos\left(\frac{l_{10}}{l_b}\right) + \arccos\left(\frac{l_{10}^2 + l_{11}^2 - l_{act}^2}{2l_{10}l_{11}}\right) \quad (3.7)$$

$$\omega = 2\gamma - \alpha + \arccos\left(\frac{l_1^2 + l_2^2 - l_3^2 - l_4^2 + 2l_1l_2 \cos \psi}{2l_3l_4}\right) \quad (3.8)$$

Since the joint ROM of the user should be considered to optimize the finger trajectory by the structure, y_2 and r_2 are the PIP joint ROM by the structure and the desired ROM, respectively. They are also included in the cost function.

$$y_2 = [\min(y_1) \quad \max(y_1)] \quad (3.9)$$

$$r_2 = [\min(r_1) \quad \max(r_1)] \quad (3.10)$$

Therefore, the cost function is expressed by the difference of the finger trajectory between the exoskeleton by the design parameter vector and that of the desired motion as follows:

$$y = [y_1 \quad y_2]^T \quad (3.11)$$

$$r = [r_1 \quad r_2]^T \quad (3.12)$$

$$z = [w_1 \quad w_2][y - r] \quad (3.13)$$

$$J = z^T z \quad (3.14)$$

where w_1 and w_2 are weight factors for the joint angles and the ROM, respectively, and J is the cost function of the design parameter vector. The optimized design parameter for maximally satisfying the desired trajectory was determined by finding the design parameter vector with the minimum cost.

The flowchart of the optimization algorithm for design parameters is shown in Fig 3-7. Since the cost function is a multivariate nonlinear equation, a numerical method was used to investigate the optimized vector for the design parameters. First of all, the available ranges of the design parameters were determined considering the finger size. To avoid the interference between the exoskeleton structure and the finger, the collision between the exoskeleton and the finger was considered in the most flexed posture where the interference occurs easily. Thus, the cost of the design parameter is calculated when the interference problem does not exist. After investigating all variable vectors, the design parameter vector with the minimum cost was chosen as the optimized design structure.

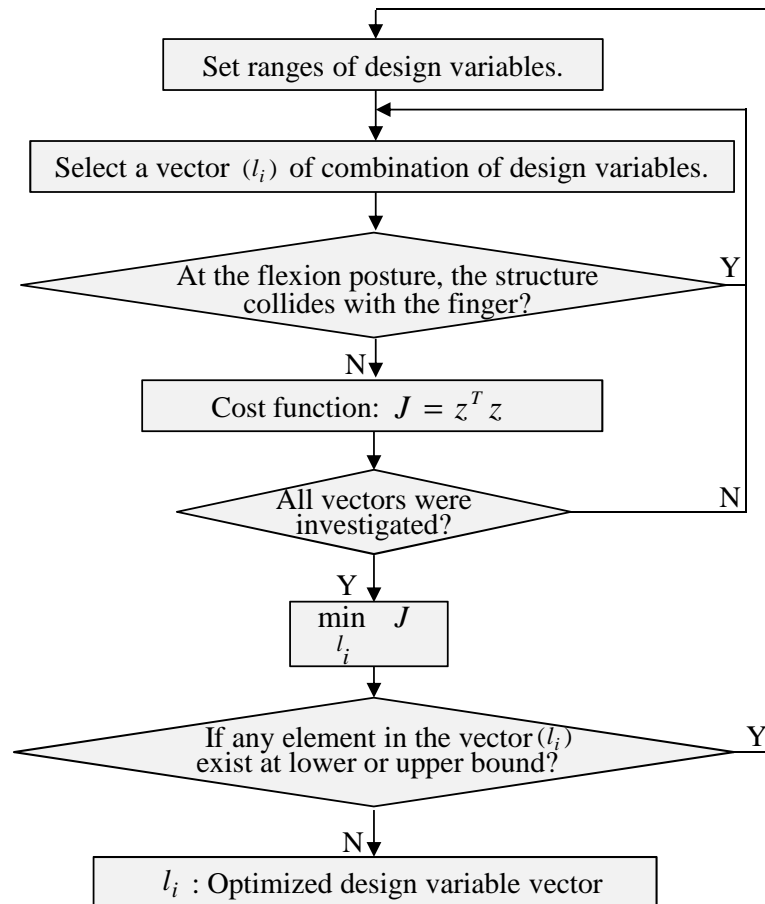


Figure 3-7: Flowchart of the optimization algorithm

Table 3.3: The optimized design vector

Variable	l_2	l_4	l_5	l_6	l_7	l_b	l_{11}	α	ϵ
Value	66 mm	54 mm	35 mm	39 mm	23 mm	93 mm	34 mm	132 °	33 °

However, if any elements of the design vector was at the lower or upper bound of the range, the design parameter ranges were reconsidered. Consequently, the optimization process is conducted again until the optimized design parameter vector with a local minimum cost is obtained.

The optimized design parameters are shown in Table. 3.3. The ratio of l_2 and l_{11} connected to the same joint is highly related to ROM of the exoskeleton with the limited motor stroke l_{act} . Therefore, the length of l_2 was determined to be about twice of the length of l_{11} to generate full joint ROM using the small length of the motor stroke (30 mm). Furthermore, since the human generally has longer proximal phalange length than the middle phalange length,, the links l_5, l_6 , and l_7 forming a 4-bar linkage around the PIP joint are shorter than the links l_2 and l_4 around MCP joint. The length of l_b is determined as 93 mm to put the system on the dorsum of the hand. The angles

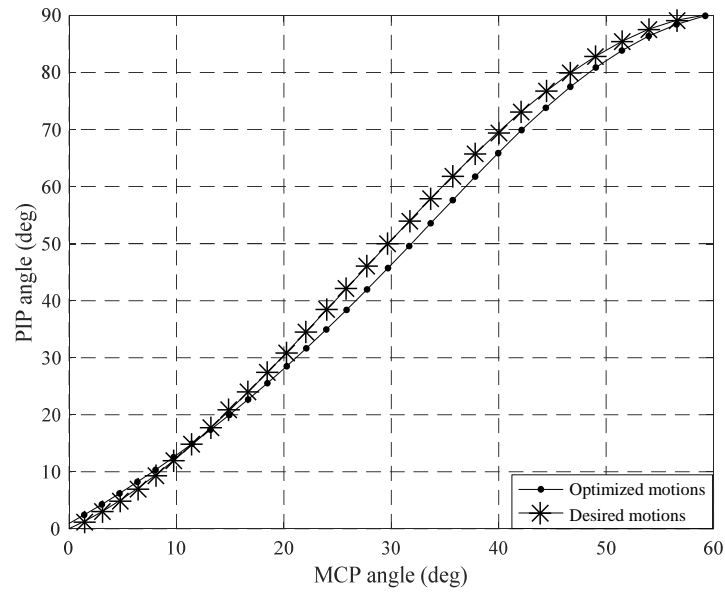


Figure 3-8: Optimized finger motions

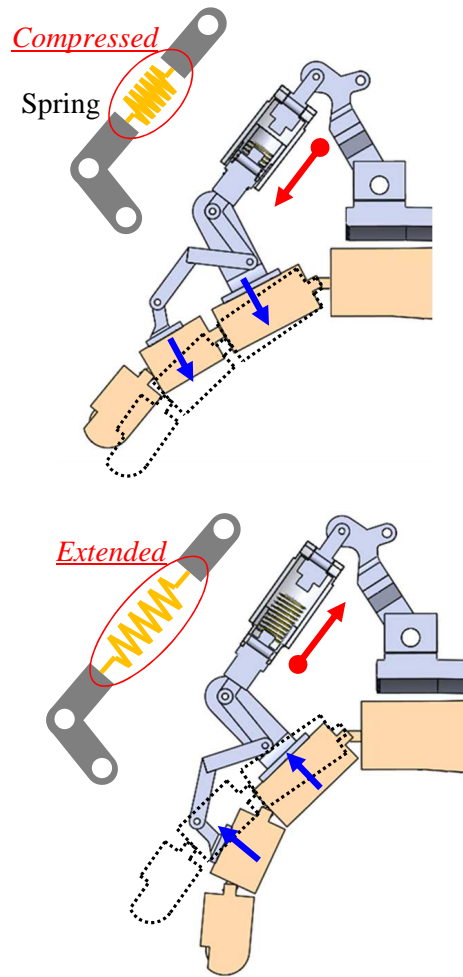
α and ϵ influence on not only the relationship between the angles of the MCP and PIP joints but also the starting angle of MCP joint, respectively. Thus, they were defined to maximally satisfy the desired joint relation and ROM through the optimization algorithm.

In the Fig. 3-8, finger joint angles by the obtained exoskeleton structure through the optimization algorithm were compared with those of the desired trajectory. The curve with stars is the desired joint trajectory by the adjusted polynomial, and the curve with dots is the joint angle obtained using the optimized exoskeleton structure. As shown in the figure, the finger motions generated by the exoskeleton were very similar to the desired motions. Thus, it is verified that the exoskeleton structure obtained by the optimization algorithm guides the fingers to the general finger motions successfully. The proposed design and the optimization algorithm could make the CPM system to perform F/E exercises of the user's fingers.

3.3.3 Spring mechanism

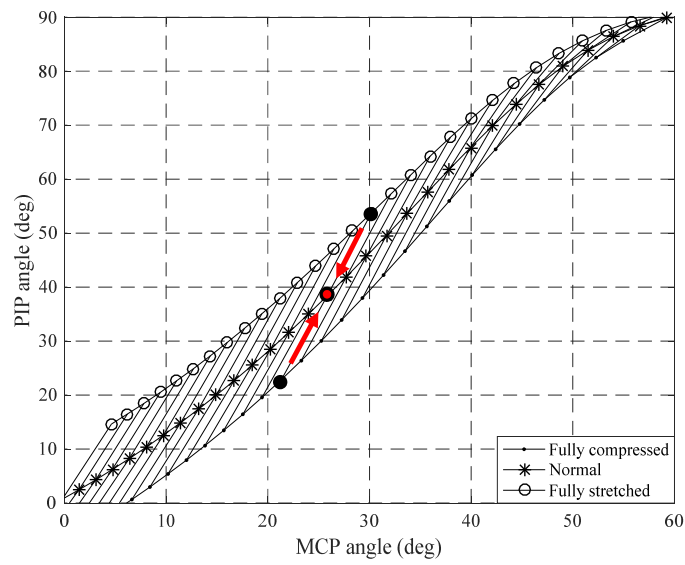
Most of the CPM systems were developed to make the user's fingers just follow the given circular trajectory using the position control [14, 107].

However, in case of surgery or accident patients, since the joint stiffness varies depending on the rehabilitation period, it is necessary to control the force feedback according to the patient's condition. Therefore, an elastic element as a passive impedance, i.e., spring, was introduced in the proposed CPM device; the generated force by the spring guides the fingers which have deviated

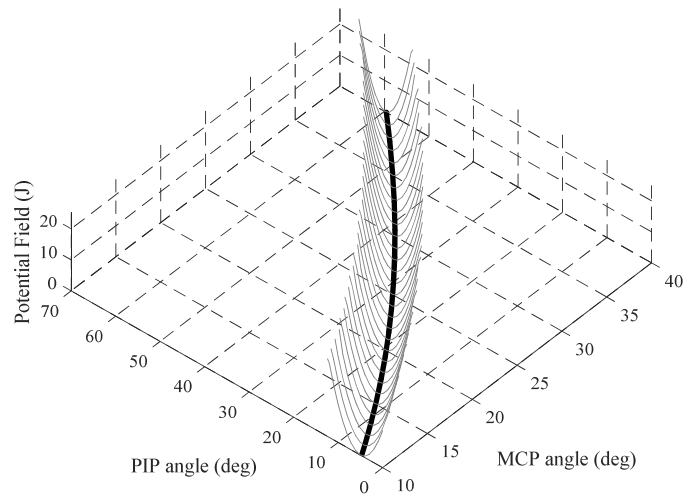


- : Desired posture
- : The direction of the spring force
- : The guidance force to the desired posture

Figure 3-9: Spring mechanism



(a) Joint angles of the fingers



(b) Potential field (gray lines: potential field, thick line: desired joint trajectory)

Figure 3-10: Deviated postures from the desired trajectory

motion from the desired posture. With the spring mechanism installed in the linkage structure, the guiding force is generated without a complex force control algorithm.

A spring was installed to the bent link, as shown in Fig. 3-9. When the user's fingers extend farther than the desired posture, the spring is compressed and the spring force is delivered in the extension direction to make the fingers move to the desired posture. Moreover, the guidance force can be easily calculated by a potentiometer measuring the deflected length of the spring without a large force sensor.

The magnitude of the guiding force is defined by not only the deflected length of the spring but also the stiffness of the spring. Since the spring constant is also an important factor to determine the magnitude of the spring force, determining appropriate spring constant is required. The spring of the exoskeleton structure was manually designed to generate a maximum force of 12 N when the angles of the MCP and PIP joint were deviated from the desired joint angles, by averages of 5 ° and 15 °, respectively. According to the patient's condition, the stiffness of the spring for the rehabilitation system can be easily adjusted by changing it with the spring with different stiffness.

The available finger postures according to the spring deflection is shown in Fig. 3-10 (a). The line-patterned area presents the available finger joint angles by the exoskeleton structure with the spring mechanism. The curve with the stars presents the finger joint angles when the spring is in normal length, and also, the curves with the circles and dots present the finger joint angles in case of the fully compressed and stretched spring, respectively. Therefore, the user's fingers are automatically returned to the desired posture from the deviated posture along the lines (in the direction of the red arrow).

The spring mechanism installed in the structure can be considered as a physical impedance mechanism [108]. One of the most widely known methods for calculating the impedance is the potential field, and the gradient of the potential field is considered as the impedance [109, 110]. In addition, the potential field is calculated using the spring force around the desired trajectory of the finger joint. The positions x_H and x_M are assumed as the end-point of the spring according to the posture of the fingers and another end-point of the spring obtained using the stroke length of the linear motor, respectively. The potential field by the spring was determined as a quadratic function of the difference between x_H and x_M as following:

$$P = \frac{1}{2}k(x_M - x_H)^2 \quad (3.15)$$

where k is the parameter of the quadratic function. By differentiating (3.15), the impedance force, F , determined in (3.16) is obtained as following:

$$F = -k(x_M - x_H) \quad (3.16)$$

The parameter k can be interpreted as a spring constant. The negative sign means that the spring force is applied in opposite direction to the deviated motion. Figure 3-10 (b) shows the potential field of the spring force; for clear expression, the area where the angle of the MCP joint is $10\sim 40^\circ$ was enlarged. As the finger postures deviates from their desired posture, the guiding force increases depending on the gradient of the potential field.

3.3.4 Force distribution analysis

The transmitted spring forces to finger joints are proportional to the deviated motions of the finger. Therefore, to investigate how the generated force by the spring is distributed to each joint, the distribution analysis of the force was conducted. A free body diagram of the exoskeleton structure was shown in Fig. 3-11 (a). The force F_s presents the force of the spring installed in the bent link and the force F_n presents the applied force to each rotational joint according to the link number. The numbers in the square indicate the required links for force distribution analysis. The transmitted moments to the MCP and PIP joints are denoted as M_{MCP} and M_{PIP} , respectively.

Since the bent link in the exoskeleton structure is an indeterminate linkage, finite element method (FEM) was used for analysis of the force distribution. The equations for FEM were derived based on the principle of minimum potential energy [111]. The equation of the spring force was given in (3.16) using the spring constant and the deflected spring length. The links in the structure were described as stiff bodies depending on the Young's modulus (E), cross-sectional area (A), length (L), and moment of inertia (I). The displacement (u, v) and slope (q) of the joint is changed by the distributed forces through the stiff bodies were obtained as follows:

$$[K][Q] = [F] \quad (3.17)$$

where K is the stiffness matrix of the links, Q is the displacement and slope vector of joints, and F

is the force vector. Each matrix and vector can be presented as following:

$$K = [f(E, A_i, I_i, L_i)], \quad i : \text{structure link} \quad (3.18)$$

$$Q = [u_j \ v_j \ q_j \ \dots]^T, \quad j : \text{rotation joint} \quad (3.19)$$

$$F = [F_s \ F_u]^T \quad (3.20)$$

where F_s is the spring force, and F_u is unknown forces transmitted to the joints. The matrix M was introduced to combine all the unknown variables (unknown displacements (Q) and forces (F_u)) into one vector, and then solve the resulting equations using linear algebra. Therefore, the above equation can be rewritten as follows:

$$\begin{bmatrix} K & M \end{bmatrix} \begin{bmatrix} Q \\ F_u \end{bmatrix} = \begin{bmatrix} F_s \\ 0 \end{bmatrix} \quad (3.21)$$

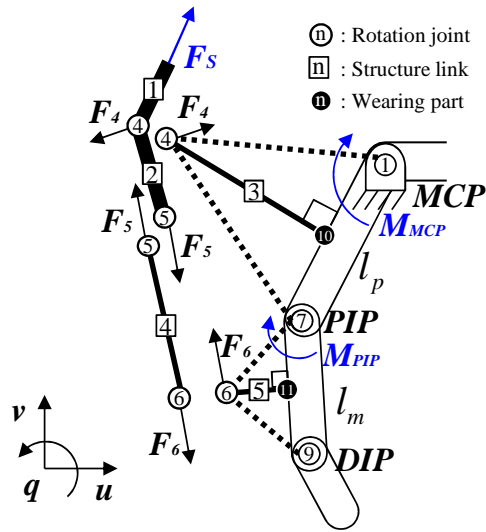
$$\begin{bmatrix} Q \\ F_u \end{bmatrix} = \begin{bmatrix} K & M \end{bmatrix}^{-1} \begin{bmatrix} F_s \\ 0 \end{bmatrix} \quad (3.22)$$

Using these equations, the unknown displacements and forces can be obtained. Furthermore, the applied moment to each joint is calculated using the transmitted force to each phalange as following:

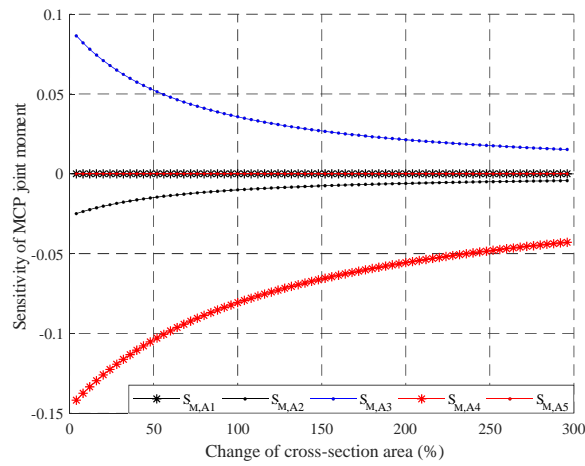
$$\overrightarrow{M_{MCP}} = \overrightarrow{l_{10 \rightarrow 1}} \times \overrightarrow{F_{10}} \quad (3.23)$$

$$\overrightarrow{M_{PIP}} = \overrightarrow{l_{11 \rightarrow 7}} \times \overrightarrow{F_{11}} \quad (3.24)$$

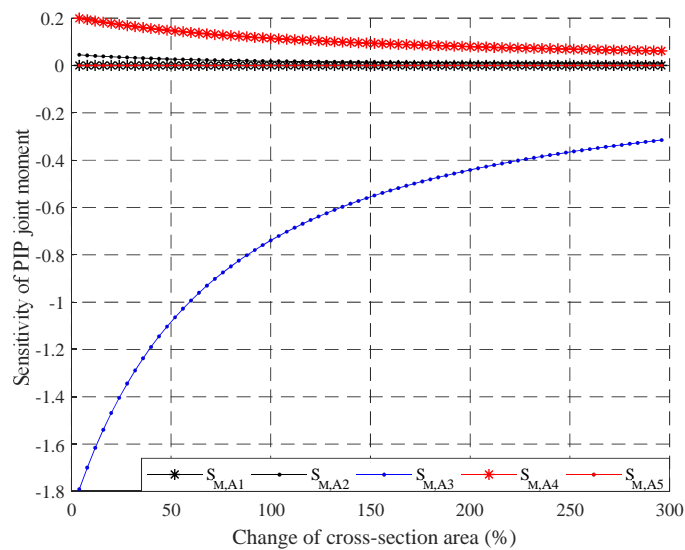
The transmitted moments were affected by stiffness of the links by Young's modulus, link length, cross-sectional area, link inertia. The links were typically made using the same material and the link lengths were determined by the optimization algorithm, and also the link inertia depends on its length and the cross-sectional area. Therefore, the cross-sectional area of the links is the only independent design factor to adjust the transmitted torque at the joints. Consequently, the sensitivity of the transmitted moment at the joint due to the cross-sectional area of links were calculated to evaluate the effect of the cross-sectional area for force distribution analysis. The joint moment sensitivity can be calculated by the changed amount of the moment due to the changed



(a) Free body diagram

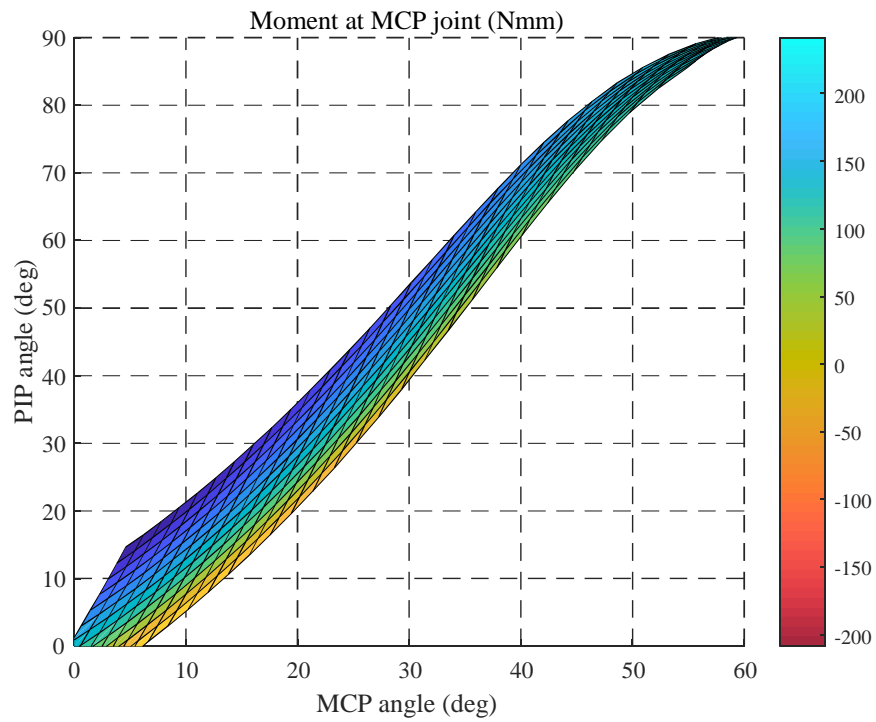


(b) Sensitivity of the force at MCP joint (A_n : Cross-section area of link n)

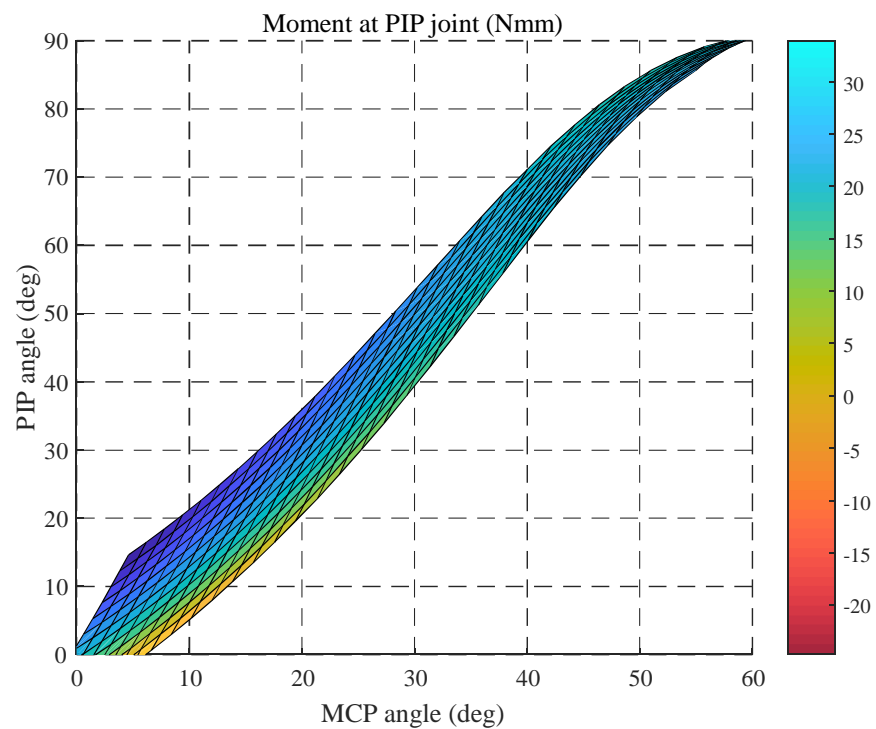


(c) Sensitivity of the force at PIP joint

Figure 3-11: Force distribution analysis



(a) Moment at MCP joint



(b) Moment at PIP joint

Figure 3-12: Applied Moment at MCP and PIP joint

cross-sectional area of link as following:

$$S_{M,A_n} = \frac{\Delta M/M}{\Delta A_n/A_n} \quad (3.25)$$

where M is the transmitted joint moment, and A_n is the cross-sectional area of link n .

Fig. 3-11 (b) and (c) show the sensitivity of the moment transmitted to the MCP and PIP joints, respectively. The figure present the joint moment sensitivity as the cross-sectional area of the chosen link varies from 9 mm^2 to 36 mm^2 while that of other links are constant as 9 mm^2 . The transmitted moment to the joints were influenced by only the links 2, 3, and 4. Especially, the transmitted moment at the PIP joint is reduced dramatically as the cross-sectional area of link 3 increases and that of link 4 decreases. It is because the link 3 and 4 are longer than other links and their inertia were dramatically varied by changing the cross-sectional area. As the link 3 gets thicker, the inertia of the structure around MCP joint increases, which increases the transmitted moment to the MCP joint. Similarly, the transmitted moment to the PIP joint is highly dependent on the thickness of link 4. Therefore, the link 3 was designed to be slim, while ensuring that it supports the exoskeleton structure, and link 4 was made thicker while making sure not to increase the system size. The finger structure was manually designed to distribute the spring force to each joint by adjusting the cross-sectional area of each link.

Fig. 3-12 (a) and (b) present the transmitted MCP and PIP joint moments by the proposed exoskeleton structure in the compressed or stretched spring condition. The negative value means that the applied joint moment is in the extended direction and vice versa. The moment is transmitted up to 230 Nmm for the MCP joint and up to 35 Nmm for the PIP joint. As the middle phalanx is more flexed than the proximal phalanx due to the PIP joint, the PIP joint moment is much smaller than the MCP joint moment.

3.4 Performance Evaluation

3.4.1 Implementation of the exoskeleton system for the hand

Figure 3-13 shows a prototype of the proposed exoskeleton for exercising hand F/E motion. The system can guide F/E motion of four fingers except the thumb as a mitten. The rigid frame for connecting four finger and the structure has a silicon layer to compensate the thickness and height difference between phalanges. Furthermore, the silicone belt was used to fasten the fingers easily.

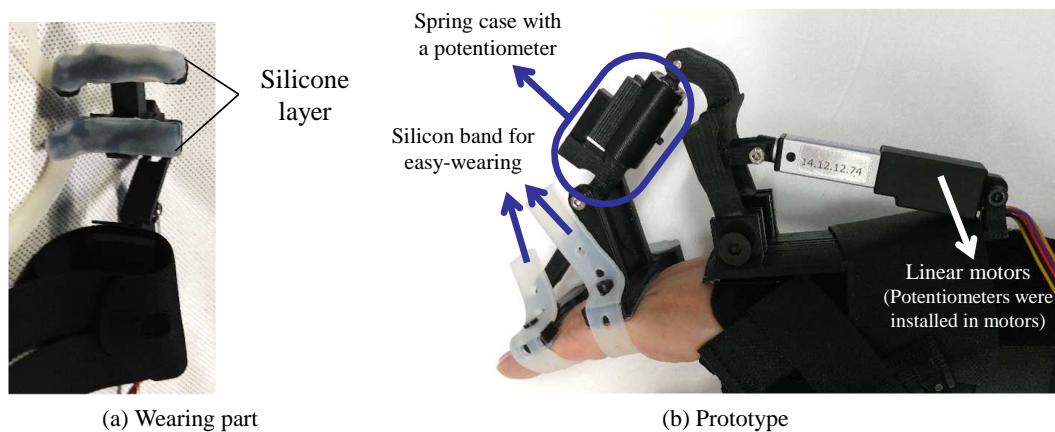


Figure 3-13: Prototype of the system

The whole system was actuated by only one linear motor for light weight and high portability. Additionally, a potentiometer embedded in the actuator measures the length of the motor stroke for estimating posture of four fingers.

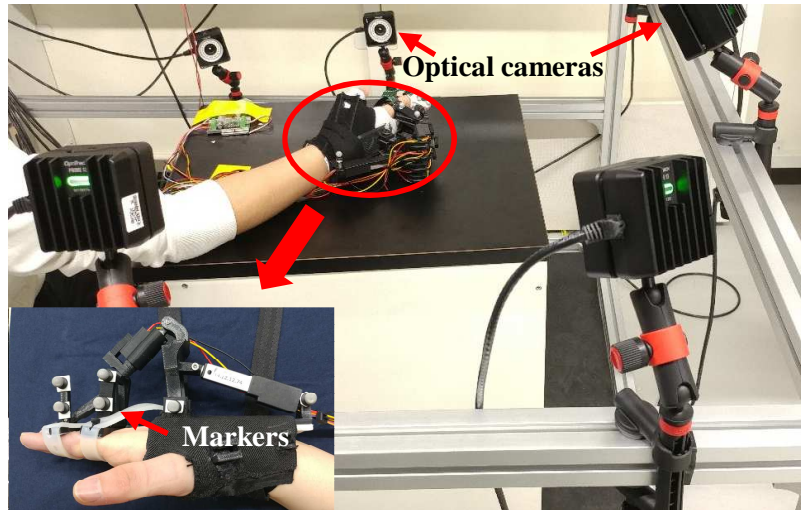
A spring installed in the bent link can produce the guiding force for four fingers. The magnitude of the spring force is calculated by the deflected length measured by a potentiometer attached on the spring case.

A linear motor with small size was attached on the dorsum of the hand for guiding the fingers (L12-P, Actixon, Canada [63]), and the exoskeleton structure was manufactured by 3D printing technology. The dimensions of the device are $120 \times 195 \times 78 \text{ mm}$, and the weight including the motor, is 156 g .

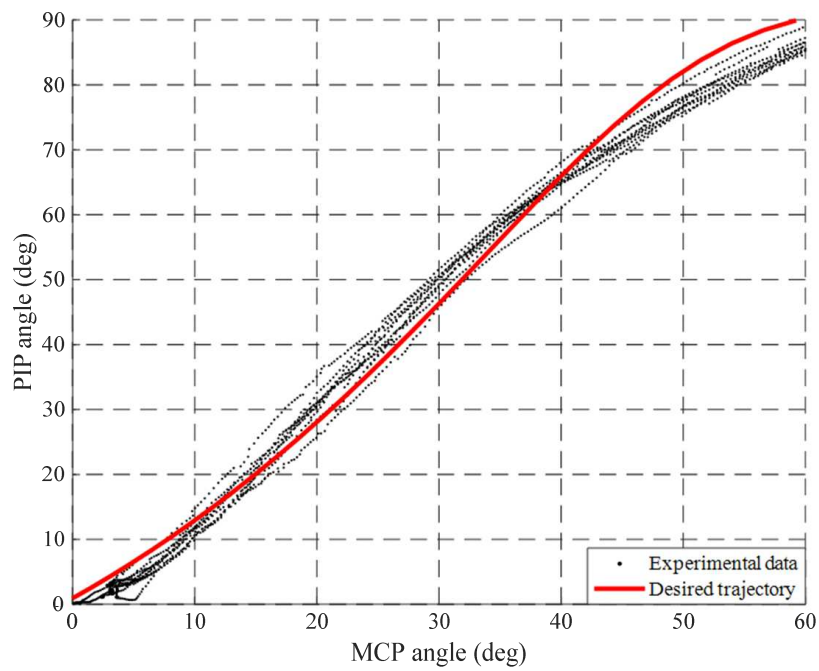
3.4.2 Finger Motion Experiment

The experiment for finger motions were conducted to verify the performance to guide the user's fingers. A subject without any muscle impairment wore the proposed exoskeleton system on the right hand and relaxed the hand during the experiment. The exoskeleton system which is optimally designed to the subject guided the relaxed hand along with the determined trajectory through the exoskeleton design process. The experimental setup for measuring the joint motions of the user's fingers is shown in Fig 3-14 (a). The markers for the motion capture system was attached to the exoskeleton structure and the joint angles of the user's fingers were measured.

Figure 3-14 (b) shows finger joint motions guided by the proposed exoskeleton. The red dots are joint trajectory of the subject's fingers, and the solid curve is the desired exoskeleton trajectory. The joint trajectory of the subject's fingers were very similar to the desired exoskeleton trajectory



(a) Experimental setup



(b) Experimental result

Figure 3-14: Experiment of finger motion

Table 3.4: Force distribution experiment

Spring condition	Desired posture (°)		Given posture (°)		Joint moment (Nmm)			
	MCP	PIP	MCP	PIP	FEM		Experiment	
					MCP	PIP	MCP	PIP
4 mm stretched (12 N)	8.1	10.4	12.7	25.0	190.2	19.4	183.7	14.4
	16.7	22.7	21.2	37.9	162.9	12.8	154.8	10.6
	25.8	38.4	30.2	53.8	123.6	5.3	117.1	4.2
4 mm compressed (12 N)	16.7	22.7	12.0	7.9	-219.3	-27.8	-214.1	-24.0
	25.8	38.4	21.3	22.9	-194.1	-20.4	-174.3	-17.2
	35.7	57.6	31.4	42.2	-152.8	-10.7	-143.1	-7.1

with 5 ° deviated angle maximally. The figure shows that the exoskeleton system for the hand can guide the patient’s fingers effectively along with the desired exoskeleton trajectory.

3.4.3 Force Distribution Experiment

The force distribution analysis by FEM was experimentally verified by comparing the simulated joint moments to the delivered joint moments of an artificial joint hand. The artificial hand with the exoskeleton structure is shown in Fig 3-15. When the spring is in normal state and the motor maintain the constant stroke length, the posture of the artificial hand is same with the desired posture. Thus, the transmitted moments to the MCP and PIP joints are zero. However, when the spring is deflected, the joint moment by the spring force is applied according to the deviated motion of the fingers. In this experiment, the joint angles of the artificial hand were maintained to deflect the spring by 4 mm with the constant length of the motor stroke. Therefore, the fixtures to maintain the determined angles of the artificial hand were manufactured and attached to the joints of the artificial hand. Therefore, the spring generated the force and the transmitted moments to the MCP and PIP joints were measured by a torque sensor.

The transmitted joint moments at MCP and PIP joints in the force distribution experiment were compared to those obtained by FEM analysis as shown in Table 3.4. The joint moments obtained by FEM analysis and the experiment show similar value. Therefore, it was validated that the transmitted moments can be successfully estimated by FEM analysis and designed by adjusting the cross-sectional area of the links. Through the performance experiment for finger motions and force distribution shows that the proposed hand exoskeleton system can guide the patient’s fingers along with the desired finger motions and distributed the expected joint moments.

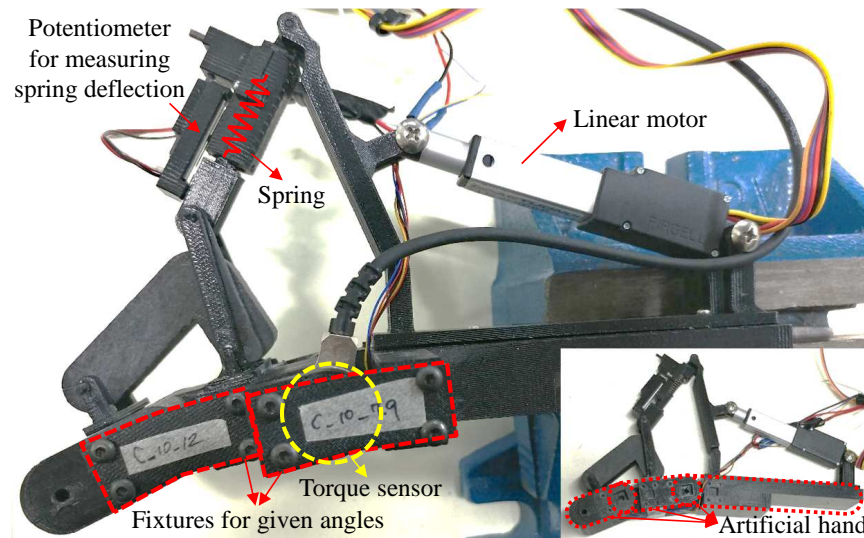


Figure 3-15: Experimental setup

3.5 Summary

In this chapter, an exoskeleton for exercise of hand F/E motion with high portability was proposed. The exoskeleton structure for MCP and PIP joint motion consists of two four-bar linkage connected to a bent link for 1 DOF actuation. The finger motions by several subjects were obtained by the hand F/E experiment to investigate general finger motion. In addition, the design parameters of the structure were determined through the optimization algorithm to maximally satisfy the desired finger trajectory based on the user's finger size, joint ROM, and the general finger motion. A spring, as a passive physical impedance, was installed at the structure to generate the guiding force for exercising the fingers; the magnitude of spring force depends on the finger's deviated motions from the desired posture. The transmitted moment to the MCP and PIP joints were estimated by FEM analysis and the cross-sectional area of the links were manually design considering the expected joint moments. Therefore, the prototype of the hand exoskeleton system with consideration of high wearability and portability was manufactured and experimentally verified. The finger motion experiment shows that the hand exoskeleton system guided the fingers well as desired and help the patient to exercise general motions of the fingers. The experiment for force distribution using the artificial hand verified that the transmitted moments to the MCP and PIP joints in the experiment were similar to the expected moments from FEM analysis. Therefore, the proposed device guides the patient's fingers along with the desired finger motions and distributed the expected moments to the joints from FEM analysis.

Chapter 4

Conclusion

4.1 Wearable Hand Exoskeleton Systems for Virtual Reality

In this chapter, a wearable hand exoskeleton featuring force-controllable actuator modules was developed. The linkage structure (with 3 DOF and a large ROM) was inspired by a study of finger anatomy. The fingertip workspace of the linkage structure was kinematically evaluated and compared to that of the functional ROM. As the structural workspace permits a ROM that is 90% of the natural value, the user can employ diverse postures when interacting with objects. The actuator modules employ an SEA mechanism (an actuator and an elastic element). The spring was manually designed to impart the required stiffness to the actuator module. The contact forces arising when subjects grasped objects were measured to determine the maximum force imparted by the actuator. Motor friction was eliminated by using a friction compensation algorithm to linearize the motor, and a DOB was employed to afford accurate force control even during motion. As the compact actuator modules are attached to the hand dorsum, the user can move both the hand and arm freely. The actuator module accurately generated the desired forces when the fingers were stationary or engaged in arbitrary motion. However, the normal fingertip force was smaller than the real-world value because of drastic changes in fingertip direction as the finger is flexed.

In addition, a wearable exoskeleton allowing measurement of finger motion and force feedback during engagement with VR was developed and verified in terms of user experience. The structure is worn only on the fingertips and palm; wearability is thus high and full, natural finger ROM is ensured. By using the proposed finger motion measurement algorithm, the system accurately measured 5 DOF thumb motion and 4 DOF motions of the index and middle fingers after a single calibration, unlike earlier systems.

To explore user experience (UX), the evaluation framework reflected the characteristics of the system; I used a questionnaire to capture the opinions of the subjects in terms of usability and utilitarianism; responses were scored using a 7-point Likert scale. The mean satisfaction score was 5.87/7; most subjects had a positive opinion of the system and many considered that learnability was excellent. In addition, as the system allows users to engage with the VR via intuitive control and feedback methods, satisfaction in terms of functional design was high. Negative aspects that were cited included the heavy and uncomfortable nature of the system, and the force feedback sensation not reflecting the 'feel' of real objects.

4.2 A Wearable Spring-guided Hand Exoskeleton for Continuous Passive Motion

In this Chapter, a highly portable exoskeleton facilitating hand F/E exercise was developed. The exoskeleton permitted MCP and PIP joint motion and included two four-bar linkages connected to a bent link; actuation allowed for 1 DOF. The finger motions of several subjects were analyzed. In addition, design parameters were optimized using an algorithm that considered the desired finger trajectory based on user finger size, joint ROMs, and general finger motion. A spring affording passive physical impedance was installed to generate the forces guiding finger exercise; the spring force depended on the extent of finger deviation from the desired posture. The moments transmitted to the MCP and PIP joints were estimated via the FEM and the link cross-sectional areas were manually designed by reference to these moments. A highly wearable and portable prototype was experimentally evaluated. The experiment showed that the exoskeleton guided the fingers as desired, and aided exercises that improved overall finger motion. The experimental force distribution over an artificial hand showed that the moments transmitted to the MCP and PIP joints were similar to those expected from FEM analysis. Therefore, the device guides the patient's fingers, achieves the desired finger motions, and distributes appropriate moments to the joints.

4.3 Open Issues

Overall, finger motion measurement was excellent and user feedback was positive. However, the force feedback does not 'feel' identical to real-world feedback because of zero impedance and the feedback direction. The most dominant reasons for degraded force feedback are zero impedance

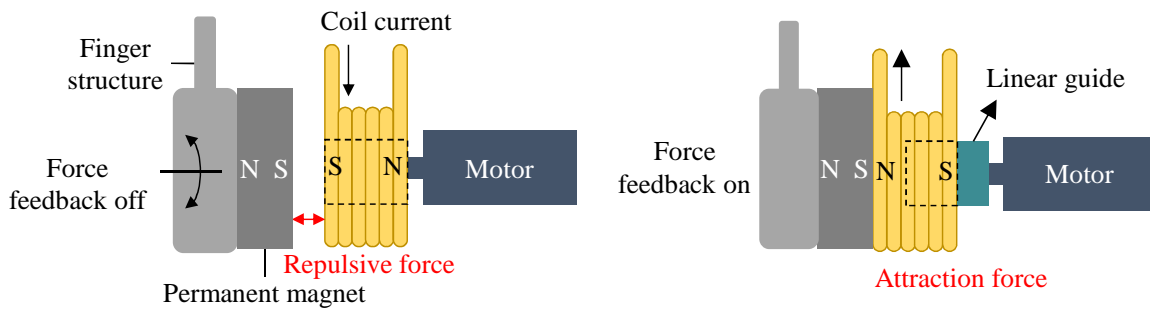


Figure 4-1: Magnetic clutch mechanism

performance and direction of the force feedback.

4.3.1 Zero Impedance Performance

To address the zero impedance issue, a complex, robust control algorithm was applied. However, the algorithm only minimizes actuator friction; perfect zero impedance is not attained. When the user interacts with the VR environment (e.g., during a game or in a training situation), fingers are typically simply moved rather than used to pick up objects. Therefore, it is important to attain zero impedance when transmitting various forces.

However, most previous studies regarded zero impedance as a form of force feedback. As zero impedance was not perfectly implemented using the control algorithm, we added an additional mechanism. In a simple braked system, zero impedance is easily realized by disengaging the clutch, but forces cannot then be delivered. On the other hand, a current-controlled actuator accurately generates forces but the zero impedance performance is worse than that of a brake. Therefore, by combining a brake and a current-controlled actuator, the actuator module can attain high-level zero impedance and generate various forces, as shown in Fig. 4-1. A magnetic clutch was created, and a permanent magnet and coil were used to engage/disengage the current-controlled motor to vary the type of force feedback given. When the impedance is zero, the coil current creates an attractive force and the current-controlled motor varies the strength of that force. If force feedback is off, the coil current is applied in the reverse direction, creating a repulsive force, and the motor is disengaged to afford zero impedance, such that the user feels only the inertia of the physical device. Thus, users do not become fatigued when using the haptic system, and can interact comfortably with the VR environment for many hours.

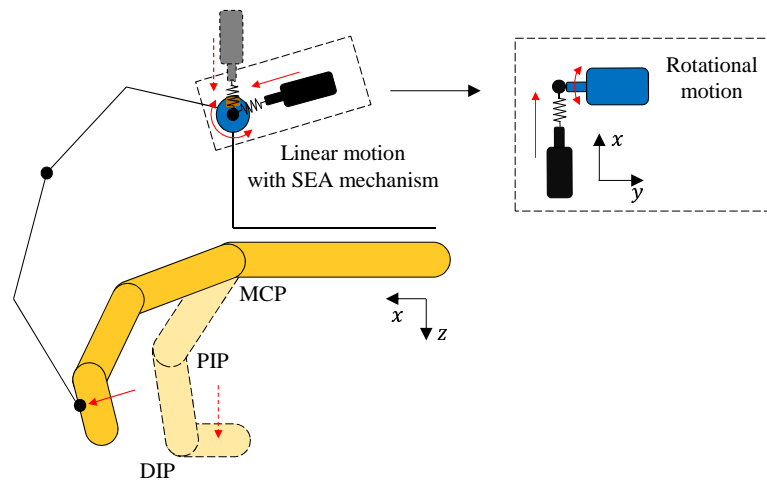


Figure 4-2: The mechanism for various force direction

4.3.2 Direction of the Force Feedback

When we grasp an object in real life, we generally receive a force normal (perpendicular) to the direction to the fingertip. Immersion in a virtual environment cannot be achieved if the direction of force feedback from the VR system differs from that in the real world. However, as the areas around all hand joints available for actuator placement are limited, the force feedback modules are attached to the hand dorsum in most hand exoskeletons, and torque generated by the actuator is transmitted to the fingertips via finger-like structures. Thus, the user does not perceive a normal force at the fingertips, but rather a force from the back of the hand such as that used to pull a finger away from an object. In the developed system, the direction of force created by the feedback actuator is changed; the actuator always imparts normal forces to the fingertips, thus reflecting reality.

Figure 4-2 shows the actuator module used to transmit forces varying in magnitude and direction to the fingertips. Two actuators were employed to generate the forces and deliver them to the fingertips. Various forces are readily generated by the combination of the linear actuator and SEA discussed in Chapter 2. The directions of applied forces vary by fingertip orientation, derived via forward kinematics. The actuator rotates the linear motor as directed by the fingertip orientation. Separate control of force magnitude and direction generates feedback very similar to that of real-life forces.

References

- [1] Forcimension. (2019) omega.6. [Online]. Available: <http://www.forcimension.com/>
- [2] D. Systems. (2019) Touch. [Online]. Available: <http://www.3dsystems.com/>
- [3] M. Sato, “Development of string-based force display:spidar,” in *8th international conference on virtual systems and multimedia*, 2002.
- [4] M. Monroy, M. Oyarzabal, M. Ferre, A. Campos, and J. Barrio, “Masterfinger: Multi-finger haptic interface for collaborative environments,” in *EuroHaptics*, 2008, pp. 411–419.
- [5] C. Systems. (2019) Cybergrasp. [Online]. Available: <http://www.cyberglovesystems.com/>
- [6] DextaRobotics. (2019) Dexmo. [Online]. Available: <https://www.dextarobotics.com/>
- [7] Festo. (2019) Exohand. [Online]. Available: <http://www.festo.com/>
- [8] M. Bouzit, G. Burdea, G. Popescu, and R. Boian, “The rutgers master ii - new design force-feedback glove,” *IEEE/ASME Transactions on Mechatronics*, vol. 7, pp. 256–263, 2002.
- [9] P. Medical. (2019) Prometheus traction splint. [Online]. Available: <https://www.prometheusmedical.co.uk/>
- [10] Saebo. (2019) Saebostretch and saeboxflex. [Online]. Available: <https://www.prometheusmedical.co.uk/>
- [11] TheraBand. (2019) Hand exerciser. [Online]. Available: <http://www.theraband.com/>
- [12] T. T. Equipment. (2019) Kinetic maestra portable hand cpm. [Online]. Available: <http://theratechequip.com/>
- [13] RemintonMedical. (2019) Waveflex hand cpm. [Online]. Available: <http://www.remingtonmedical.com/>

- [14] C. N. Schabowsky, S. B. Godfrey, R. J. Holley, and P. S. Lum, “Development and pilot testing of hexorr: hand exoskeleton rehabilitation robot,” *Journal of NeuroEngineering and Rehabilitation*, vol. 7, 2010.
- [15] E. B. Brokaw, R. J. Holley, and P. S. Lum, “Hand spring operated movement enhancer (handsome) device for hand rehabilitation after stroke,” in *Annual International Conference of the IEEE EMBS*, 2011.
- [16] Rehab-Robotics. (2019) Hand of hope. [Online]. Available: <http://www.rehab-robotics.com/>
- [17] N. Ho, K. Tong, X. Hu, K. Fung, X. Wei, W. Rong, and E. Susanto, “An emg-driven exoskeleton hand robotic training device on chronic stroke subjects,” in *IEEE International Conference on Rehabilitation Robotics (ICORR)*, 2011.
- [18] Gloreha. (2019) Sinfonia. [Online]. Available: <https://www.gloreha.com/>
- [19] B. B. Kang, H. Choi, H. Lee, and K.-J. Cho, “Exo-glove poly ii: A polymer-based soft wearable robot for the hand with a tendon-driven actuation system,” *Soft Robotics*.
- [20] D. Neumann and E. Rowan, *Kinesiology of the musculoskeletal system: foundations for physical rehabilitation*. Mosby, 2002.
- [21] E. Samur, *Performance Metrics for Haptic Interfaces*. Springer, 2012.
- [22] Y. W. Kim, S. H. Yoon, H. Hwangbo, and Y. G. Ji, “Development of a user experience evaluation framework for wearable devices,” in *International Conference on Human Aspects of IT for the Aged Population*, 2017.
- [23] G. Pfurtscheller and C. Neuper, “Dynamics of sensorimotor oscillations in a motor task,” in *Brain-Computer Interfaces*. Springer, Berlin, Heidelberg, 2009, pp. 47–64.
- [24] W. Penfield and E. Boldrey, “Somatic motor and sensory representation in the cerebral cortex of man as studied by electrical stimulation,” *Brain*, vol. 60, pp. 389–443, 1937.
- [25] R. L. Drake, A. W. Vogl, and A. W. M. Mitchell, *Gray’s anatomy for students*. Elsevier, 2010.
- [26] N. G. Kutner, R. Zhang, A. J. Butler, S. L. Wolf, and J. L. Alberts, “Quality-of-life change associated with robotic-assisted therapy to improve hand motor function in patients with subacute stroke: A randomized clinical trial,” *Physical Therapy*, vol. 90, pp. 493–504, 2010.

- [27] G. B. Prange, M. J. A. Jannink, C. G. M. Groothuis-Oudshoorn, H. J. Hermens, and M. J. IJzerman, “Systematic review of the effect of robot-aided therapy on recovery of the hemiparetic arm after stroke,” *Journal of Rehabilitation Research and Development*, vol. 43, pp. 171–184, 2006.
- [28] J. D. Schaechter, E. Kraft, T. S. Hilliard, R. M. Dijkhuizen, T. Benner, S. P. Finklestein, B. R. Rosen, and S. C. Cramer, “Motor recovery and cortical reorganization after constraint-induced movement therapy in stroke patients: a preliminary study,” *Neurorehabilitation and neural repair*, vol. 16, pp. 326–338, 2002.
- [29] S. Wist, J. Clivaz, and M. Sattelmayer, “Muscle strengthening for hemiparesis after stroke: A meta-analysis,” *Annals of physical and rehabilitation medicine*, vol. 59, pp. 114–124, 2016.
- [30] M. L. Giudice, “Effects of continuous passive motion and elevation on hand edema,” *American Journal of Occupational Therapy*, vol. 44, pp. 914–921, 1990.
- [31] S. W. O’Driscoll and N. J. Giori, “Continuous passive motion (cpm) : Theory and principles of clinical application,” *American Journal of Occupational Therapy*, vol. 37, pp. 179–188, 2000.
- [32] I. Jo and J. Bae, “Design and control of a wearable and force-controllable hand exoskeleton system,” *Mechatronics*, vol. 41, pp. 90–101, 2017.
- [33] Y. Park, I. Jo, J. Lee, and J. Bae, “Wehaptic: A wearable haptic interface for accurate position tracking and interactive force control,” *IEEE Robotics and Automation Letters*, vol. in press, 2019.
- [34] I. Jo, Y. Park, H. Kim, and J. Bae, “Evaluation of a wearable hand kinesthetic feedback system for virtual reality: Psychophysical and user experience (ux) evaluation,” *IEEE Transactions on Human-Machine Systems*, vol. in press, 2019.
- [35] I. Jo and J. Bae, “Kinematic analysis of a hand exoskeleton structure,” in *International Conference on Ubiquitous Robots and Ambient Intelligence (URAI)*, 2013, pp. 457–458.
- [36] ———, “A force-controllable compact actuator module for a wearable hand exoskeleton,” in *19th World Congress The International Federation of Automatic Control (IFAC WC)*, 2014, pp. 4453–4458.

- [37] —, “Design and control of a wearable hand exoskeleton with force-controllable and compact actuator modules,” in *IEEE International Conference on Robotics and Automation (ICRA)*, 2015.
- [38] Y. Park, I. Jo, J. Lee, and J. Bae, “A wearable hand system for virtual reality,” in *IEEE/RSJ International Conference on Intelligent Robots and Systems (IROS)*, 2017.
- [39] S. K. Banala, S. H. Kim, S. K. Agrawal, and J. P. Scholz, “Robot Assisted Gait Training With Active Leg Exoskeleton (ALEX),” *IEEE Trans. on Neural System Rehabilitation Engineering*, vol. 17, pp. 2–8, 2009.
- [40] J. C. Perry, J. Rosen, and S. Burns, “Upper-limb powered exoskeleton design,” *IEEE/ASME Trans. Mechatron.*, vol. 12, pp. 408–417, 2007.
- [41] R. Riener, L. Lunenburger, S. Jezernik, M. Anderschitz, G. Colombo, and V. Dietz, “Patient-cooperative strategies for robot-aided treadmill training: first experimental results,” *IEEE Trans. Neural Syst. Rehabil. Eng.*, vol. 13, pp. 380–394, 2005.
- [42] J. F. Veneman, R. Kruidhof, E. E. Hekman, R. Ekkelenkamp, E. H. V. Asseldonk, and H. van der Kooij, “Design and Evaluation of the LOPES Exoskeleton Robot for Interactive Gait Rehabilitation,” *IEEE Trans. on Neural System Rehabilitation Engineering*, vol. 15, pp. 379–386, 2007.
- [43] A. Zoss, H. Kazerooni, and A. Chu, “Biomechanical design of the berkeley lower extremity exoskeleton (BLEEX),” *IEEE/ASME Trans. Mechatronics*, vol. 11, pp. 128–138, 2006.
- [44] Samsung. (2019) Gearvr. [Online]. Available: <http://www.samsung.com/>
- [45] Oculus. (2019) Oculus rift. [Online]. Available: <http://www.oculus.com/>
- [46] SONY. (2019) 3d personal viewer. [Online]. Available: <http://www.sony.com/>
- [47] Samsung. (2019) Hmd odyssey. [Online]. Available: <http://www.samsung.com/>
- [48] HTC. (2019) Vive. [Online]. Available: <http://www.vive.com/>
- [49] H. In, B. B. Kang, M. Sin, and K.-J. Cho, “Exo-glove: A wearable robot for the hand with a soft tendon routing system,” *IEEE Robotics & Automation Magazine*, vol. 22, pp. 97–105, 2015.

- [50] A. Chiri, N. Vitiello, F. Giovacchini, S. Roccella, F. Vecchi, and M. C. Carrozza, “Mechatronic design and characterization of the index finger module of a hand exoskeleton for post-stroke rehabilitation,” *IEEE/ASME Transactions on Mechatronics*, vol. 17, pp. 884–894, 2012.
- [51] M. Fontana, A. Dettori, F. Salsedo, and M. Bergamasco, “Mechanical design of a novel hand exoskeleton for accurate force displaying,” in *IEEE International Conference on Robotics and Automation (ICRA)*, 2009, pp. 1704–1709.
- [52] J. Iqbal, O. Ahmad, and A. Malik, “Hexosys ii-towards realization of light mass robotics for the hand,” in *IEEE International Multitopic Conference (INMIC)*, 2011, pp. 115–119.
- [53] M. Hume, H. Gellman, H. McKellop, and R. Brumfield, “Functional range of motion of the joints of the hand,” *The Journal of hand surgery*, vol. 15, no. 2, pp. 240–243, 1990.
- [54] D. Ruth and J. McCarthy, “The design of spherical 4r linkages for four specified orientations,” *Mechanism and Machine Theory*, vol. 34, pp. 677–692, 1999.
- [55] Y. Tian, B. Shirinzadeh, and D. Zhang, “Stiffness estimation of the flexure-based five-bar micro-manipulator,” in *Intl. Conf. on Control, Automation, Robotics and Vision*, 2008, pp. 599–604.
- [56] J. Bae, K. Kong, and M. Tomizuka, “Gait phase-based control for a rotary series elastic actuator assisting the knee joint,” *ASME Journal of Medical Devices*, vol. 5, pp. 031 010–1–6, 2011.
- [57] J. Bae and M. Tomizuka, “A gait rehabilitation strategy inspired by an iterative learning algorithm,” *Mechatronics*, vol. 22, pp. 213–221, 2012.
- [58] J. Bae, W. Zhang, and M. Tomizuka, “Network-based rehabilitation system for improved mobility and tele-rehabilitation,” *IEEE Transactions of Control Systems Technology*, vol. 21, pp. 1980–1987, 2013.
- [59] D. Paluska and H. Herr, “Series elasticity and actuator power output,” in *IEEE International Conference on Robotics and Automation (ICRA)*, 2006, pp. 1830–1833.
- [60] G. Pratt and M. Williamson, “Series elastic actuators,” in *IEEE/RSJ International Conference on Intelligent Robots and Systems (IROS)*, 1995, pp. 399–406.

- [61] J. Pratt, B. Krupp, and C. Morse, “Series elastic actuators for high fidelity force control,” *Int. J. Ind. Robot*, vol. 29, pp. 234–241, 2002.
- [62] Tekscan, *Grip System*, 2019. [Online]. Available: <https://www.tekscan.com>
- [63] Actuonix. (2017) L12 series. [Online]. Available: <http://www.actuonix.com/>
- [64] H. Z. Tan, M. A. Srinivasan, B. Eberman, and B. Cheng, “Human factors for the design of force-reflecting haptic interfaces,” *Dynamic Systems and Control*, vol. 55, pp. 353–359, 1994.
- [65] R. G. Budynas and J. K. Nisbett, *Shigley’s Mechanical Engineering Design*. McGraw-Hill, 2011.
- [66] H. Rijkema and M. Girard, “Computer animation of knowledge-based human grasping,” *ACM Siggraph Computer Graphics*, vol. 25, pp. 339–348, 1991.
- [67] TML, *CLS-20NA*, 2019. [Online]. Available: <http://www.tml.jp/>
- [68] J. Ponce and B. Faverjon, “On computing three-finger force-closure grasps of polygonal objects,” *IEEE Transactions on Robotics and Automation*, vol. 11.6, pp. 868–881, 1995.
- [69] A. A. Amis, “Variation of finger forces in maximal isometric grasp tests on a range of cylinder diameters,” *Journal of biomedical engineering*, vol. 9(4), pp. 313–320, 1987.
- [70] D. Jeong, I. Jo, and J. Bae, “Analysis on the force distribution of various grasps for the design of a hand exoskeleton,” in *Proc. the IEEE International Conference on Ubiquitous Robots and Ambient Intelligence(URAI)*, 2014, pp. 127–131.
- [71] Maxon motor. (2019) Dcx 16 series. [Online]. Available: <https://www.maxonmotor.com/>
- [72] W. Park, K. Ro, S. Kim, and J. Bae, “A soft sensor-based three-dimensional (3-d) finger motion measurement system,” *Sensors*, vol. 17(2), 2017.
- [73] Y. Park, J. Lee, and J. Bae, “Development of a wearable sensing glove for measuring the motion of fingers using linear potentiometers and flexible wires,” *IEEE Transactions on Industrial Informatics*, vol. 11, pp. 198–206, 2015.

- [74] S. Ryu, P. Lee, J. B. Chou, R. Xu, R. Zhao, A. J. Hart, and S.-G. Kim, “Extremely elastic wearable carbon nanotube fiber strain sensor for monitoring of human motion,” *ACS Nano*, vol. 9, pp. 5929–5936, 2015.
- [75] K. Li, I.-M. Chen, S. H. Yeo, and C. K. Lim, “Development of finger-motion capturing device based on optical linear encoder,” *Journal of Rehabilitation Research & Development*, vol. 48, pp. 69–82, 2011.
- [76] J. T. Muth, D. M. Vogt, R. L. Truby, Y. Meng, D. B. Kolesky, R. J. Wood, and J. A. Lewis, “Embedded 3d printing of strain sensors within highly stretchable elastomers,” *Advanced Materials*, vol. 26, pp. 6307–6312, 2014.
- [77] B. Alexander and K. Viktor, “Proportions of hand segments,” *Int. J. Morphol.*, vol. 28(3), pp. 755–758, 2010.
- [78] J. Leijnse, P. Quesada, and C.W.Spoor, “Kinematic evaluation of the finger’s interphalangeal joints coupling mechanism-variability, flexion-extension differences, triggers, locking swan-neck deformities, anthropometric correlations.” *Journal of biomechanics*, vol. 43, pp. 2381–2393, 2010.
- [79] E. Kunesch, F. Binkofski, and H.-J. Freund, “Invariant temporal characteristics of manipulative hand movements,” *Experimental Brain Research*, vol. 78(3), pp. 539–546, 1989.
- [80] D. A. Neumann, *Kinesiology of the Musculoskeletal System : Foundations for Rehabilitation*. Elsevier Health Sciences., 2013.
- [81] Z.-M. Li and J. Tang, “Coordination of thumb joints during opposition,” *Journal of Biomechanics*, vol. 40, pp. 502–510, 2007.
- [82] W. P. Cooney, M. J. Lucca, E. Y. S. Chao, and R. L. Linscheid, “The axes of rotation of the thumb carpometacarpal joint,” *Journal of Bone and Joint Surgery*, vol. 63, pp. 1371–1381, 1981.
- [83] ———, “The kinesiology of the thumb trapeziometacarpal joint,” *The Journal of Bone & Joint Surgery*.
- [84] Optitrack. (2019) Motion capture system. [Online]. Available: <http://www.optitrack.com/>

- [85] T. Feix, J. Romero, H.-B. Schmiedmayer, A. M. Dollar, and D. Kragic, “The grasp taxonomy of human grasp types,” *IEEE Transactions on Human-Machine Systems*, vol. 46, pp. 66–77, 2016.
- [86] H. Z. Tan, M. A. Srinivasan, B. Eberman, and B. Cheng, “Human factors for the design of force-reflecting haptic interfaces,” *Dynamic Systems and Control*, vol. 55.1, pp. 353–359, 1994.
- [87] G. Gescheider, *Psychophysics: the fundamentals*. Psychology Press, 2013.
- [88] A. M. Murray, R. L. Klatzky, and P. K. Khosla, “Psychophysical characterization and testbed validation of a wearable vibrotactile glove for telemanipulation,” *Presence*, vol. 12, 2003.
- [89] M. Maisto, C. Pacchierotti, F. Chinello, G. Salvietti, A. D. Luca, and D. Prattichizzo, “Evaluation of wearable haptic systems for the fingers in augmented reality applications,” *IEEE Transactions on Haptics*, vol. 10, 2017.
- [90] D. Prattichizzo, F. Chinello, C. Pacchierotti, and M. Malvezzi, “Evaluation of wearable haptic systems for the fingers in augmented reality applications,” *IEEE Transactions on Haptics*, vol. 10, 2017.
- [91] I. D. 9241-210:2010, “Ergonomics of human system interaction - part 210: Human-centred design for interactive systems,” International Standardization Organization (ISO), Tech. Rep.
- [92] V. Roto, M. Obrist, and K. Vaananen-Vainio-Mattila, “User experience evaluation methods in academic and industrial contexts,” in *Proceedings of the Workshop UXEM*, 2009.
- [93] A. Bangor, P. T. Kortum, , and J. T. Miller, “An empirical evaluation of the system usability scale,” *International Journal of Human-Computer Interaction*, vol. 24, 2008.
- [94] A. M. Lund, “Measuring usability with the use questionnaire,” *Usability Interface*, vol. 8, 2001.
- [95] J. Brooke, “Sus-a quick and dirty usability scale,” *Usability evaluation in industry*.
- [96] J. F. Knight and C. Baber, “A tool to assess the comfort of wearable computers,” *Human factors*, vol. 47, 2005.

- [97] SizeKorea, *The length of the hand*, 2019. [Online]. Available: <https://sizekorea.kr/measurement-data/hand>
- [98] I. Jo, Y. Park, J. Lee, and J. Bae, “A portable and spring-guided hand exoskeleton for exercising flexion/extension of the fingers,” *Mechanism and Machine Theory*, vol. 135, pp. 176–191, 2019.
- [99] I. Jo, J. Lee, Y. Park, and J. Bae, “Design of a wearable hand exoskeleton for exercising flexion/extension of the fingers,” in *International Conference on Rehabilitation Robotics (ICORR)*, 2017.
- [100] F. Zhang, X. Wang, Y. Fu, and S. K. Agrawal, “A human-robot interaction modeling approach for hand rehabilitation exoskeleton using biomechanical technique,” in *International Conference on Intelligent Robots and Systems (IROS)*, 2015.
- [101] Y. Yun, P. Agarwal, J. Fox, K. E. Madden, and A. D. Deshpande, “Accurate torque control of finger joints with ut hand exoskeleton through bowden cable sea,” in *International Conference on Intelligent Robots and Systems (IROS)*, 2016.
- [102] T. Worsnopp, M. Peshkin, J. Colgate, and D. Kamper, “An actuated finger exoskeleton for hand rehabilitation following stroke,” in *IEEE International Conference on Rehabilitation Robotics (ICORR)*, 2007, pp. 896–901.
- [103] D. G. Kamper, E. G. Cruz, and M. Siegel, “Stereotypical fingertip trajectories during grasp,” *Journal of neurophysiology*, vol. 90, pp. 3702–3710, 2003.
- [104] A. R. R. Conti, E. Meli, “A novel kinematic architecture for portable hand exoskeletons,” *Mechatronics*, vol. 35, pp. 192–207, 2016.
- [105] J. Yang, H. Xie, and J. S. School, “A novel motion-coupling design for a jointless tendon-driven finger exoskeleton for rehabilitation,” *Mechanism and Machine Theory*, vol. 99, pp. 83–102, 2016.
- [106] S. W. O’Driscoll and N. J. Giori, “Continuous passive motion (cpm) : Theory and principles of clinical application,” *Journal of Rehabilitation Research and Development*, vol. 37, pp. 179–188, 2000.

- [107] J. Li, R. Zheng, Y. Zhang, and J. Yao, “ihand rehab: An interactive hand exoskeleton for active and passive rehabilitation,” in *International Conference on Rehabilitation Robotics (ICORR)*, 2011.
- [108] N. Hogan, “Impedance control: An approach to manipulation. parts i, ii, and iii,” *Journal of Dynamic Systems, Measurement, and Control*, vol. 107, pp. 1–24, 1985.
- [109] J. Bae and M. Tomizuka, “A gait rehabilitation strategy inspired by an iterative learning algorithm,” *Mechatronics*, vol. 22, pp. 213–221, 2012.
- [110] H. Krebs, J. Palazzolo, L. Dipietro, M. F. J. Krol, K. Rannekleiv, B. Volpe, and N. Hogan, “Rehabilitation robotics: Performance-based progressive robot-assisted therapy,” *Autonomous robots*, vol. 15, pp. 7–20, 2003.
- [111] N. Kim and B. V. Sankar, *Introduction to Finite Element Analysis and Design*. John Wiley and Sons, 2009.

Acknowledgement (감사의 글)

6년 반이라는 시간동안 석박사 통합과정을 공부하면서 저에게 많은 도움을 주셨던 분들이 계셨고, 그 덕분에 포기하지 않고 무사히 졸업할 수 있었습니다. 학위 논문의 마지막 장에서는 그분들께 감사의 인사를 드리고자 합니다.

먼저 부족한 저에게 아낌없는 조언을 주시고 연구의 방향성을 잃지 않도록 도와주신 저의 지도 교수님이신, 배준범 교수님께 진심으로 감사드립니다. 교수님의 가르침 덕분에 연구가 무엇인지 깊이 고민해볼 수 있었고, 어려움이 있어도 포기하지 않는 마음을 배울 수 있었습니다. 또한, 대학원 과정동안 도움을 주시고 귀한 시간을 내어 저의 학위 논문을 심사하고 조언해주신 신관섭, 강상훈, 오현동, 손홍선 교수님께 감사드립니다.

다음으로, 좋은 연구를 위해 함께 고생한 Bio-Robotics and Control (BiRC) 연구실 멤버들에게 감사드립니다. 특히, 가장 많은 시간을 함께 보내며 고생한 VR 그룹 멤버들, 박연규, 이정수, 김현준, 인턴으로 고생한 백승호, 윤서연, 이상엽에게 고맙습니다. 모두와 함께 했던 덕분에 연구를 마무리할 수 있었습니다.

더불어, 제가 연구에 어려움을 느껴 지쳤을 때, 가까이에서 아낌없는 조언을 주셨던 구자환, 김수현, 이지혜 선생님께 감사드립니다. 가장 힘들었던 시기에 선생님들을 만났기에 포기하지 않을 수 있었습니다. 힘든 대학원 생활을 함께 도전하며 고민을 나누었던 박현하, 곽송미, 박상아, 박은구에게 고맙습니다. 덕분에 대학원생 시절 동안 즐겁게 지낼 수 있었습니다. 또한, 각자의 자리에게 최선을 다하면서 서로 응원을 보내주는 김지선, 김예원, 김윤경, 한다혜, 졸업 논문 작성에 많은 도움을 준 정영태, 윤소라에게 고맙습니다.

마지막으로 제가 포기하지 않도록 격려해 주셨던 제가 가장 사랑하는 우리 부모님, 조화훈, 송영숙, 어려울 때마다 고민을 듣고 조언해 주었던 언니와 형부, 조진영, 박희정, 조승현, 김현진, 사랑스러운 조카, 박서진, 박서인에게 고맙습니다. 가족의 사랑과 응원 덕분에 무사히 졸업할 수 있었습니다.

그 동안 저를 지켜봐 주신 모든 분들께 다시 한번 진심으로 감사드리며 앞으로도 꾸준히 성장하는 연구자가 되겠습니다.

